FEDERAL UNIVERSITY OF PARANÁ

FREDERICO ALVES JAHNERT

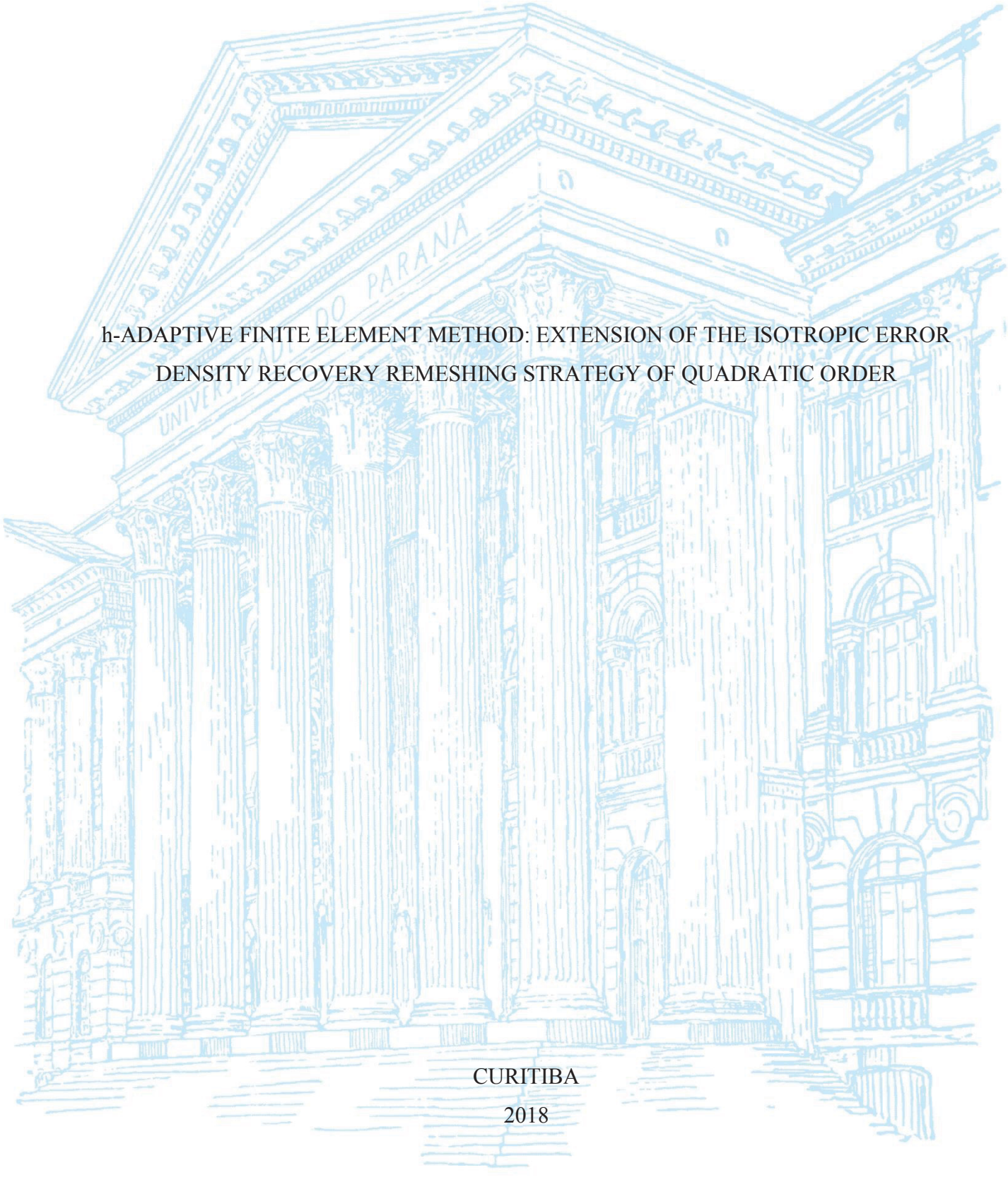

h-ADAPTIVE FINITE ELEMENT METHOD: EXTENSION OF THE ISOTROPIC ERROR DENSITY RECOVERY REMESHING STRATEGY OF QUADRATIC ORDER

CURITIBA

2018

FREDERICO ALVES JAHNERT

MÉTODO DOS ELEMENTOS FINITOS h-ADAPTATIVO: EXTENSÃO DA TÉCNICA DE RECUPERAÇÃO DA DENSIDADE DE ERRO ISOTRÓPICA DE ORDEM QUADRÁTICA

h-ADAPTIVE FINITE ELEMENT METHOD: EXTENSION OF THE ISOTROPIC ERROR DENSITY RECOVERY REMESHING STRATEGY OF QUADRATIC ORDER

Dissertação apresentada como requisito parcial à obtenção do grau de Mestre em Engenharia Mecânica, no Programa de Pós-Graduação em Engenharia Mecânica, Área de Concentração em Mecânica dos Sólidos e Vibrações, Setor de Tecnologia, Universidade Federal do Paraná.

Orientador: Prof. Dr. Jucélio Tomás Pereira.

Dissertation submitted as partial fulfillment of the requirements for the degree of Master in Mechanical Engineering, in the Post-Graduate Program in Mechanical Engineering of the Federal University of Paraná, Area of Solid Mechanics and Vibrations.

Supervisor: Prof. Dr. Jucélio Tomás Pereira.

CURITIBA

2018

Catalogação na Fonte: Sistema de Bibliotecas, UFPR
Biblioteca de Ciência e Tecnologia

J25h Jahnert, Frederico Alves
H-adaptive finite element method: extension of the isotropic error density recovery remeshing strategy of quadratic order [recurso eletrônico] / Frederico Alves Jahnert. – Curitiba, 2018.

Dissertação - Universidade Federal do Paraná, Setor de Tecnologia, Programa de Pós-Graduação em Engenharia Mecânica, 2018.

Orientador: Jucélio Tomás Pereira.

1. Método dos elementos finitos. 2. H-adaptividade. 3. Recuperação da densidade do erro isotrópica. I. Universidade Federal do Paraná. II. Pereira, Jucélio Tomás. III. Título.

CDD: 518.25

Bibliotecária: Vanusa Maciel CRB- 9/1928

MINISTÉRIO DA EDUCAÇÃO
SETOR TECNOLOGIA
UNIVERSIDADE FEDERAL DO PARANÁ
PRÓ-REITORIA DE PESQUISA E PÓS-GRADUAÇÃO
PROGRAMA DE PÓS-GRADUAÇÃO ENGENHARIA MECÂNICA

TERMO DE APROVAÇÃO

Os membros da Banca Examinadora designada pelo Colegiado do Programa de Pós-Graduação em ENGENHARIA MECÂNICA da Universidade Federal do Paraná foram convocados para realizar a arguição da Dissertação de Mestrado de **FREDERICO ALVES JAHNERT** intitulada: **H-ADAPTIVE FINITE ELEMENT METHOD: EXTENSION OF THE ISOTROPIC ERROR DENSITY RECOVERY REMESHING STRATEGY OF QUADRATIC ORDER**, após terem inquirido o aluno e realizado a avaliação do trabalho, são de parecer pela sua APROVAÇÃO no rito de defesa.

A outorga do título de mestre está sujeita à homologação pelo colegiado, ao atendimento de todas as indicações e correções solicitadas pela banca e ao pleno atendimento das demandas regimentais do Programa de Pós-Graduação.

Curitiba, 05 de Julho de 2018.

JUCÉLIO TOMAS PEREIRA
Presidente da Banca Examinadora (UFPR)

LUCIVAL MALCHER
Avaliador Externo (UNB)

MARCO ANTONIO LUERSEN
Avaliador Externo (UTFPR)

ACKNOWLEDGEMENTS

I would like to express my sincere gratitude to my supervisor Prof. Dr. Jucélio Tomás Pereira for his continuous guidance, encouragement and inspiration. His trust in my work greatly motivated me to succeed and, as a friend, his advices helped me in my career and life.

In addition, I would like to thank Prof. Jéderson da Silva for his significant assistance throughout the research project and the opportunity to work with someone who is so dedicated and determined. Also, I thank Prof. Carlos Alberto Bavastri, Prof. Eduardo Márcio de Oliveira Lopes and the thesis committee: Prof. Lucival Malcher, Prof. Marco A. Luersen and Prof. Jucélio Tomás Pereira.

My sincere gratitude to my colleagues and friends of the Laboratory of Vibrations (LaVIBS) and the Laboratory of Computational Solid Mechanics (LaSCom): Fabio Junkes, Jéssica Vieira, Gabriela Dicati, José Gubaua, Thiago da Silva, Tiago Sousa, Cintia Préve and others.

I thank my parents Ricardo and Rosimeri Jahnert for their unconditional support in every stage of my life, to my grandparents Frederico (*in memoriam*) and Helga Jahnert for their kindness and humility and my friends: Rafael Vandresen, Aline and Giselle Jahnert, Caio Fortes, among others for the stress relief and, especially, Hamish McKenzie for all his assistance.

I would like to express my profound appreciation to my girlfriend Izadora Rifiski for providing me unfailing support and understanding throughout this journey.

I thank the *Coordenação de Aperfeiçoamento de Pessoal de Nível Superior* (CAPES) for the financial support and I thank the Federal University of Paraná (UFPR) and the Post-Graduate Program in Mechanical Engineering (PGMec) for providing the appropriate foundations required to make this research possible.

"*The man who moves a mountain begins by carrying away small stones.*"

Confucius

RESUMO

O Método de Elementos Finitos (MEF) é uma técnica para resolver numericamente problemas físicos comumente utilizada na engenheria. Um fator importante na obtenção de uma solução precisa e eficiente decorre da utilização adequada da malha de discretização. Tipicamente, técnicas h-adaptativas são empregadas para projeção de uma malha ótima, onde o erro estimado em cada elemento é distribuído e minimizado de acordo com um critério de malha ótima. Neste contexto, o presente trabalho estende e avalia o método de refino h-adaptativo denominado de Recuperação da Densidade do Erro Isotrópica (IEDR) para elementos triangulares quadráticos. Inicialmente desenvolvida para elementos lineares, esta técnica baseia-se na recuperação de uma função densidade do erro em energia em conjunto com a solução de um problema de otimização que busca o tamanho do novo elemento. Dessa maneira, a metodologia IEDR aborda os erros provenientes do MEF de maneira que contenha informações locais com maior abrangência, já que, nesta metodologia, uma função densidade do erro é recuperada. Os parâmetros de qualidade de malha, obtidos através desta técnica, são comparados à tradicionais técnicas de projeto de malha denominada de Ch^p e à técnica Li-Bettess (LB). A estimativa dos erros de discretização é realizada através do estimador de erro *a posteriori* baseado em recuperação, onde os gradientes recuperados são obtidos pelo método Superconvergente de Recuperação de Padrões (*Superconvergent Patch Recovery* - SPR). A implementação computacional é elaborada no software Matlab®, sendo a geração de malha realizada pelo gerador *Bidimensional Anisotropic Mesh Generator* (BAMG). Resultados numéricos demonstram que o processo h-adaptativo baseado na técnica IEDR obtém malhas convergentes para problemas com e sem singularidade, as quais apresentam, em geral, vantagens em relação ao número de graus de liberdade, à convergência e aos parâmetros de malha em comparação à tradicional técnica Ch^p e vantagens comparada à técnica LB para elementos quadráticos.

Palavras-chave: *Elemento Triangular de Deformações Lineares. h-adaptividade. Método dos Elementos Finitos. Estimadores de erro a posteriori. Recuperação da Densidade do Erro Isotrópica.*

ABSTRACT

The finite element method (FEM) is a technique used to numerically solve physics problems which is often used in engineering. One factor in obtaining a solution that has acceptable accuracy is using adequate mesh discretization. Typically, h-adaptive techniques are used to determine new element sizes based on errors distributed among each element following an optimum mesh criterion. In this context, the current work proposes to extend and analyze the Isotropic Error Density Recovery (IEDR) h-refinement method for quadratic triangular finite elements. Initially developed for linear triangular finite elements, the extended technique is based on the recovery of an error density function, such that an optimization technique is used to search for the new element sizes. Hence, the IEDR technique utilizes more information of the local errors to design element sizes due to the recovery of an element error density function. The h-adaptive finite element method process based on the IEDR technique is compared to the traditionally used Ch^p and Li-Bettess mesh design techniques found in the literature. The discretization error estimates are achieved via a recovery based *a posteriori* error estimator, whereas the recovered gradients are obtained using the Superconvergent Patch Recovery Method. The algorithm is implemented using Matlab®, while the mesh generation is done by the *Bidimensional Anisotropic Mesh Generator* (BAMG). Results show, overall, that the meshes designed through the proposed methodology obtain superior mesh quality parameters, less degrees of freedom and better convergence in comparison with the traditional Ch^p remeshing methodology and advantages compared to the Li-Bettess element size estimation technique for quadratic elements.

Keywords: *Linear Strain Triangle. h-adaptativity. Finite Element Method. a posteriori Error Estimates. Isotropic Error Density Recovery.*

LIST OF FIGURES

LIST OF TABLES

LIST OF ABREVIATIONS

BAMG	Bidimensional Anisotropic Mesh Generator
CST	Constant Strain Triangle.
DPE	Differential Partial Equations.
FEM	Finite Element Method.
IEDR	Isotropic Error Density Recovery.
L_2	Quadratic vector norm.
LSM	Least Squares Method.
LST	Linear Strain Triangle.
MATLAB	Matrix Laboratory software.
PPR	Polynomial Preserving Recovery.
PSS	Plane Stress State.
RCP	Recovery by Compatibility in Patches.
REP	Recovery by Equilibration of Patches.
RQE	*Recuperação Quadratica do Erro.*
SCR	Superconvergent Cluster Recovery.
SPR	Superconvergent Patch Recovery.
SPRE	Superconvergent Patch Recovery with Equilibrium.
SPREB	Superconvergent Patch Recovery incorporating Equilibrium and Boundary conditions.
ZZ	Zienkiewicz-Zhu Estimator.

LIST OF SYMBOLS

Latin alphabet

a	Thermal conductivity problem's constant.
$\boldsymbol{a}$	Vector composed by coefficients of the recovered polynomial.
$\boldsymbol{A}$	Characteristic matrix associated with the SPR method.
b	Thermal conductivity problem's constant.
$\boldsymbol{b}_{SPR}$	Characteristic vector associated with the SPR method.
B	Terms of the recovered strain field.
$\boldsymbol{B}_{\varepsilon}$	Matrix composed by the terms of the recovered strain field.
C	Mesh convergence criterion's constant.
C_i	Coefficients of the error density function for the *i*-th order term (old mesh).
$\overline{C}$	Convergence acceleration constant.
d	Domain dimension.
D_i	Coefficients of the error density function for the *i*-th order term (new mesh).
$D_{\bar{\zeta}}$	Standard deviation of the local error parameter.
$\boldsymbol{D}$	Constitutive elasticity tensor.
$\boldsymbol{D}_g$	Generic constitutive tensor.
el	Generic element of the mesh.
$\boldsymbol{e}_{\boldsymbol{u}}$	Error measured as function of displacement.
$\boldsymbol{e}_{\varepsilon}$	Error measured as function of strain.
$\boldsymbol{e}_{\sigma}$	Error measured as function of stress.
$\lVert\boldsymbol{e}\rVert$	Energy error norm.
$\lVert\boldsymbol{e}^*\rVert$	Energy error norm obtained through the error estimator.
$\lVert\boldsymbol{e}_m\rVert$	Total error in the energy norm for the current mesh (old mesh).
$\lVert\boldsymbol{e}_{m+1}\rVert$	Total error in the energy norm for the next mesh (new mesh).
$\lVert\boldsymbol{e}\rVert_{lim}$	Limit error for an element.
$\lVert\boldsymbol{e}\rVert_{ie}$	Error in the energy norm for the *ie*-th element.
E	Material's modulus of elasticity.

E_{ie}	Error estimate for a generic triangular region.
f	Domain excitation.
$g(h)$	Constraint function in terms of element error.
G	First order terms of the error density function.
$\boldsymbol{G}$	Vector composed by first order terms of the error density function.
h	Element's edge size for a triangular element.
h_m	Element's edge size for a triangular element for the current mesh.
h_{m+1}	Element's edge size for a triangular element for the next mesh.
$\overline{h}_{ie}$	Inverse average of element sizes which share a common vertex node.
H	Second order term of the error density function.
H_0^1	first-order Hilbert space.
$\boldsymbol{H}$	Matrix composed by second order terms of the error density function.
k	Index of superconvergent point associated with the SPR method.
L	Third order terms of the error density function.
LC	Maximum element size for analysed problems.
L'	Simplified third order term of the error density function.
$\boldsymbol{L}$	Matrix composed by the third order terms of the error density function.
m	Adapted mesh iteration number.
n	Highest order of differentiation in the strain-displacement operator.
nsp	Number of superconvergent points.
NEl	Total number of elements in the mesh.
NE	Number of nodes in an element.
NDF	Number of degrees of freedom.
p	Polynomial order of element approximation.
P	Optimization problem.
$\boldsymbol{P}$	Vector composed by relative coordinates.
$\boldsymbol{P}^*$	Matrix composed of approximation functions.
Q	Fourth order terms of the error density function.
Q_s	Constant describing the plane elasticity problem with stress singularity.
$\boldsymbol{Q}$	Matrix composed by fourth order terms of the error density function.
r	Radius.

ref_{max}	Maximum refinement percentage compared to original element size.
t	Thickness.
T	Analytical solution of the thermal conductivity problem.
u	Analytical solution.
$\boldsymbol{u}$	Analytical displacement solution of the plane elasticity problem.
$\boldsymbol{u}_i^e$	Displacement vector for the i-th node and e-th element.
$\boldsymbol{u}^{FEM}$	Approximate displacement solution obtained via the Finite Element Method.
$\|\boldsymbol{u}\|$	Measurement of the total energy accumulated by the system.
$\|\boldsymbol{u}_m\|$	Measurement of the total energy accumulated by the system in the current mesh.
U	Energy error density function.
U_0	Constant term of the energy error density function.
v	Kinematically admissible variation.
x_k	Coordinate of the superconvergent point k.
$\boldsymbol{x}$	Vector composed by coordinates x and y.
$\boldsymbol{x}'$	Vector composed by coordinates x^2 and y^2.
$\boldsymbol{x}''$	Vector composed by coordinates xy, x^2 and y^2.
y_k	Coordinate of the superconvergent point k.
$\boldsymbol{Z}$	Symmetric characteristic matrix of the error density function.

Greek alphabet

α	Element error convergence rate.
α'	Problem constant of the thermal conductivity problem.
β	Geometrical constant related to the second moment of area of a circular element domain.
β'	Geometrical constant related to the first moment of area of a circular element domain.
λ	Regularity parameter defining the presence of singularity in the solution of a problem.
γ^{FEM}	Shear strain field calculated via the Finite Element Method.
γ^{REC}	Recovered shear strain field.
ε_{adm}	Admissible element error.
$\boldsymbol{\varepsilon}$	Strain fields.
$\boldsymbol{\varepsilon}^{FEM}$	Strain fields obtained via the Finite Element Method.
ϕ	Angle.
φ	Angle of rotation of element.
ζ_g	Global error parameter.
$\overline{\zeta}_{ie}$	Local element error parameter.
$\overline{\zeta}_{av}$	Average of the local element error parameter values.
$\overline{\zeta}_{max}$	Maximum value of the local element error parameter.
ζ_{ie}	Element refinement parameter.
$\overline{\eta}$	Relative admissible global energy error percentage.
η	Analytical global energy error percentage.
η	Coordinate.
θ	Effectivity index.
π	Pi ($\pi = 3.141592...$).
Π	Quadratic distance functional.
ρ	Problem constant of the thermal conductivity problem.
$\boldsymbol{\sigma}$	Analytical stress fields.
$\boldsymbol{\sigma}^{FEM}$	Stress fields measured via the Finite Element Method.

$\boldsymbol{\sigma}^{SPR}$	Recovered stress fields found using the Superconvergent Patch Recovery method.
$\boldsymbol{\sigma}^{REC}$	Recovered stress fields.
$\bar{\boldsymbol{\sigma}}^{*}$	Nodal vector of recovered stresses.
Γ	Boundary of the problem domain.
υ	Poisson ratio.
ξ	Coordinate.
$\boldsymbol{\psi}_e$	Element shape functions vector.
∂	Partial differentiation operator.
Ω	Problem domain.
Ω_{ie}	Domain of *ie*-th element.

TABLE OF CONTENTS

1 INTRODUCTION

Today's engineering challenges are becoming more complex, while requiring more rapid and precise solutions. In this context, it is of utmost importance to develop new techniques to achieve these requirements with low costs. Hence, numerical methods have become valuable tools to solve a vast number of engineering problems, especially, those which its physical phenomena can be modelled mathematically as partial differential equations and imposed boundary conditions.

The finite element method (FEM) is a numerical method based on solving the problem's partial differential equations using an equivalent wighted-integral form aiming at the minimal potentional energy of the system, i.e. the Variational Principle. Hence, the equivalent form, called weak form, can be solved by discrete approximations through the discretization of the given domain of analysis into a set of subdomains (REDDY, 2006). Accordingly, the solution achieved using FEM can contain approximation errors. Thus, considerable effort has been invested in developing error estimators (NADAL *et al*., 2015). These, in general, can be classified as *a priori* and *a posteriori* error estimators, which are applied, respectively, before the finite element solution is obtained, providing information related to the asymptotic behavior of the discretization errors, and after the solution is obtained, providing more precise information of the field variables and comparison to the approximated solution. Considering *a posteriori* error estimators, two distinct types are defined: recovery-based estimation and residual based estimation.

The recovery-based error estimator, according to Zienkiewicz and Zhu (1987), uses the numerical solution itself to obtain a more accurate recovered solution and evaluate, through a given error norm, the error estimation.

The use of precise error estimators provides information regarding the local distribution of errors. Hence, it becomes possible to modify the finite element mesh through adaptive algorithms, seeking a solution that satisfies a pre-determined error criterion (PRUDHOMME *et al.*, 2003). According to Cook *et al.* (2002), three categories of adaptive mesh refinement are available: **h-adaptivity**, related to the adjustment of the element size, **p-adaptivity**, related to the alteration of the order *p* of the element approximation, and **r-adaptivity**, concerning the adjustment of the location of the nodes of the mesh. On account of its broad use and the opportunity of improvement, the versatile h-adaptive mesh refinement is considered in the current study.

Recently, Pereira, Silva and Gonçalves (2016) and Silva (2017) proposed a new methodology of determining the element sizes for the h-adaptive finite element method, denominated Isotropic Error Density Recovery (IEDR). According to their studies, this mesh design technique, based on the recovery of an error density function, shows promising results. However, it has been exclusively applied and analyzed for linear triangular finite elements.

Therefore, the current work proposes to extend and analyze the quality and performance of the IEDR mesh design technique for quadratic triangular elements applied to elliptic problems. The proposed methodology is compared to the classic element size design technique proposed by Zienkiewicz and Zhu (1987), defined as the Ch^p technique, as well as the method proposed by Li and Bettess (1995) and Li *et al*. (1995), called the Li-Bettess (LB) technique.

1.1 OBJECTIVES

The main objective of this study is to extend, implement and analyze the h-adaptive FEM technique named IEDR for quadratic triangular elements and compare it to the classic remeshing strategies available in the literature.

The main objectives can be divided into the following specific objectives:

- Develop a formulation for the h-adaptive refinement for triangular quadratic elements based on the IEDR technique for linear elements;
- Implement a numerical structure for the h-adaptive finite element method using the developed formulation for the following classic problems of engineering:
    - Scalar plane problem of thermal conductivity for a squared domain;
    - Plane elasticity vectorial problem for a squared domain;
    - Plane elasticity problem for an L shaped domain with the presence of a singularity.
- Validate the results obtained through the adaptive FEM based on the IEDR technique in view of parameters of the analytical solution;
- Analyze and compare the behavior and efficiency in global and element levels of the h-adaptive refinement based on the Ch^p, Li-Betess and IEDR element size design techniques for triangular elements with a quadratic shape function.

1.2 DISSERTATION STRUCTURE

The structure of this dissertation is discussed in this section. In the current Chapter, the relevance of the study is put forward. The importance of the finite element method is introduced, as well as the use of adaptive refinement. The objectives of the dissertation are also discussed.

In Chapter 2, the ideas introduced in the first chapter are discussed in view of relevant articles in the literature. The parameters which influence the accuracy of the FEM, the derivative recovery techniques, the error estimation methods and, especially, the h-adaptive strategies based on the Ch^p, Li-Bettess and IEDR element size designs are discussed.

In Chapter 3, the numerical formulations and mathematical concepts as introduced in the literature are revised. These include *a posteriori* recovery-based error estimation, the Ch^p and LB element size design techniques based on the element error equidistribution criterion and the convergence criteria of the adaptive processes.

In Chapter 4, the IEDR design technique is developed for triangular quadratic finite elements. In this chapter, mathematical formulas regarding the optimization of each element's size are defined in relation to the error in energy density function.

In Chapter 5, the results of the analysis are discussed. Final considerations are made in Chapter 6. Lastly, the references used in the development of this dissertation are listed in the final section.

2 LITERATURE REVIEW

In this Chapter, the literature review is presented with relevant studies pertaining to the current work. The advancements in the h-refinement strategies are discussed emphasizing the error estimators used and the element size design techniques employed.

2.1 THE FINITE ELEMENT METHOD

In most engineering problems, solutions are obtained through the modeling of physical phenomena. These models, described with the laws of physics, relate the variables of the problem in order to achieve a required solution. The analytical description of the models is developed using assumption applied to the context of the problem to be solved. However, the formulation and solution of such problems can become highly burdensome in the presence of complex domain geometries (REDDY, 2006).

Traditionally, numerical methods are employed to achieve an acceptable solution for the governing differential equations. A variety of numerical methods is available today, such as the Finite Difference Method, the Boundary Element Method, the Finite-Volume Method, and others. In the Finite Element Method, the formulation of the governing differential equations is expressed in an equivalent variational form and boundary conditions are used to solve the problem. Consequently, it is possible to approximate the problem's variables in each subdomain (element) of the discretization mesh, and, thereafter, an approximate solution for the whole domain is obtained. In a general sense, the FEM has the following characteristics:

- The domain of the problem is represented as a set of simpler subdomains, denominated elements. The conjunction of these elements is called a mesh of elements (FIGURE 1);
- The elements are defined by shape functions and nodes which introduce degrees of freedom to the domain system;
- In each finite element, the solution is approximated by a polynomial shape function of order *p*;
- Boundary conditions are applied to the domain of analysis, which are then used as constraints in determining the FEM solution.

FIGURE 1 – REPRESENTATION OF A BIDIMENSIONAL DOMAIN: (a) PROBLEM DIAGRAM. (b) DISCRETIZATION OF THE DOMAIN BY TRIANGULAR AND QUADRILATERAL ELEMENTS.

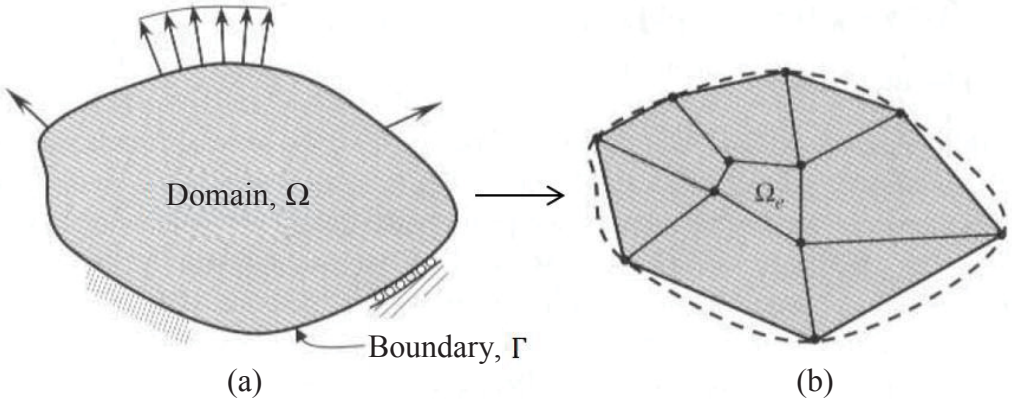

SOURCE: Modified from Reddy (2006).

Therefore, the approximate solution obtained through FEM introduces errors that degrade the solution's quality when compared to the analytical solution. Hence, it is important to evaluate and develop techniques to reduce these errors. FIGURE 1 shows (a) the domain formed by a contour which has forces applied to it and, (b) the discretization of this domain by finite elements.

According to Cook *et al*. (2002), several error sources exist in FEM, such as the numerical errors related to the rounding of numbers, user errors and discretization errors. However, only the discretization errors come solely from the representation of the mathematical model and are inherent to FEM. According to Reddy (2006), these errors can be divided into two categories: approximation errors due to the domain and approximation errors due to the FEM solution.

Domain approximation errors can occur in bidimensional and tridimensional problems when the domain geometry cannot be represented accurately by the mesh of finite elements. This error can be defined as errors in the problem's specification, leading to a solution of a modified domain boundary problem.

On the other hand, approximation errors due to the finite element solution ($\boldsymbol{u}_h$), arise from the approximation the primary variable in each element's domain Ω_{te}. In this case, the exact solutions, $\boldsymbol{u}$, is approximated as

$$\boldsymbol{u} \approx \boldsymbol{u}^{FEM} = \sum_{e=1}^{NEl} \sum_{i=1}^{NE} \boldsymbol{u}_i^e \boldsymbol{\psi}_e \tag{1}$$

where $\boldsymbol{u}_i^e$ is the nodal displacement vector for the *ie*-th element, $\boldsymbol{\psi}_e$ defines the element interpolation function, while NEl is the total number of elements in the finite element mesh and NE is the number of nodes in an element.

Thus, this dissertation focuses in controlling and reducing the solution's approximation error through the use of h-adaptive mesh refinement, where error estimation is used to guide the process of acquiring suitable element sizes of the finite element mesh.

2.2 DISCRETIZATION ERROR ESTIMATION

As discussed by González-Estrada *et al* (2014), the quality assessment of the numerical solution through FEM has become a critical research topic since the 1970s. This assessment, denominated error estimation, can be divided into two main categories: *a posteriori* error estimation and *a priori* error estimation (ZIENKIEWICZ; TAYLOR, 2000).

In the *a priori* error estimation, the process occurs before the approximate solution is obtained. Thus, this error estimation provides information concerning the behavior of the error caused by changes in the discretization mesh rather than a direct error estimation related to the FEM solution (GRÄTSCH; BATHE, 2005). This category of error estimation techniques usually provides advantages in solving complex problems, where the computational are too costly to use *a posteriori* error estimation (FRAYSSE; VALERO; RUBIO, 2013). Fraysse, Valero and Rubio (2013), for example, analyzed the use of *a priori* discretization error estimation for tridimensional non-linear problems of computational fluid dynamics.

On the other hand, *a posteriori* error estimators are currently used in several FEM algorithms due to their simplicity and robustness (CAO, 2014). These methods, in contrast to *a priori* estimators, use the computed numerical solution itself obtained through FEM (ZIENKIEWICZ; TAYLOR, 2000). Pioneering studies of *a posteriori* error estimation of discretization error were done by Babuska and Rheinboldt (1978a, 1978b, 1981) focusing on its use in h-adaptivity mesh refinement. These initial developments introduced residual based methodologies for unidimensional and bidimensional problems, achieving moderate success in decreasing the approximation error via mesh refinement. Since then, a vast number of studies have been produced on this topic. A more detailed literature review can be found in Ainsworth and Oden (2000).

Furthermore, *a posteriori* error estimators can be divided in two main categories: residual based estimators (implicit or explicit) and recovery-based estimators (ZIENKIEWICZ; TAYLOR, 2000). These techniques are briefly described in the following section.

2.2.1 *a posteriori* residual based error estimators

The residual based error estimators are methodologies which use a residual equation to provide information about the discretization errors. This residual equation calculates two sources of errors: the element errors associated to the uncertainty of the differential equation solution in the element's interior and the error present from the discontinuities of the derivative field between elements (GRÄTSCH; BATHE, 2005). The residual based error estimator can use and explicit or implicit formulation. The explicit formulation calculates the error directly thought the residual equation and the data finite element solution. On the other hand, the implicit formulation requires the solution of auxiliary boundary value problems to estimate an approximation to the actual error. As a result, the explicit formulation usually requires less computational costs (AINSWORTH; ODEN, 2000). The implicit formulation, initially developed by Demkowicz and Oden (1986), lead to studies such as, Bank and Weiser (1985), Ainsworth and Oden (1993a, 1993b, 1993c) and others. More information about explicit error estimators can be found in Babuska and Rheinboldt (1978), Johnson and Hansbo (1992) e Stewart and Hughes (1997).

2.2.2 *a posteriori* recovery based error estimators

Regarding recovery-based error estimators, two important features should be considered, the gradient recovery procedures and the error estimation itself (ZIENKIEWICZ; ZHU, 1992a). This is due to the fact that recovery-based estimators are heavily dependent on the difference between the solution obtained through FEM and the recovered solution obtained through recovery procedures. In the current literature, many solution recovery methods are available due to the close relation between the quality of the recovered values and the accuracy of the error estimate (PEREIRA; SILVA; GONÇALVES, 2016). As demonstrated by Zienkiewicz and Zhu (1992b), the recovery based *a posteriori* error estimator, denominated Zienkiewicz-Zhu (ZZ) estimator, provides highly accurate error

estimation compared to previous methodologies. For this reason and due to its robustness and simplicity, recovery-based error estimators have been used predominately in adaptive refinement processes (ZIENKIEWICZ; ZHU, 1992b; ZIENKIEWICZ; TAYLOR, 2000).

Recovery based error estimators were introduced by Zienkiewicz and Zhu (1987), where they were used as basis for h-adaptive mesh refinement for a linear elastic problem. In this article, the authors defined an optimal mesh criterion based on the equidistribution of the element error, thus, a way to estimate the sizes of the new elements was developed. This criterion is used extensively in this field of the literature.

In order to improve the solution recovery procedure, Zienkiewicz and Zhu (1992a, 1992b), introduced a new technique named Superconvergent Patch Recovery (SPR). According to Zienkiewicz and Zhu (1992a, 1992b), the ZZ error estimator demonstrated significant improvements in the estimation of error using the SPR methodology when compared to other recovery techniques.

The ZZ error estimator uses a gradient recovery method to obtain a higher-order improved solution. The recovered solution is then used as a substitute to the analytical solution. The error function for an elastic linear problem, for example, can be expressed as a function of the displacement ($\boldsymbol{e}_u$), strain ($\boldsymbol{e}_\varepsilon$) or stress ($\boldsymbol{e}_\sigma$), given by, respectively as

$$\boldsymbol{e}_u = \boldsymbol{u} - \boldsymbol{u}^{FEM}, \tag{2}$$

$$\boldsymbol{e}_\varepsilon = \boldsymbol{\varepsilon} - \boldsymbol{\varepsilon}^{FEM}, \tag{3}$$

$$\boldsymbol{e}_\sigma = \boldsymbol{\sigma} - \boldsymbol{\sigma}^{FEM}, \tag{4}$$

where $\boldsymbol{u}$, $\boldsymbol{\varepsilon}$ and $\boldsymbol{\sigma}$ are analytical displacement, strain and stress fields and $\boldsymbol{u}^{FEM}$, $\boldsymbol{\varepsilon}^{FEM}$ and $\boldsymbol{\sigma}^{FEM}$ are the respective approximate solution fields obtained using FEM.

Many norms can be used to calculate the error predicted by the error estimator, such as the L_2 norm and the energy norm. The energy norm can be expressed as

$$\|\boldsymbol{e}\| = \left[\int_\Omega (\boldsymbol{\sigma} - \boldsymbol{\sigma}^{FEM})^T \, \boldsymbol{D}^{-1} (\boldsymbol{\sigma} - \boldsymbol{\sigma}^{FEM}) \, d\Omega \right]^{\frac{1}{2}}, \tag{5}$$

where $\boldsymbol{D}$ is the constitutive elasticity tensor of the material, in this work, an elastic linear isotropic material. The recovery-based estimator essentially consists of substituting the

unknown analytical stress field solution, $\boldsymbol{\sigma}$, which is unavailable in most cases, by a recovered stress field, $\boldsymbol{\sigma}^{REC}$, thus

$$\|\boldsymbol{e}^*\| = \left[\int_{\Omega} \left(\boldsymbol{\sigma}^{REC} - \boldsymbol{\sigma}^{FEM}\right)^T \boldsymbol{D}^{-1} \left(\boldsymbol{\sigma}^{REC} - \boldsymbol{\sigma}^{FEM}\right) d\Omega \right]^{\frac{1}{2}}, \tag{6}$$

In such cases, the value of $\boldsymbol{\sigma}^{REC}$ is recovered using the FEM solution $\boldsymbol{\sigma}^{FEM}$. Therefore, $\|\boldsymbol{e}^*\|$ is denoted as the error in the energy norm obtained via error estimation.

2.2.3 Element solution recovery methods

The development of recovery based *a posteriori* error estimators introduced a great necessity of improving the precision of solution recovery techniques in order to provide data for efficient adaptive methods (PEREIRA; SILVA; GONÇALVES, 2016). For this reason, Zienkiewicz and Zhu (1992a, 1992b, 1995) created and analyzed the ***Superconvergent Patch Recovery*** (SPR) method for unidimensional and bidimensional problems, using linear, quadratic and cubic elements. The SPR method makes use of a local patch of elements to adjust the gradient of the FEM solution by the Least Squares Method (LSM), where specific points with higher convergence rates are sampled in the process. These points are defined as superconvergente points which usually coincide with Gauss quadrature points (BARLOW; 1976). The usage of points with higher convergence rates in the solution recovery process offers an asymptotically exact error estimate. In other words, the ratio between the estimated error and the real error tends to unity as the mesh is refined (CAO; 2014). In the works of Zienkiewicz and Zhu (1992a, 1992b), it was noted, heuristically, that, while using triangular quadratic elements, the SPR method results in a convergence rate for the gradient recovered solution proportional to $O(h^{p+2})$, that is, two orders higher than the asymptotic convergence of the finite element approximation. This phenomenon is called ultraconvergence.

Zhang (1996, 2000) mathematically proved the existence of ultraconvergence in the recovered derivatives obtained through the SPR method for uniform unidimensional meshes. It is shown that ultraconvergence will occur for any even-order finite element. Zhu and Meng (2004) investigated the presence of ultraconvergence in triangular quadratic finite elements. In this study, an asymptotic expansion was used to prove mathematically the presence of ultraconvergence for these elements in elliptic boundary value problems. Subsequently, many

studies have been produced aiming at the investigation of optimal sampling points for the SPR process. For triangular quadratic elements, it was concluded that superconvergent points, those which have strictly highest convergence, do not exist (RAJENDRAN; LIEW, 2003; ZIENKIEWICZ; TAYLOR, 2000).

In order to assist the SPR methodology, Rajendran and Liew (2003) analyzed the use of Gauss quadrature points in the SPR procedure for quadratic and linear elements. In this study, it was shown that, when utilizing 3 sampling points, the Gauss quadrature points had the best performance in recovering the gradient of the solution when compared to the Barlow and pseudo-Barlow points for quadratic triangular elements. Rajendran and Liew (2003) concluded that the recovered gradient, using the aforementioned points, is superconvergent even though the actual points are not superconvergent. Thus, the analyzed points are called optimal sampling points. Heuristically, Zienkiewicz and Taylor (2000) indicate that the Gauss quadrature with 4 sampling points are best sampling points for quadratic triangular elements, however they also affirm that superconvergent points (unique arrangement of points with optimal convergence), for these elements do not exist.

Other studies have been produced to evaluate the SPR procedure for non-uniform meshes in view of h-adaptive FEM processes. Some of these studies are: Bank and Xu (2003) for linear elements and Huang and Xu (2008) for quadratic elements. These studies show that the high level of convergence is still present for non-uniform patches of elements. However, the ultraconvergence phenomenon is present exclusively in nodes located in the interior of the domain, where sufficient domain elements are present to form complete patches. For this reason, the rate of convergence of the calculated error in the energy norm is decreased when considering the whole domain (ZIENKIEWICZ; ZHU, 1992a, 1992b).

Therefore, modifications to the SPR recovery technique were proposed in the literature. Initially, Wiberg and Abdulwahab (1992) and Wiberg, Abdulwahab and Ziukas (1994) introduced the Superconvergent Patch Recovery with Equilibrium (SPRE). In this method, an improvement in the recovered values is observed by satisfying the equilibrium condition through restrictions. Having in mind the low quality of the SPR recovery technique in the boundaries of the domain, Wiberg and Li (1994) modified the SPRE and created a new method called Superconvergent Patch Recovery Incorporating Equilibrium and Boundary Conditions (SPREB). This methodology uses weight functions in the gradient recovery procedure at nodes located near the boundaries, which imposes the recovered polynomial to satisfy, approximately the boundary conditions. Wiberg and Abdulwahab (1997) compared the three methods in unidimensional and bidimensional problems using various element types.

It was observed that the SPREB method showed robust results, with convergence rates for quadratic elements 1,5 above the convergence rates for linear elements using this technique.

Henceforth, Boroomand and Zienkiewicz (1997) developed a new recovery technique denominated *Recovery by Equilibration of Patches* (REP). The formulation behind this technique is based on satisfying equilibrium conditions between recovered stress fields in each patch of elements through adjustments via the LSM of the stress fields obtained through FEM. This method does not require the identification of superconvergent points, thus, it is applicable for any element type. Specifically, for quadratic elements, the REP methodology obtained convergence rates similar to those obtained through SPR for the evaluation of the error in the energy norm.

The recovery methods mentioned above are used as basis for the development of other recovery methods, which seek to improve the quality of the recovered values, such as: The *Recovery by Compatibility in Patches (RCP)* by Ubertini (2004); the *Polynomial Preserving Recovery (PPR)* by Zhang and Naga (2004, 2005); the Superconvergent Cluster Recovery Method (SCR) by Huang and Yi (2010). However, the SPR method, in account of its robustness and simplicity, provides an adequate solution recovery methodology and is a suitable alternative for problems with simple domains (Silva, 2015).

2.3 ISOTROPIC MESH ADAPTIVITY STRATEGIES

The *a posteriori* error estimators, discussed previously, serve as foundation for the adaptive mesh refinement processes. As mentioned, in broad terms, these processes are divided into three categories (ZIENKIEWICZ; TAYLOR, 2000): the h-adaptive version, the p-adaptive version and the r-adaptive version. These methodologies use a stipulated discretization error distribution criterion, which has essential importance in the adaptive process. Thus, the h-adaptive process, in general, starts with a coarse uniform mesh that is iteratively refined following this pre-determined optimal mesh criterion.

Zhu and Zienkiewicz (1992a, 1992b) analyzed an h-adaptive mesh refinement process using the ZZ error estimator and the SPR solution recovery technique for isotropic elements (quasi-equilateral elements). The authors defined the error equidistribution criterion, which requires the global error to be divided equally between each element of the mesh and limited by a maximum error value. In these articles, triangular and quadrangular elements of different orders are used in classical problems, such as plane elasticity problems and others.

The results show excellent effectiveness of the error estimator in the energy norm as basis of an h-adaptive process. Specifically, for quadratic triangular elements, and global relative error percentage of 1% is achieved in only 2 iterations.

Since then, many authors applied the error estimators developed by Zienkiewicz and Zhu as the basis for adaptive processes. For example, Katragadda and Grosse (1996) applied the ZZ error estimator to analyze three h-adaptive mesh refinement methods for an adjunct elasticity and thermal problem. Novotny and Fancello (1998) employed an h, p and hp adaptive refinement in the investigation of elastic bending of plates. In these studies, high convergence rates are achieved.

Recently, Nicolas *et al*. (2016) developed and analyzed the usage of pyramidal and tetrahedral elements in h-adaptive refinement for a tridimensional crack analysis, aiming at an efficient subdivision of hexahedral elements.

As seen in the literature, great effort has been applied into using *a posteriori* error estimators in h-adaptive mesh refinement (AINSWORTH; ODEN, 2000). After determining the error distribution in the mesh of elements, in general, the refinement process employs an element design technique to define each new element size. A commonly used remeshing strategy, called ZZ or Ch^p remeshing strategy, is based on the criterion of asymptotic convergence of the error, thus, for a sufficiently regular problem (absence of singularities), the error norm is said to be proportional to the element size to the power of p, the order of the element (ZIENKIEWICZ; TAYLOR, 2000).

Another h-adaptive mesh refinement strategy, based on the same criterion, was introduced by Li and Bettess (1995). The essence of this methodology is to use the element error convergence rate in conjunction with an *a priori* estimation of the number of elements required in the new mesh thus calculating the optimal element sizes. This method, named Li-Bettess (LB), achieved more efficient meshes when compared to the Ch^p technique for certain problems (LI *et al.*, 1995, LI, BETTESS, 1995; DIEZ, HUERTA, 1999). Li and Bettess (1995) mathematically proved that the errors in the mesh should be distributed based on the optimum mesh criterion introduced by Zienkiewicz and Zhu (1987), however using the appropriate number of elements of the new mesh, instead of the current mesh. Furthermore, Diéz and Huerta (1999) affirm that the LB technique achieves mesh optimality in the sense that it furnishes meshes with the minimum number of elements.

Pereira, Silva and Gonçalves (2016) developed an alternative methodology to determine the element sizes, called the Isotropic Error Density Recovery (IEDR). This technique is based on recovering an error in the energy norm density function for each

element such that, by solving an optimization problem, the new element sizes are found. Using the SPR recovery technique as precursor for *a posteriori* error estimation, a comparison between h-adaptive processes based on the Ch^p and IEDR mesh design techniques was presented.

FIGURE 2 – (a) SOLUTION OF PROBLEM PROPOSED BY MITCHELL (2013). (b) INITIAL MESH USED IN h-ADAPTIVE MESH REFINEMENT.

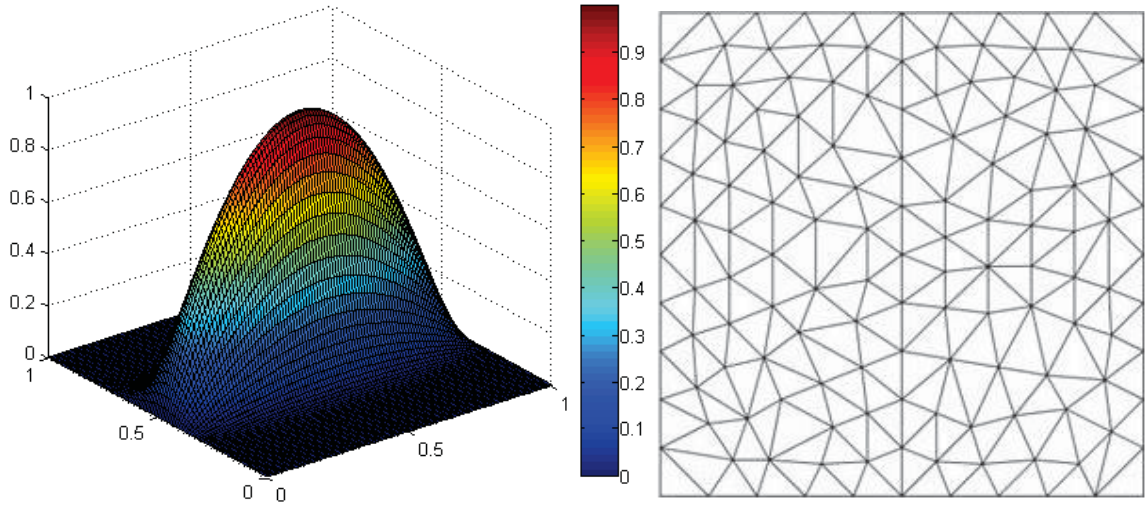

(a) (b)

SOURCE: Pereira, Silva and Gonçalves (2016).

The problem introduced by Mitchell (2013) (FIGURE 2(a)) was used by Pereira, Silva and Gonçalves (2016) to compare the mentioned h-adaptive refinement strategies for linear triangular elements (Constant Strain Triangle – CST) considering the same limit error throughout the mesh. The initial coarse mesh is shown in FIGURE 2(b). Starting at the first iteration at the top of FIGURE 3, the h-adaptive refinement process based on the Ch^p remeshing strategy, FIGURE 3(a), produces meshes with a visible higher number of elements in regions of elevated gradient, whereas the process based on the IEDR methodology, FIGURE 3(b), fewer of elements are generated in these regions. As demonstrated, the IEDR element design methodology accurately estimates the new element sizes, producing a mesh with fewer degrees freedom in comparison with the Ch^p methodology. Thus, the average element error and maximum element error parameters are improved (PEREIRA; SILVA; GONÇALVES, 2016).

FIGURE 3 – SEQUENCE OF h-ADAPTIVE MESH REFINEMENTS: (a) Ch^P REMESHING STRATEGY, (b) ISOTROPIC ERROR DENSITY RECOVERY (IEDR) REMESHING STRATEGY.

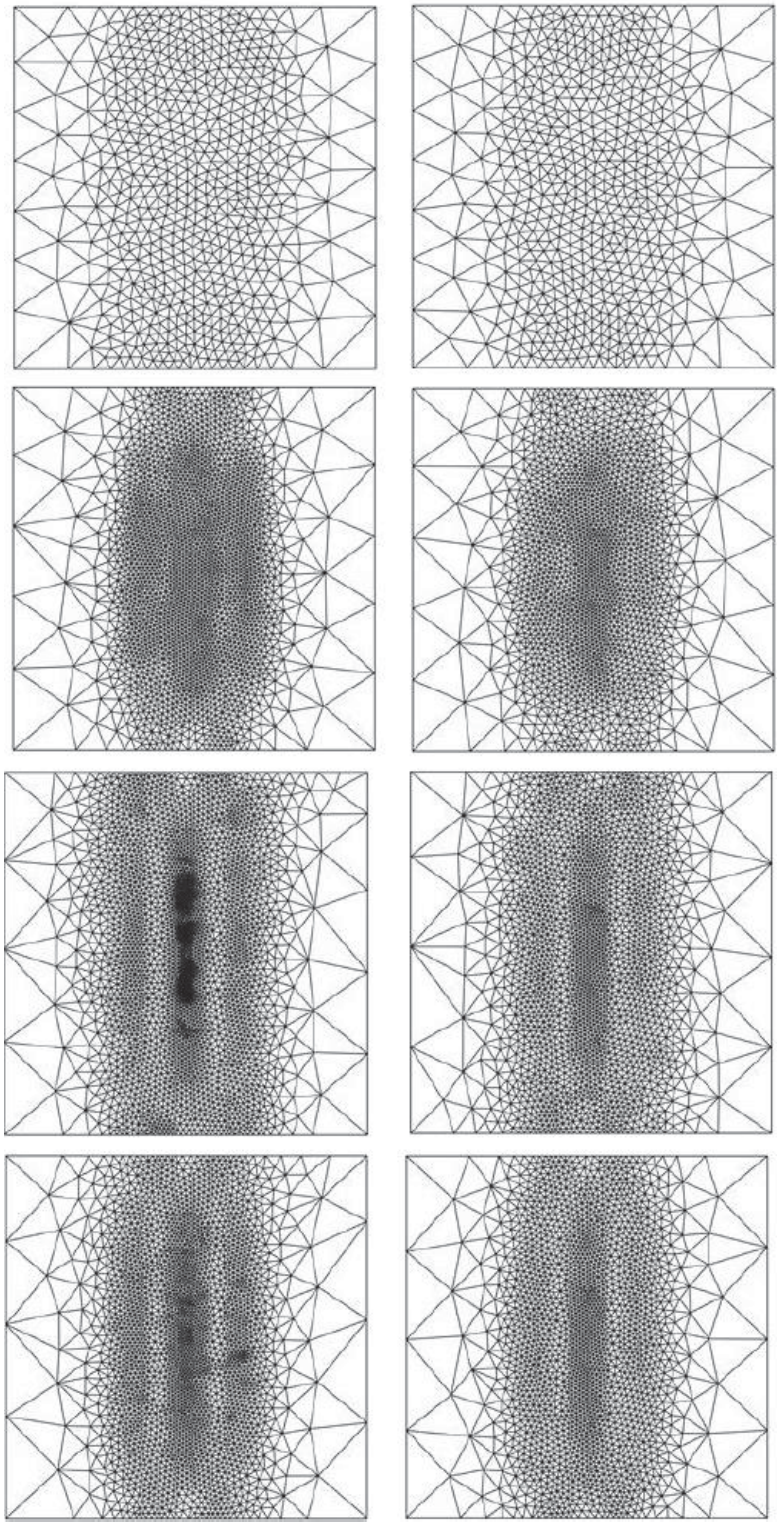

(a) (b)

SOURCE: Pereira, Silva and Gonçalves (2016).

2.4 SUMMARY

Many studies have been developed to assess h-adaptive mesh refinement techniques using *a posteriori* error estimators and the Ch^p element size design procedure. However, the LB element size design methodology showed more effective results for some problems investigated in the literature in comparison to the Ch^p technique. Furthermore, the promising isotropic element design technique called IEDR, however, was only implemented and analyzed using linear elements, where better performance was attained compared to the Ch^p technique. In this context, it is evident the need for further studies related to the application of the IEDR technique considering quadratic ordered elements. This study aims at validating: the practicability of the IEDR technique for quadratic elements and the advantages and disadvantages in using each of the remeshing strategies, called Ch^p, LB and IEDR techniques.

3 THEORETICAL BACKGROUND

The current Chapter aims at reviewing relevant theoretical concepts regarding the methodologies used in this dissertation. Initially, the mathematical formulation of the error estimation process is described, focusing on the energy norm of the error for plane elasticity problems. The SPR recovery method is defined for quadratic triangular elements. Also, in relation to the h-adaptive FEM, expressions deemed relevant in the literature are presented, such as the convergence criteria of the process and the remeshing strategies, Ch^p and LB. It is important to notice that these expressions serve as a basis for the extension of the IEDR technique presented in Chapter 4, which characterizes one of the main contributions of the research.

3.1 RECOVERY BASED ERROR ESTIMATION IN THE ENERGY NORM

The discretization error present in the finite element computations can be defined as the difference between the approximate FEM solution and the analytical solution (ZIENKIEWICZ; ZHU, 1992b; ZIENKIEWICZ; TAYLOR, 2000). In linear elasticity problems, the error function can defined in terms of the displacement field ($\boldsymbol{e}_u$), the strain field ($\boldsymbol{e}_\varepsilon$) or the stress field ($\boldsymbol{e}_\sigma$). These functions are defined, respectively, through Eq. (2), Eq. (3) and Eq. (4).

In order to obtain a scalar value for the error intensity, several error norms are studied in the literature such as the L_2 norm and the strain energy norm. This dissertation uses the energy error norm $\|\boldsymbol{e}\|$. For linear elasticity problems, the error energy norm is given by (ZIENKIEWICZ; ZHU, 1987)

$$\|\boldsymbol{e}\| = \left[\int_{\Omega} (\boldsymbol{\sigma} - \boldsymbol{\sigma}^{FEM})^T \, \boldsymbol{D}^{-1} (\boldsymbol{\sigma} - \boldsymbol{\sigma}^{FEM}) \, d\Omega \right]^{\frac{1}{2}}, \tag{7}$$

where $\boldsymbol{D}$ is the material's constitutive elasticity tensor.

However, since the analytical solution of a given problem is usually unknown, a recovered stress field ($\boldsymbol{\sigma}^{REC}$) with higher rates of convergence than those of FEM can be used ($\boldsymbol{\sigma}^{FEM}$). This process, introduced by Zienkiewicz and Zhu (1987) is the essence of *a posteriori* recovery-based error estimators. Based on the energy norm, this error estimation can be expressed as

$$\|\boldsymbol{e}^*\| = \left[\int_{\Omega} \left(\boldsymbol{\sigma}^{REC} - \boldsymbol{\sigma}^{FEM}\right)^T \boldsymbol{D}^{-1} \left(\boldsymbol{\sigma}^{REC} - \boldsymbol{\sigma}^{FEM}\right) d\Omega \right]^{\frac{1}{2}}. \tag{8}$$

Due to the use of a recovered solution with higher rates of convergence than the FEM solution, an asymptotically exact estimate is obtained i.e. the error estimator converges to the true error as element sizes get smaller (ZIENKIEWICZ; TAYLOR, 2000).

In stress analysis problems, a relative measure of the error is defined in order to describe the behavior of the problem. This parameter is called the relative energy norm error percentage, η, given by

$$\eta = \frac{\|\boldsymbol{e}\|}{\|\boldsymbol{u}\|} 100(\%), \tag{9}$$

where $\|\boldsymbol{u}\|$ is the total strain energy accumulated by the system.

A measurement of the quality of the error estimator is defined as the effectivity index. This index is given by the ratio between the estimated error and true error, which is defined as

$$\theta = \frac{\|\boldsymbol{e}^*\|}{\|\boldsymbol{e}\|}. \tag{10}$$

3.2 SUPERCONVERGENT PATCH RECOVERY METHOD (SPR)

The Superconvergent Patch Recovery method, developed by Zienkiewicz and Zhu (1992a, 1992b), is an important tool used to obtain accurate recovered gradient solutions. This method is based on obtaining a recovered polynomial which describes the recovered gradient

field, thus, recovered values in the nodes can be calculated. This polynomial is found by using a least squares fit (LSM) of the FEM solution calculated on superconvergent points or optimal sampling points. These points present higher convergence rates than any other point in the element. By using these points, the recovered solution converges to the analytical solution with a higher rate than the solution via FEM (BARLOW, 1976).

In this process, a patch of elements is used instead of recovering the approximation polynomial throughout the domain. A recovered polynomial is calculated in a patch of elements formed by all the elements which share a common vertex node. Thus, the recovered stress or strain solution can be calculated at that node.

FIGURE 4 illustrates a patch of elements for triangular quadratic elements formed by elements around a central node. In this figure, the SPR method uses the superconvergent (represented by △) points to obtain the recovered polynomial through LSM. After evaluating this polynomial, a nodal value of stress (or strain) can be calculated for the central node of the patch (denoted as ●) which will have a higher convergence rate. This is accomplished by using the central node's coordinates in the recovered polynomial. In regards to the nodes in the edge of the triangle, which share more than one patch, an average between recovered values, calculated using each patch's recovered polynomial and node coordinate, is used.

FIGURE 4 – THE SPR METHOD FOR QUADRATIC TRIANGULAR ELEMENTS

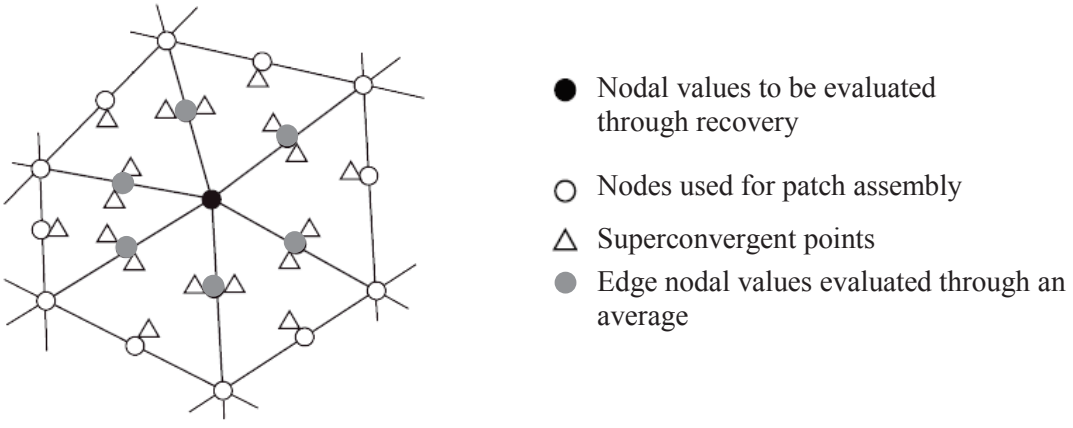

SOURCE: Modified from Zienkiewicz and Zhu (1992a).

In FIGURE 4, the arrangement of superconvergent points (△) used by Zienkiewicz and Zhu (1992a, 1992b) in the introduction of the method is shown. An alternative selection of superconvergent points for triangular quadratic elements is presented in FIGURE 5, in generalized coordinates η e ξ (RAJENDRAN; LIEW, 2003). Recently, Rajendran and Liew (2003) investigated optimal sampling points for the SPR method using triangular quadratic

elements. It was shown that the arrangement given by FIGURE 5 offer the best performance for the SPR method when using a 3-point arrangement. In the other hand, Zienkiewicz and Taylor (2000), indicate that using a 4-point arrangement, as described in FIGURE 6, a high convergence rate (two orders higher than the FEM solution) of the error estimation is acquired with the use of the SPR method. Thus, as shown in FIGURE 4, 5 and 6 divergences regarding the definition of best sampling points for triangular quadratic elements is present in the literature. The arrangement given by Zienkiewicz and Taylor (2000) (FIGURE 6) is used in this dissertation since small improvements were found using this arrangement.

FIGURE 5 – QUADRATIC ELEMENT'S CONTOUR PLOT OF THE SUM OF SQUARE OF RESIDUES. LOCATIONS OF MINIMA DEMONSTRATE POINTS WITH HIGHER CONVERGENCE.

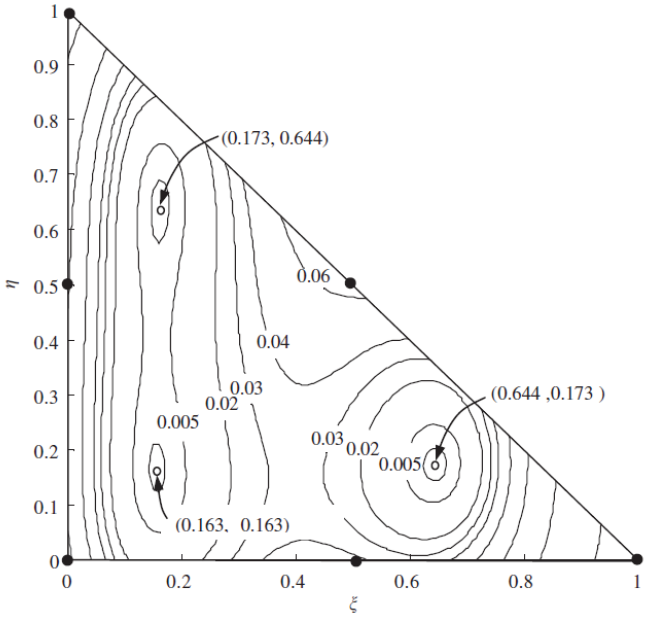

SOURCE: Rajendran and Liew (2003).

FIGURE 6 – REPRESENTATION OF THE SUPERCONVERGENT 4-POINT ARRANGEMENT INDICATED FOR THE SPR TECHNIQUE.

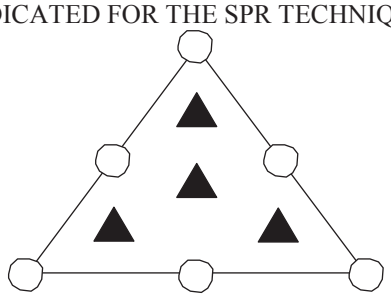

SOURCE: Zienkiewicz and Taylor (2000).

The recovered stress solution, for a generic patch, can be expressed as (ZIENKIEWICZ e ZHU, 1992a)

$$\boldsymbol{\sigma}^{SPR} = \boldsymbol{P}^{*}\boldsymbol{a}, \tag{11}$$

where $\boldsymbol{P}^{*}$ is a matrix formed by the interpolation function polynomial terms and $\boldsymbol{a}$ is the vector of unknown coefficients of the recovery polynomial.

It is defined a quadratic distance function, $\Pi(\boldsymbol{a})$, between the polynomial and the stress values obtained through FEM at the superconvergent points of each element formed around the *i*-th node. The minimization of $\Pi(\boldsymbol{a})$, in relation to the vector of unknown coefficients, results in a linear system of equations which can be solved as

$$\boldsymbol{a} = \boldsymbol{A}^{-1}\boldsymbol{b}_{SPR}, \tag{12}$$

where the matrix $\boldsymbol{A}$ is given by

$$\boldsymbol{A} = \sum_{k=1}^{nsp} \boldsymbol{P}^{*T}(x_k, y_k)\boldsymbol{P}^{*}(x_k, y_k), \tag{13}$$

and nsp is the total number of superconvergente points in the analyzed patch. The vector $\boldsymbol{b}_{SPR}$ is given by

$$\boldsymbol{b}_{SPR} = \sum_{k=1}^{nsp} \boldsymbol{P}^{*T}(x_k, y_k)\boldsymbol{\sigma}_i^{FEM}(x_k, y_k). \tag{14}$$

while (x_k, y_k) represents the coordinates of superconvergent point *k*.

Once the coefficients of the recovery polynomial ($\boldsymbol{a}$) are determined, the recovered nodal values of the patch can be calculated by substituting the appropriate nodal coordinates into Eq. (11). The order of the recovered stress (or strain) field obtained through the SPR method is the same as the shape function used for the FEM solution After obtaining the recovered stress value for each node of the element, the element's shape functions can used to

interpolate these values and create a smoothed field which is continuous between elements. For the *e*-th element, this interpolation is expressed as

$$\boldsymbol{\sigma}^{REC} = \boldsymbol{\psi}_e \bar{\boldsymbol{\sigma}}^{*}, \tag{15}$$

where $\boldsymbol{\sigma}^{REC}$ is the recovered stress field vector and $\bar{\boldsymbol{\sigma}}^{*}$ is the recovered stresses for each node of the element as obtained previously. Applying the energy norm, Eq. (8), at element level, it is possible to calculate the local error.

3.3 CONVERGENCE CRITERIA AND ERROR PARAMETERS OF THE h-ADAPTIVE FEM

The estimated finite element errors can be used as basis for a process of finite element mesh adaptation. This process requires a convergence criterion in order to obtain the optimal sizes of each element while maintaining a uniform error distribution between elements.

A FEM solution is considered convergent if it satisfies the convergence criterion at element and global levels. The latter refers to the global error of the solution. In this case, it is required that the total error of the mesh in the energy norm ($\|\boldsymbol{e}\|$) shall not surpass a percentage of the total energy accumulated in the system ($\|\boldsymbol{u}\|$). Mathematically, the global acceptability criterion can be expressed as

$$\|\boldsymbol{e}\| \leq \bar{\eta} \|\boldsymbol{u}\|, \tag{16}$$

where $\bar{\eta}$ is the global admissible error. Henceforth, it is defined a global error parameter, ζ_g, as

$$\zeta_g = \frac{\|\boldsymbol{e}\|}{\bar{\eta} \|\boldsymbol{u}\|}. \tag{17}$$

This parameter indicates whether the mesh satisfies the global convergence criterion ($\zeta_g \leq 1$) or does not ($\zeta_g > 1$), i.e. the mesh is inadequate.

The usage of the global convergence criterion alone may create a mesh where some elements present high levels (and low levels) of errors. Instead, by using the global convergence criterion in conjunction with a local convergence parameter, a better mesh refinement is produced. Thus, the error distribution throughout the mesh can also satisfy a local convergence criterion in order to achieve an optimal mesh. This concept can be expressed as

$$\|\boldsymbol{e}\|_{ie} \leq \|\boldsymbol{e}\|_{lim}, \tag{18}$$

where $\|\boldsymbol{e}\|_{ie}$ is the error in the *ie*-th element and $\|\boldsymbol{e}\|_{lim}$ represents the admissible element error. The local error parameter, $\bar{\zeta}_{ie}$, can be defined as (OÑATE; BUGEDA, 1993)

$$\bar{\zeta}_{ie} = \frac{\|\boldsymbol{e}\|_{ie}}{\|\boldsymbol{e}\|_{lim}}. \tag{19}$$

Thus, for an element with optimal size, its local error parameter should be equal to unity. In contrast, $\bar{\zeta}_{ie} > 1$ or $\bar{\zeta}_{ie} < 1$ indicate that the element should be refined or made coarser, respectively.

It is important to note that the definition of the admissible element error, $\|\boldsymbol{e}\|_{lim}$, makes a great influence in the adaptive process (OÑATE; BUGEDA, 1993). Thus, a single refinement parameter can be defined, which satisfies approximately both convergence criteria simultaneously. This parameter, called the element refinement parameter, ζ_{ie}, is defined by the multiplication of ζ_g and $\bar{\zeta}_{ie}$, given as (OÑATE; BUGEDA, 1993)

$$\zeta_{ie} = \zeta_g \bar{\zeta}_{ie} = \frac{\|\boldsymbol{e}\|}{\bar{\eta}\,\|\boldsymbol{u}\|} \frac{\|\boldsymbol{e}\|_{ie}}{\|\boldsymbol{e}\|_{lim}}. \tag{20}$$

This parameter is used in the evaluation of the quality of the h-adaptive mesh refinement.

3.4 Ch^P ELEMENT DESIGN TECHNIQUE BASED ON THE ELEMENT ERROR EQUIDISTRIBUTION CRITERION

The Ch^p mesh design methodology, introduced by Zienkiewicz and Zhu (1987), is based on estimating the new size of each element by using the asymptotic convergence rate of the error and the error equidistribution criterion. Thus, the remeshing strategy seeks to obtain a mesh where the error is limited and equally distributed between each element of the mesh. The total error in the energy norm of the current mesh, $\|\boldsymbol{e}_m\|$, can be expressed in terms of each element's error $\|\boldsymbol{e}\|_{ie}$:

$$\|\boldsymbol{e}_m\|^2 = \sum_{ie=1}^{NEl} \|\boldsymbol{e}\|_{ie}^2 . \tag{21}$$

Assuming a constant limiting value for the error in each element, $\|\boldsymbol{e}\|_{lim}$, Eq. (21) can be rearranged as

$$\|\boldsymbol{e}_{m+1}\|^2 = NEl \, \|\boldsymbol{e}\|_{lim}^2 , \tag{22}$$

where $\|\boldsymbol{e}_{m+1}\|$ is the total error in the energy norm for the next mesh (adapted mesh). Thus, the limiting error for each element, $\|\boldsymbol{e}\|_{lim}$, can be expressed as

$$\|\boldsymbol{e}\|_{lim} = \left(\frac{\|\boldsymbol{e}_{m+1}\|^2}{NEl} \right)^{\frac{1}{2}} . \tag{23}$$

The local error parameter can be defined by combining Eqs. (23) and (19), given by

$$\bar{\zeta}_{ie} = \frac{\|\boldsymbol{e}\|_{ie}}{\|\boldsymbol{e}\|_{lim}} = \frac{\|\boldsymbol{e}\|_{ie} \sqrt{NEl}}{\|\boldsymbol{e}\|} . \tag{24}$$

thus, the element refinement parameter is given as

$$\zeta_{ie} = \zeta_g \bar{\zeta}_{ie} = \frac{\|\boldsymbol{e}\|_{ie} \sqrt{NEl}}{\bar{\eta} \|\boldsymbol{u}_m\|}. \tag{25}$$

Zienkiewicz and Zhu (1987), based on the asymptotic convergence rate of the error, proposed that the relation between the total error in a mesh, $\|\boldsymbol{e}\|$, and the characteritc element size in the mesh, h, is given by

$$\|\boldsymbol{e}\| \leq C h^{min(p,\lambda)}, \tag{26}$$

where C is a constant related to the problem, p is the polynomial order of element approximation and λ is a parameter which defined the regularity of the solution $\boldsymbol{u}$.

In this study, the premise that the error convergence rate for a problem without singularities, ($\lambda > p$), is proportional to O(h^p) is adopted. Thus, it is possible to obtain an estimate of the size of the new element, h_{m+1}, from the relationship between the error in the current mesh and the new mesh. For a generic element, *ie*, the error in that element for the current mesh is given by

$$\|\boldsymbol{e}_m\|_{ie} \leq C h_{m,ie}^p, \tag{27}$$

and for the next mesh (*m+1*), the error for that element should be equal to the element limit error

$$\|\boldsymbol{e}_{m+1}\|_{ie} \leq C h_{m+1,ie}^p = \|\boldsymbol{e}\|_{lim}. \tag{28}$$

Dividing Eq. (27) by Eq. (28) and considering that

$$\zeta_{ie} = \frac{\|\boldsymbol{e}_m\|_{ie}}{\|\boldsymbol{e}_{m+1}\|_{ie}}, \tag{29}$$

an estimation of the new element size is found, such that

$$h_{m+1} = \frac{h_m}{\zeta_{ie}^{1/p}}, \tag{30}$$

where h_m represents the size of the edges of that element in the current mesh (old mesh) and h_{m+1} is the size of the edges of the element in the next mesh (new mesh).

3.5 LB REMESHING STRATEGY BASED ON THE ELEMENT ERROR EQUIDISTRIBUTION CRITERION

Introduced by Li and Bettess (1995), the element design technique called Li-Bettess (LB) aims at predicting the number of elements necessary for the convergence of the h-adaptive process while using the error equidistribution criterion to design the optimal element size. In view of the global convergence rate of the error in the mesh, Eq. (27), the element local convergence rate can be expressed as

$$\|\boldsymbol{e}\|_{ie} \leq Ch^{min(\lambda,p)-n+2}, \tag{31}$$

where $\|\boldsymbol{e}\|_{ie}$ represents the error in the energy norm for the element *ie*, C is a constant, h represents the edge's size of the finite element, p is the polynomial order of the element approximation and n is the highest order of differentiation of the solution which it remains continuous. Therefore, for FEM plane elasticity problems without singularities occurring, the element errors for the old mesh and new mesh, respectively, are expressed as

$$\|\boldsymbol{e}\|_{ie} \leq Ch_{ie}^{p+1} \tag{32}$$

$$\|\boldsymbol{e}\|_{ie,m+1} \leq Ch_{ie,m+1}^{p+1}. \tag{33}$$

The convergence rate of the error in the element is one order higher than that of the whole mesh (Eq. 27). Consequently, the relation between the sizes and the error in the energy norm for each element, considering both old and new mesh, is given by

$$h_{m+1} = h_m \left[\frac{\|\boldsymbol{e}\|_{ie,m+1}}{\|\boldsymbol{e}\|_{ie,m}} \right]^{1/p+1} . \tag{34}$$

The admissible error per element in the next mesh, $\|\boldsymbol{e}\|_{lim}$, is defined by the division of the global admissible error by an estimation of the number of elements required in that mesh, denoted as Nel_{m+1}, given by

$$\|\boldsymbol{e}\|_{lim} = \frac{\eta \|\boldsymbol{u}\|}{\sqrt{NEl_{m+1}}} \tag{35}$$

Thus, a prediction of the number of elements in the new mesh is required as mentioned. To do that, a geometrical relationship between the element sizes in the current mesh and new mesh for the same domain is used, such that

$$NEl_{m+1} = \sum_{ie=1}^{Nel} \left[\frac{h_m}{h_{m+1}} \right]^2 \tag{36}$$

By rearranging Eqs. (34), (35) and (36), an expression for the predicted number of elements in the new mesh is found. This calculation uses the element errors in the current mesh as calculated using the error estimator:

$$NEl_{m+1} = \left(\bar{\eta} \|\boldsymbol{u}\| \right)^{-2/p} \left\{ \sum_{ie=1}^{Nel} \|\boldsymbol{e}\|_{ie,m}{}^{2/(p+1)} \right\}^{(p+1)/p} . \tag{37}$$

Finally, the new element sizes can be found using the predicted number of elements in the optimal mesh, as

$$h_{m+1} = h_m \left[\frac{\bar{\eta} \|\boldsymbol{u}\|}{\|\boldsymbol{e}\|_{ie,m} \sqrt{NEl_{m+1}}} \right]^{1/p+1} . \tag{38}$$

3.6 IEDR ELEMENT DESIGN BASED ON THE ELEMENT ERROR EQUIDISTRIBUTION CRITERION

The Isotropic Error Density Recovery (IEDR) element design methodology, introduced by Pereira, Silva and Gonçalves (2016), named *Recuperação Quadratica do Erro* (RQE) in this article, seeks to search for the optimal element size in which the admissible element error is not surpassed. In this process, the technique is based on the recovery of a density function of the error in the energy norm and an optimization method used to maximize the element size restricted by the admissible error.

Silva (2017) proposed a modification of the RQE technique, renamed as IEDR, that directly evaluates the optimal triangular sized element and added an iterative process to estimate the number of elements in the new adapted mesh, while adjusting each element's error density function accordingly. The present dissertation develops a new methodology for this iterative process considering an *a posteriori* estimate of the error density function based on the asymptotic convergence rate of the error, which is developed in the next section. Silva (2017) analyzed the technique in plane elasticity problems while using linear triangular finite elements. In this thesis, the error in the energy norm, E_k^2, for a given a triangular domain, Ω_{ie}, is expressed as

$$\begin{aligned} E_{ie}^2 &= \int_{\Omega_{ie}} U \, d\Omega = \int_{\Omega_{ie}} \left[U_0 + (G_1 x + G_2 y) + \left(H_{11} x^2 + 2H_{12} xy + H_{22} y^2 \right) \right] d\Omega \\ &= U_0 \int_{\Omega_{ie}} d\Omega + G_1 \int_{\Omega_{ie}} x \, d\Omega + G_2 \int_{\Omega_{ie}} y \, d\Omega + H_{11} \int_{\Omega_{ie}} x^2 \, d\Omega \ldots \\ &\quad \ldots + 2H_{12} \int_{\Omega_{ie}} xy \, d\Omega + H_{22} \int_{\Omega_{ie}} y^2 d\Omega. \end{aligned} \tag{39}$$

where U_0, $\boldsymbol{G}$ and $\boldsymbol{H}$ correspond to the constant, linear and quadratic terms of the error density function, respectively. In order to calculate the optimal element sizes for the new mesh, an optimization problem is posed, where the maximization of the element size, constrained by the prescribed admissible error, is sought. In the standard notation, the problem is represented as

$$P : \begin{cases} \text{Minimize} & -h \\ \text{Constraint :} & g(h) \leq 0, \end{cases} \tag{40}$$

where $g(h) = E_{ie}^2 - \varepsilon_{adm}^2 = h^2\left[\beta' U_0 + \beta tr(\boldsymbol{H}) h^2\right] - \varepsilon_{adm}^2$. The problem can be solved, for example, by the Langrange multiplier method. Thus, the optimal element size is given by

$$h_{m+1} = \left(\frac{\sqrt{(\beta' U_0)^2 + 4\beta tr(\boldsymbol{H})\varepsilon_{adm}^2} - \beta' U_0}{2\beta tr(\boldsymbol{H})} \right)^{1/2}, \tag{41}$$

where β' and β are constants.

3.7 QUALITY PARAMETERS OF THE ADAPTED MESH

An important factor in the analysis of h-adaptive FEM is to quantify the quality of the meshes produced throughout the process. In broad terms, the literature usually only compares the global convergence curves between processes and number of elements in the mesh. Pereira, Silva and Gonçalves (2016) introduced three auxiliary measurements to better quantify and compare the quality of each h-adaptive methodology and mesh design strategy. These are: the maximum value of the local error parameter ($\overline{\zeta}_{máx}$), the average of the local error parameter for each element ($\overline{\zeta}_{ave}$) and the standard deviation of the local error parameter ($D_{\overline{\zeta}}$). The latter indicates a measurement of the variation of the local error parameter compared to unity and can be expressed as

$$D_{\overline{\zeta}} = \sqrt{\frac{\sum_{ie=1}^{NEl}\left(\overline{\zeta}_{ie} - 1\right)^2}{NEl}}, \tag{42}$$

where $\overline{\zeta}_{ie}$ is the local error parameter given by Eq. (18). Note that for an optimal mesh, $\overline{\zeta}_{ave} = 1$, $\overline{\zeta}_{máx} = 1$ e $D_{\overline{\zeta}} = 0$.

4 THE ISOTROPIC ERROR DENSITY RECOVERY (IEDR) ELEMENT SIZE DESIGN FOR QUADRATIC TRIANGULAR ELEMENTS (LST)

In this Section, the IEDR formulation is developed for quadratic elements. This characterizes the main contribution of this dissertation. The formulation is developed for 2D problems. 3D problems can be solved via an extension of this formulation for 3D elements.

4.1 QUADRATIC STRAIN FIELD RECOVERY

A plane elasticity problem is considered such that the approximate solution is known for mesh composed of quadratic triangular elements, also called Linear Strain Triangle (LST) elements. The strain field obtained through FEM ($\boldsymbol{\varepsilon}^{FEM}$) and the strain field obtained via a recovery technique ($\boldsymbol{\varepsilon}^{REC}$) are defined as, respectively

$$\boldsymbol{\varepsilon}^{FEM} = \begin{Bmatrix} \varepsilon_{11}^{FEM} \\ \varepsilon_{22}^{FEM} \\ \gamma_{12}^{FEM} \end{Bmatrix} \quad \text{and} \quad \boldsymbol{\varepsilon}^{REC} = \begin{Bmatrix} \varepsilon_{11}^{REC} \\ \varepsilon_{22}^{REC} \\ \gamma_{12}^{REC} \end{Bmatrix}. \tag{43}$$

In the present study, the recovered strain vector $\boldsymbol{\varepsilon}^{REC}$ is calculated using the SPR method. The recovered strain fields in each direction are obtained as polynomials with the same order as the element's shape functions. Thus, for quadratic elements, the recovered strain fields can be expressed in matrix form as

$$\boldsymbol{\varepsilon}^{REC} = \boldsymbol{\varepsilon}^{REC}(x,y) = \begin{Bmatrix} \varepsilon_{11}^{REC} \\ \varepsilon_{22}^{REC} \\ \gamma_{12}^{REC} \end{Bmatrix} = \begin{Bmatrix} B_0^{11} + B_1^{11}x + B_2^{11}y + B_3^{11}x^2 + B_4^{11}xy + B_5^{11}y^2 \\ B_0^{22} + B_1^{22}x + B_2^{22}y + B_3^{22}x^2 + B_4^{22}xy + B_5^{22}y^2 \\ B_0^{12} + B_1^{12}x + B_2^{12}y + B_3^{12}x^2 + B_4^{12}xy + B_5^{12}y^2 \end{Bmatrix}. \tag{44}$$

Alternatively, Eq. (44) can be rearranged as

$$\boldsymbol{\varepsilon}^{REC} = \begin{Bmatrix} \varepsilon_{11}^{REC} \\ \varepsilon_{22}^{REC} \\ \gamma_{12}^{REC} \end{Bmatrix} = \begin{bmatrix} B_0^{11} & B_1^{11} & B_2^{11} & B_3^{11} & B_4^{11} & B_5^{11} \\ B_0^{22} & B_1^{22} & B_2^{22} & B_3^{22} & B_4^{22} & B_5^{22} \\ B_0^{12} & B_1^{12} & B_2^{12} & B_3^{12} & B_4^{12} & B_5^{12} \end{bmatrix} \begin{Bmatrix} 1 \\ x \\ y \\ x^2 \\ xy \\ y^2 \end{Bmatrix} = \boldsymbol{B}_{\varepsilon}^{REC} \boldsymbol{P}, \tag{45}$$

where $\boldsymbol{B}_{\varepsilon}^{REC}$ denotes a matrix composed by the coefficients of the recovered strain fields expansion, x and y are the relative coordinates of a given point, where the barycenter of the element is defined as origin, and $\boldsymbol{P}$ is a vector with relative coordinates in different orders. Thus, any recovered strain component, ε_{ij}^{REC}, is defined as

$$\varepsilon_{ij}^{REC} = B_0^{ij} + B_1^{ij} x + B_2^{ij} y + B_3^{ij} x^2 + B_4^{ij} xy + B_5^{ij} y^2 = \boldsymbol{B}_{\varepsilon}^{ij^T} \boldsymbol{P}. \tag{46}$$

Applying Eq. (46) to the coordinates of each of the 6 nodes of the triangular element, the following equations are derived

$$\varepsilon_{ij_{(node\ 1)}}^{REC} = B_0^{ij} + B_1^{ij} x_1 + B_2^{ij} y_1 + B_3^{ij} x_1^2 + B_4^{ij} x_1 y_1 + B_5^{ij} y_1^2, \tag{47}$$

$$\varepsilon_{ij_{(node\ 2)}}^{REC} = B_0^{ij} + B_1^{ij} x_2 + B_2^{ij} y_2 + B_3^{ij} x_2^2 + B_4^{ij} x_2 y_2 + B_5^{ij} y_2^2, \tag{48}$$

$$\varepsilon_{ij_{(node\ 3)}}^{REC} = B_0^{ij} + B_1^{ij} x_3 + B_2^{ij} y_3 + B_3^{ij} x_3^2 + B_4^{ij} x_3 y_3 + B_5^{ij} y_3^2, \tag{49}$$

$$\varepsilon_{ij_{(node\ 4)}}^{REC} = B_0^{ij} + B_1^{ij} x_4 + B_2^{ij} y_4 + B_3^{ij} x_4^2 + B_4^{ij} x_4 y_4 + B_5^{ij} y_4^2, \tag{50}$$

$$\varepsilon_{ij_{(node\ 5)}}^{REC} = B_0^{ij} + B_1^{ij} x_5 + B_2^{ij} y_5 + B_3^{ij} x_5^2 + B_4^{ij} x_5 y_5 + B_5^{ij} y_5^2, \tag{51}$$

$$\varepsilon_{ij_{(node\ 6)}}^{REC} = B_0^{ij} + B_1^{ij} x_6 + B_2^{ij} y_6 + B_3^{ij} x_6^2 + B_4^{ij} x_6 y_6 + B_5^{ij} y_6^2. \tag{52}$$

This system of equations can be expressed in matrix form as

$$\begin{Bmatrix} \varepsilon_{ij(node\ 1)}^{REC} \\ \varepsilon_{ij(node\ 2)}^{REC} \\ \varepsilon_{ij(node\ 3)}^{REC} \\ \varepsilon_{ij(node\ 4)}^{REC} \\ \varepsilon_{ij(node\ 5)}^{REC} \\ \varepsilon_{ij(node\ 6)}^{REC} \end{Bmatrix} = \begin{bmatrix} 1 & x_1 & y_1 & x_1^2 & x_1y_1 & y_1 \\ 1 & x_2 & y_2 & x_2^2 & x_2y_2 & y_2 \\ 1 & x_3 & y_3 & x_3^2 & x_3y_3 & y_3 \\ 1 & x_4 & y_4 & x_4^2 & x_4y_4 & y_4 \\ 1 & x_5 & y_5 & x_5^2 & x_5y_5 & y_5 \\ 1 & x_6 & y_6 & x_6^2 & x_6y_6 & y_6 \end{bmatrix} \begin{Bmatrix} B_0^{ij} \\ B_1^{ij} \\ B_2^{ij} \\ B_3^{ij} \\ B_4^{ij} \\ B_5^{ij} \end{Bmatrix}. \tag{53}$$

The solution of this system of equations gives the term $\boldsymbol{B}_{\varepsilon}^{ij}$ of the quadratic approximation for the *i*-th recovered strain components for a given element in analysis. The same process is done for each of the strain components and the coefficients of the $\boldsymbol{B}_{\varepsilon}^{REC}$ are found.

4.2 TOTAL ERROR CALCULATION IN A TRIANGULAR REGION AROUND THE ELEMENT

As expressed in Eqs. (2) - (4), the error can be defined as the difference between the analytical solution and the approximate solution obtained through FEM. The quantification of pointwise error can be done using the error energy norm, given by

$$\|\boldsymbol{e}\|_{ie}^2 = \int_{\Omega} U \, d\Omega = \int_{\Omega} \Delta\boldsymbol{\varepsilon}^T \boldsymbol{D} \, \Delta\boldsymbol{\varepsilon} \, d\Omega \,, \tag{54}$$

where $\|\boldsymbol{e}\|_{ie}$ is the energy error in a generic triangular region of the domain, Ω, $U = U(x, y)$ is the error density function and $\Delta\boldsymbol{\varepsilon}$ is the vector composed by the difference between the strain fields obtained through recovery and directly from the FEM solution, described as

$$\Delta\boldsymbol{\varepsilon} = \boldsymbol{\varepsilon}^{REC} - \boldsymbol{\varepsilon}^{FEM} \,. \tag{55}$$

Rearranging Eq. (45) and Eq. (55)

$$\Delta\boldsymbol{\varepsilon} = \boldsymbol{\varepsilon}^{REC} - \boldsymbol{\varepsilon}^{FEM} = \boldsymbol{B}_{\boldsymbol{\varepsilon}}^{REC}\boldsymbol{P} - \boldsymbol{\varepsilon}^{FEM}, \tag{56}$$

where $\boldsymbol{\varepsilon}^{FEM}$ can be represented by linear functions representing the strain fields in the use of LST elements. Eq. (56) can be expanded in the form

$$\Delta\boldsymbol{\varepsilon} = \begin{bmatrix} B_0^{11} & B_1^{11} & B_2^{11} & B_3^{11} & B_4^{11} & B_5^{11} \\ B_0^{22} & B_1^{22} & B_2^{22} & B_3^{22} & B_4^{22} & B_5^{22} \\ B_0^{12} & B_1^{12} & B_2^{12} & B_3^{12} & B_4^{12} & B_5^{12} \end{bmatrix} \begin{Bmatrix} 1 \\ x \\ y \\ x^2 \\ xy \\ y^2 \end{Bmatrix} - \begin{bmatrix} A_0^{11} & A_1^{11} & A_2^{11} & 0 & 0 & 0 \\ A_0^{22} & A_1^{22} & A_2^{22} & 0 & 0 & 0 \\ A_0^{12} & A_1^{12} & A_2^{12} & 0 & 0 & 0 \end{bmatrix} \begin{Bmatrix} 1 \\ x \\ y \\ x^2 \\ xy \\ y^2 \end{Bmatrix}, \tag{57}$$

where A_1^{ij} and B_1^{ij} are the coefficients of the polynomials related to the recovered strain and the strain solution via FEM, respectively, in the direction *ij*.

Rearranging Eq. (57), the following is obtained

$$\Delta\boldsymbol{\varepsilon} = \begin{bmatrix} (B_0^{11} - A_0^{11}) & (B_1^{11} - A_1^{11}) & (B_2^{11} - A_2^{11}) & B_3^{11} & B_4^{11} & B_5^{11} \\ (B_0^{22} - A_0^{22}) & (B_1^{22} - A_1^{22}) & (B_2^{22} - A_2^{22}) & B_3^{22} & B_4^{22} & B_5^{22} \\ (B_0^{12} - A_0^{12}) & (B_1^{12} - A_1^{12}) & (B_2^{12} - A_2^{12}) & B_3^{12} & B_4^{12} & B_5^{12} \end{bmatrix} \begin{Bmatrix} 1 \\ x \\ y \\ x^2 \\ xy \\ y^2 \end{Bmatrix} = \boldsymbol{B}_{\varepsilon}\boldsymbol{P}, \tag{58}$$

where $\boldsymbol{B}_{\varepsilon}$ is a matrix composed by the differences between the recovered and FEM strain fields. As shown in Eq. (54) and based on Eq. (58), the error density function in the energy norm, U, can be expressed as

$$U = U(x,y) = \Delta\boldsymbol{\varepsilon}^T\boldsymbol{D}\Delta\boldsymbol{\varepsilon} = \boldsymbol{P}^T\boldsymbol{B}_{\boldsymbol{\varepsilon}}^T\boldsymbol{D}\boldsymbol{B}_{\boldsymbol{\varepsilon}}\boldsymbol{P} = \boldsymbol{P}^T\boldsymbol{Z}\boldsymbol{P}, \tag{59}$$

where matrix $\boldsymbol{Z}$ is symmetric and defined by the product

$$\boldsymbol{Z} = \boldsymbol{B}_{\varepsilon}^T\boldsymbol{D}\boldsymbol{B}_{\varepsilon}. \tag{60}$$

Rearranging Eq. (59) in terms of the matrix $\boldsymbol{Z}$, the error density function is expressed as

$$U = \begin{Bmatrix} 1 & x & y & x^2 & xy & y^2 \end{Bmatrix} \begin{bmatrix} Z_{11} & Z_{21} & Z_{31} & Z_{41} & Z_{51} & Z_{61} \\ Z_{12} & Z_{22} & Z_{32} & Z_{42} & Z_{52} & Z_{62} \\ Z_{13} & Z_{23} & Z_{33} & Z_{43} & Z_{53} & Z_{63} \\ Z_{14} & Z_{24} & Z_{34} & Z_{44} & Z_{54} & Z_{64} \\ Z_{15} & Z_{25} & Z_{35} & Z_{45} & Z_{55} & Z_{65} \\ Z_{16} & Z_{26} & Z_{36} & Z_{46} & Z_{56} & Z_{66} \end{bmatrix} \begin{Bmatrix} 1 \\ x \\ y \\ x^2 \\ xy \\ y^2 \end{Bmatrix}, \tag{61}$$

in expanded form, the error density function is derived in terms of the coefficients of matrix $\boldsymbol{Z}$, given as

$$\begin{aligned} U = {} & Z_{11} + (Z_{21} + Z_{12})x + (Z_{31} + Z_{13})y + (Z_{41} + Z_{22} + Z_{14})x^2 + (Z_{61} + Z_{16} + Z_{33})y^2 + \\ & (Z_{51} + Z_{15} + Z_{32} + Z_{23})xy + (Z_{42} + Z_{24})x^3 + (Z_{63} + Z_{36})y^3 + (Z_{52} + Z_{25} + Z_{43} + Z_{34})x^2 y \\ & + (Z_{53} + Z_{35} + Z_{62} + Z_{26})xy^2 + (Z_{66})y^4 + (Z_{44})x^4 + (Z_{46} + Z_{55} + Z_{64})x^2 y^2 + (Z_{45} + Z_{54})x^3 y \\ & + (Z_{65} + Z_{56})xy^3. \end{aligned} \tag{62}$$

Aiming at simplifying the equation above, the error density function can be expressed in terms of the constant, first order, second order, third order and fourth order terms. Thus,

$$\begin{aligned} U(x,y) &= U_0 + (G_1 x + G_2 y) + (H_{11}x^2 + 2H_{12}xy + H_{22}y^2) + (L_{11}x^3 + L_{12}x^2 y + L_{21}xy^2 + L_{22}y^3) \\ &\quad + (Q_{22}x^4 + 2Q_{12}x^3 y + 3Q_{11}x^2 y^2 + 2Q_{13}xy^3 + Q_{33}y^4) \\ &= U_0 + \boldsymbol{G}\boldsymbol{x} + \boldsymbol{x}^T \boldsymbol{H}\boldsymbol{x} + \boldsymbol{x}'^T \boldsymbol{L}\boldsymbol{x} + \boldsymbol{x}''^T \boldsymbol{Q}\boldsymbol{x}'', \end{aligned} \tag{63}$$

where U_0, $\boldsymbol{G}$, $\boldsymbol{H}$, $\boldsymbol{L}$, $\boldsymbol{Q}$, $\boldsymbol{x}$, $\boldsymbol{x}'$ and $\boldsymbol{x}''$ are defined as

$$U_0 = Z_{11}, \tag{64}$$

$$\boldsymbol{G} = \begin{Bmatrix} G_1 \\ G_2 \end{Bmatrix} = \begin{Bmatrix} Z_{12} + Z_{21} \\ Z_{13} + Z_{31} \end{Bmatrix}, \tag{65}$$

$$\boldsymbol{H} = \begin{bmatrix} H_{11} & H_{12} \\ H_{21} & H_{22} \end{bmatrix} = \begin{bmatrix} Z_{22} & Z_{23} \\ Z_{32} & Z_{33} \end{bmatrix}, \tag{66}$$

$$\boldsymbol{L} = \begin{bmatrix} L_{11} & L_{12} \\ L_{21} & L_{22} \end{bmatrix} = \begin{bmatrix} Z_{42} + Z_{24} & Z_{52} + Z_{25} + Z_{43} + Z_{34} \\ Z_{53} + Z_{35} + Z_{62} + Z_{26} & Z_{36} + Z_{63} \end{bmatrix}, \tag{67}$$

$$\boldsymbol{L} = \begin{bmatrix} L_{11} & L_{12} \\ L_{21} & L_{22} \end{bmatrix} = \begin{bmatrix} 2Z_{42} & 2Z_{52} + 2Z_{43} \\ 2Z_{53} + 2Z_{62} & 2Z_{36} \end{bmatrix}, \tag{68}$$

$$\boldsymbol{Q} = \begin{bmatrix} Q_{11} & Q_{21} & Q_{31} \\ Q_{12} & Q_{22} & Q_{32} \\ Q_{13} & Q_{23} & Q_{33} \end{bmatrix} = \begin{bmatrix} (2Z_{46} + Z_{55})/3 & Z_{45} & Z_{56} \\ Z_{54} & Z_{44} & (2Z_{46} + Z_{55})/3 \\ Z_{65} & (2Z_{46} + Z_{55})/3 & Z_{66} \end{bmatrix}, \tag{69}$$

$$\boldsymbol{x} = \begin{Bmatrix} x \\ y \end{Bmatrix}, \ \boldsymbol{x}' = \begin{Bmatrix} x^2 \\ y^2 \end{Bmatrix} \text{ e } \boldsymbol{x}'' = \begin{Bmatrix} xy \\ x^2 \\ y^2 \end{Bmatrix} \tag{70}$$

Considering a triangular domain, Ω_{ie}, with origin at the barycenter of the element, the total error in the energy norm, E_{ie}^2, can be obtained by the integral of the error density function:

$$\begin{aligned} \|\boldsymbol{e}\|_{ie}^2 = E_{ie}^2 &= \int_{\Omega_{ie}} U(x,y)\, d\Omega \\ &= \int_{\Omega_{ie}} U_0 + (G_1 x + G_2 y) + (H_{11}x^2 + 2H_{12}xy + H_{22}y^2) + (L_{11}x^3 + L_{12}x^2 y + L_{21}xy^2 + L_{22}y^3) \\ &+ (Q_{22}x^4 + 2Q_{12}x^3 y + 3Q_{11}x^2 y^2 + 2Q_{13}xy^3 + Q_{33}y^4)\, d\Omega, \end{aligned} \tag{71}$$

$$\begin{aligned} E_{ie}^2 = U_0 &\int_{\Omega_{ie}} d\Omega + G_1 \int_{\Omega_{ie}} x\, d\Omega + G_2 \int_{\Omega_{ie}} y\, d\Omega + H_{11} \int_{\Omega_{ie}} x^2\, d\Omega + 2H_{12} \int_{\Omega_{ie}} xy\, d\Omega \\ &+ H_{22} \int_{\Omega_{ie}} y^2 d\Omega + L_{11} \int_{\Omega_{ie}} x^3\, d\Omega + L_{12} \int_{\Omega_{ie}} x^2 y\, d\Omega + L_{21} \int_{\Omega_{ie}} xy^2\, d\Omega + L_{22} \int_{\Omega_{ie}} y^3\, d\Omega \\ &+ Q_{22} \int_{\Omega_{ie}} x^4\, d\Omega + 2Q_{12} \int_{\Omega_{ie}} x^3 y\, d\Omega + 3Q_{11} \int_{\Omega_{ie}} x^2 y^2\, d\Omega + 2Q_{13} \int_{\Omega_{ie}} xy^3\, d\Omega + Q_{33} \int_{\Omega_{ie}} y^4\, d\Omega, \end{aligned} \tag{72}$$

The integral of each term of the function is shown in TABLE 1, where φ refers to the angle of rotation of the base of the triangular element and the x axis. Due to the geometrical properties of the equilateral triangle, some area integrals are equal to zero.

TABLE 1 – MOMENT OF AREA INTEGRAL TERMS FOR QUADRATIC TRIANGULAR ELEMENTS.

MOMENT OF AREA	INTEGRAL SOLUTION
$\int_{\Omega_k} d\Omega$	$\frac{\sqrt{3}}{4}h^2$
$\int_{\Omega_k} x\, d\Omega$	0
$\int_{\Omega_k} y\, d\Omega$	0
$\int_{\Omega_k} x^2\, d\Omega$	$\frac{\sqrt{3}}{96}h^4$
$\int_{\Omega_k} xy\, d\Omega$	0
$\int_{\Omega_k} y^2 d\Omega$	$\frac{\sqrt{3}}{96}h^4$
$\int_{\Omega_k} x^3\, d\Omega$	$-sin\varphi\ \frac{1}{480}h^5$
$\int_{\Omega_k} x^2 y\, d\Omega$	$-cos\varphi\ \frac{1}{480}h^5$
$\int_{\Omega_k} xy^2\, d\Omega$	$sin\varphi\ \frac{1}{480}h^5$
$\int_{\Omega_k} y^3\, d\Omega$	$cos\varphi\ \frac{1}{480}h^5$
$\int_{\Omega_k} x^4\, d\Omega$	$\frac{\sqrt{3}}{960}h^6$
$\int_{\Omega_k} x^3 y\, d\Omega$	0
$\int_{\Omega_k} x^2 y^2\, d\Omega$	$\frac{\sqrt{3}}{2880}h^6$
$\int_{\Omega_k} xy^3\, d\Omega$	0
$\int_{\Omega_k} y^4\, d\Omega$	$\frac{\sqrt{3}}{960}h^6$

SOURCE: The author (2018).

Thus, the total error in the energy norm for an equilateral triangular region with edge's size h is given by the following expression:

$$E_{ie}^2 = U_0 \frac{\sqrt{3}}{4}h^2 + \left(H_{11}+H_{22}\right)\frac{\sqrt{3}}{96}h^4 + \left(cos\,\varphi\left(L_{22}-L_{12}\right) - sin\,\varphi\left(L_{11}-L_{21}\right)\right)\frac{1}{480}h^5 + \left(\frac{3Q_{11}}{3}+Q_{33}+Q_{22}\right)\frac{\sqrt{3}}{960}h^6. \quad (73)$$

Since the orientation of each element is dependent exclusively on the mesh generation, the angle of rotation φ is unknown at this point of the process. Thus, a negative average of the sum of the absolute values corresponding to each direction *x* and *y* is used for the third order terms corresponding to the sine and cosine functions in Eq. (73). The coefficient of the h^5 exponent is simplified as

$$\left(cos\,\varphi\left(L_{22}-L_{12}\right)-sin\,\varphi\left(L_{11}-L_{21}\right)\right)\cong L^{'}=-\frac{\left(\left|L_{11}\right|+\left|L_{22}\right|\right)}{2}-\frac{\left(\left|L_{12}\right|+\left|L_{21}\right|\right)}{2}. \tag{74}$$

where, empirically, the values obtained through $\left(cos\,\varphi\left(L_{22}-L_{12}\right)-sen\,\varphi\left(L_{11}-L_{21}\right)\right)$ are mostly negative. It is important to notice that this term has little importance in the function since the even ordered terms, which are less dependant on mixed *xy* coefficients, represent the core behavior of the function. Finally, the error in the energy norm can be defined as a function of the element size h and the coefficients of the error density function

$$E_{ie}^2=U_0\frac{\sqrt{3}}{4}h^2+tr\left(\boldsymbol{H}\right)\frac{\sqrt{3}}{96}h^4+L^{'}\frac{1}{480}h^5+tr\left(\boldsymbol{Q}\right)\frac{\sqrt{3}}{960}h^6, \tag{75}$$

where $tr\left(\mathbf{H}\right)=H_{11}+H_{22}$ and $tr\left(\boldsymbol{Q}\right)=Q_{11}+Q_{22}+Q_{33}$.

Through an optimization problem, the optimal element size can be calculated satisfying the error constraint $E_{ie}^2\le\varepsilon_{adm}^2$. This is the topic of the next section.

4.3 DESIGN OF NEW ELEMENT SIZE VIA OPTIMIZATION

This subsection aims at finding the new equilateral triangle with edge size h_{m+1} and with origin at the barycenter of the element which satisfies the error constraint. In other words, the new element size is maximized such that, in its interior, the value of the total error, E_{ie}, is limited by the admissible element error, ε_{adm}. Thus, an optimization problem is developed searching for the optimal element size (maximum) that is constrained by the admissible error, $E_{ie}^2\le\varepsilon_{adm}^2$. This problem is illustrated in FIGURE 7, where the error density function's isolines (U^1, U^2, U^3 ...) are shown and the optimal element size, h_{New}, is sought.

The admissible element error is limited based on the error equidistribution criterion as aforementioned (ZIENKIEWICZ; ZHU, 1987). The optimization problem, as shown in FIGURE 7, is expressed in its standard form in Eq. (40) where the constraint function, $g(h)$, is related to the element error given by

$$\begin{aligned} g(h) &= E_{ie}^2 - \varepsilon_{adm}^2 \\ &= U_0 \frac{\sqrt{3}}{4} h^2 + tr(\boldsymbol{H}) \frac{\sqrt{3}}{96} h^4 + L' \frac{1}{480} h^5 + tr(\boldsymbol{Q}) \frac{\sqrt{3}}{960} h^6 - \varepsilon_{adm}^2 \end{aligned} \tag{76}$$

FIGURE 7 – SEARCH PROCESS OF THE OPTIMAL ELEMENT SIZE.

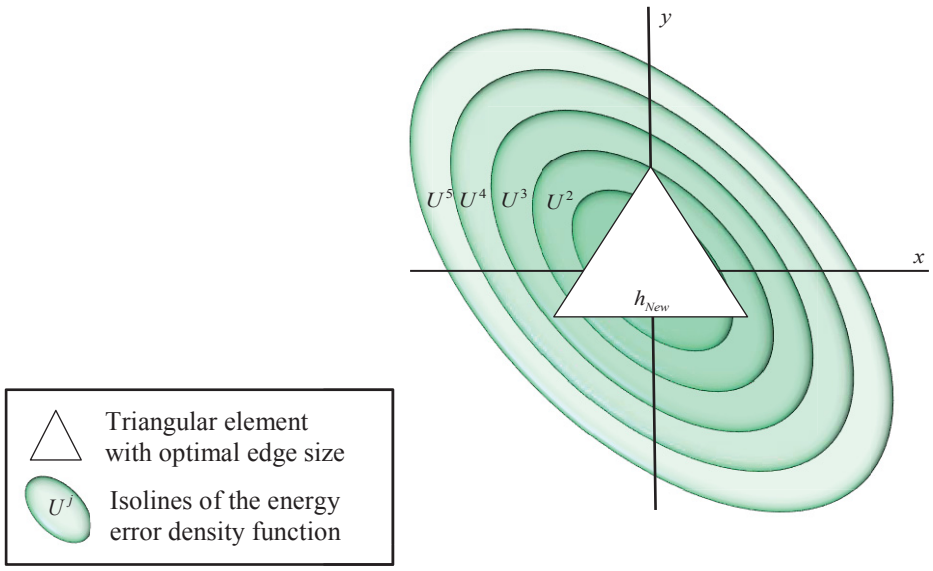

SOURCE: The author (2018).

The optimization problem is solved by finding the first positive root of the constraint function. To achieve this, the necessary conditions for a local minimum are applied. The solution of this resultant equation can be found by a unidimensional search which combines the minimization techniques based on constant-sized steps and the bisection method. As a result, the optimal new element size can be found which satisfies the condition $E_{ie} \leq \varepsilon_{adm}$. The size h_{m+1} of each element in the mesh is calculated according to the procedure mentioned above. The coefficients of the error density function of each element are stored in memory since they are used in the iterative process described in the next section.

4.4 ESTIMATE OF THE ELEMENT ERROR DENSITY FUNCTIONS IN THE NEW MESH

The IEDR technique aims at searching for the optimal element sizes for the new generated mesh. Thus, in order to calculate the element sizes considering the new mesh, the error density functions for these new elements (region) can be estimated through the use of the error asymptotic convergence rate. This is done by calculating the predicted number of elements in the new mesh and adjusting the error density functions according to the new element sizes until no adjustments are required. Hence, an iterative process is implemented where each element's error density function and number of elements for the new mesh are recalculated until convergence.

In this section, the subscript $m+1$ refers to the next mesh while subscript m refers to the current mesh being analyzed. Considering a generic element, the error in the energy norm for the current mesh, $\|\boldsymbol{e}_m\|$, and new mesh, $\|\boldsymbol{e}_{m+1}\|$, respectively, can be expressed as

$$\|\boldsymbol{e}_m\|^2 = \int_{\Omega_{ie}} U_m \, d\Omega \le C^2 h_m^{2\alpha}, \tag{77}$$

$$\|\boldsymbol{e}_{m+1}\|^2 = \int_{\Omega_{ie}} U_{m+1} \, d\Omega \le C^2 h_{m+1}^{2\alpha}, \tag{78}$$

where $\alpha = min(\lambda, p) - n + 2$, i.e. the element error convergence criterion as mentioned in Eq. (31). The integrals of the error density functions, for the old and new element, respectively. are given by

$$\int_{\Omega_{ie}} U_m \, d\Omega = U_{0_m} \frac{\sqrt{3}}{4} h_m^2 + tr(\boldsymbol{H})_m \frac{\sqrt{3}}{96} h_m^4 + L'_m \frac{1}{480} h_m^5 + tr(\boldsymbol{Q})_m \frac{\sqrt{3}}{960} h_m^6, \tag{79}$$

$$\begin{aligned} \int_{\Omega_{ie}} U_{m+1} \, d\Omega = {} & U_{0_{m+1}} \frac{\sqrt{3}}{4} h_{m+1}^2 + tr(\boldsymbol{H})_{m+1} \frac{\sqrt{3}}{96} h_{m+1}^4 \\ & + L'_{m+1} \frac{1}{480} h_{m+1}^5 + tr(\boldsymbol{Q})_{m+1} \frac{\sqrt{3}}{960} h_{m+1}^6 \end{aligned} \tag{80}$$

By rearranging Eqs. (77) and (78) into Eqs. (79) and (80), the element error convergence rate can be expressed in terms of the error density function for the old and new element:

$$U_{0_m}\frac{\sqrt{3}}{4}h_m^2+tr(\boldsymbol{H})_m\frac{\sqrt{3}}{96}h_m^4+L'_m\frac{1}{480}h_m^5+tr(\boldsymbol{Q})_m\frac{\sqrt{3}}{960}h_m^6\le\left(Ch_m^{\alpha}\right)^2, \tag{81}$$

$$U_{0_{m+1}}\frac{\sqrt{3}}{4}h_{m+1}^2+tr(\boldsymbol{H})_{m+1}\frac{\sqrt{3}}{96}h_{m+1}^4+L'_{m+1}\frac{1}{480}h_{m+1}^5+tr(\boldsymbol{Q})_{m+1}\frac{\sqrt{3}}{960}h_{m+1}^6\le\left(Ch_{m+1}^{\alpha}\right)^2, \tag{82}$$

By relating Eqs. (81) and (82) and cancelling the constants C, the element's error density function in the current mesh can be expressed in terms of its error density function in the next mesh following the error convergence rate criterion. Thus,

$$\begin{aligned}U_{0_{m+1}}\frac{\sqrt{3}}{4}h_{m+1}^2+tr(\boldsymbol{H})_{m+1}\frac{\sqrt{3}}{96}h_{m+1}^4+L'_{m+1}\frac{1}{480}h_{m+1}^5+tr(\boldsymbol{Q})_{m+1}\frac{\sqrt{3}}{960}h_{m+1}^6=\\ \left(\frac{h_{m+1}}{h_m}\right)^{2\alpha}\left[U_{0_m}\frac{\sqrt{3}}{4}h_m^2+tr(\boldsymbol{H})_m\frac{\sqrt{3}}{96}h_m^4+L'_m\frac{1}{480}h_m^5+tr(\boldsymbol{Q})_m\frac{\sqrt{3}}{960}h_m^6\right]\end{aligned} \tag{83}$$

To predict the element's new error density function (in the energy norm), the method of equating coefficients h_{m+1}^2, h_{m+1}^4, h_{m+1}^5, h_{m+1}^6 of the polynomials is used. Thus, each term can be expressed as

$$U_{0_{m+1}}\frac{\sqrt{3}}{4}h_{m+1}^2=\left(\frac{h_{m+1}}{h_m}\right)^{2\alpha}U_{0_m}\frac{\sqrt{3}}{4}h_m^2, \tag{84}$$

$$tr(\boldsymbol{H})_{m+1}\frac{\sqrt{3}}{96}h_{m+1}^4=\left(\frac{h_{m+1}}{h_m}\right)^{2\alpha}tr(\boldsymbol{H})_m\frac{\sqrt{3}}{96}h_m^4, \tag{85}$$

$$L'_{m+1}\frac{1}{480}h_{m+1}^5=\left(\frac{h_{m+1}}{h_m}\right)^{2\alpha}L'_m\frac{1}{480}h_m^5, \tag{86}$$

$$tr(\boldsymbol{Q})_{m+1}\frac{\sqrt{3}}{960}h_{m+1}^6=\left(\frac{h_{m+1}}{h_m}\right)^{2\alpha}tr(\boldsymbol{Q})_m\frac{\sqrt{3}}{960}h_m^6. \tag{87}$$

Isolating the h_{m+1}^2, h_{m+1}^4, h_{m+1}^5, h_{m+1}^6 terms in Eqs. (84) – (87) and further cancelling constants

$$U_{0_{m+1}}h_{m+1}^2=\left(\frac{h_{m+1}}{h_m}\right)^{2\alpha}\frac{h_{m+1}^2}{h_{m+1}^2}U_{0_{old}}h_m^2, \tag{88}$$

$$tr(\boldsymbol{H})_{m+1}\, h_{m+1}^4 = \left(\frac{h_{m+1}}{h_m}\right)^{2\alpha} \frac{h_{m+1}^4}{h_{m+1}^4}\, tr(\boldsymbol{H})_m\, h_m^4, \tag{89}$$

$$L'_{m+1} h_{m+1}^5 = \left(\frac{h_{m+1}}{h_m}\right)^{2\alpha} \frac{h_{m+1}^5}{h_{m+1}^5}\, L'_m h_m^5, \tag{90}$$

$$tr(\boldsymbol{Q})_{m+1}\, h_{m+1}^6 = \left(\frac{h_{m+1}}{h_m}\right)^{2\alpha} \frac{h_{m+1}^6}{h_{m+1}^6}\, tr(\boldsymbol{Q})_m\, h_m^6. \tag{91}$$

Thus, after further rearranging of Eqs. (88) – (91), each term of the error density function can be isolated. The element's new error density function can be estimated using the following equations

$$U_{0_{m+1}} = \left(\frac{h_{m+1}}{h_m}\right)^{2\alpha-2} U_{0_m}, \tag{92}$$

$$tr(\boldsymbol{H})_{m+1} = \left(\frac{h_{m+1}}{h_m}\right)^{2\alpha-4} tr(\boldsymbol{H})_m, \tag{93}$$

$$L'_{m+1} = \left(\frac{h_{m+1}}{h_m}\right)^{2\alpha-5} L'_m, \tag{94}$$

$$tr(\boldsymbol{Q})_{m+1} = \left(\frac{h_{m+1}}{h_m}\right)^{2\alpha-6} tr(\boldsymbol{Q})_m. \tag{95}$$

In broad terms, the error density function for any isotropic element, for a bidimensional problem, can be represented as

$$C_1 h_{m+1}^1 + C_2 h_{m+1}^2 + C_3 h_{m+1}^3 \cdots + C_i h_{m+1}^i = \left(\frac{h_{m+1}}{h_m}\right)^{2\alpha} \left[D_1 h_m^1 + D_2 h_m^2 + D_3 h_m^3 \cdots + D_i h_m^i \right] \tag{96}$$

where, C_i and D_i represent the coefficients of the error density function for the *i*-th order term. Therefore, an *a priori* estimation of the *i*-th order term in accordance to the asymptotic error convergence rate is given by

$$C_i = D_i \left(\frac{h_{m+1}}{h_m}\right)^{2\alpha-i}. \tag{97}$$

In summary, the terms of the error density function for a given element in current mesh element can be adjusted considering the error convergence rate such that the new adjusted error density function represents more precisely the error in the new element leading to better element size calculations.

The process mentioned above can be used as the basis for an iterative process of redefining each element's error density function considering the estimated element sizes in the new mesh and its number of elements. The implementation, FIGURE 8, can be summarized in the following steps:

***Step* 1**: Considering the current mesh, estimate the element's error density parameters, i.e., U_0, $tr(\boldsymbol{H})$, L', $tr(\boldsymbol{Q})$ according to Eq. (63), ε_{adm}^2 according to Eq. (23) and the new element size according to the optimization problem stated in Eq. (40).

***Step* 2**: For each element, the parameters calculated in the first step are adjusted considering Eqs. (48) – (51), using the element size in the current mesh and the element size calculated for the next mesh, h_m and h_{m+1}.

***Step* 3**: The number of elements in the new mesh (NEl_{new}) is estimated and the element admissible error, ε_{adm}, is updated. These parameters are calculated according to the following equations:

$$NEL_{new} = \sum_{ie=1}^{NEl} \left(h_{m+1} / h_m \right)^2 \quad \text{and} \quad \varepsilon_{adm} = \bar{\eta} \left\| \boldsymbol{u} \right\| / \sqrt{NEl_{new}} .$$

***Step* 4**: Check if convergence is reached (mesh energy error is lower than admissible error).

FIGURE 8 exhibits the iterative process described above. Convergence is reached when there is no significant change in the number of elements and, consequently, in the admissible error.

FIGURE 8 – FLOW DIAGRAM OF ITERATIVE ELEMENT DESIGN PROCESS USED BY THE IEDR METHODOLOGY.

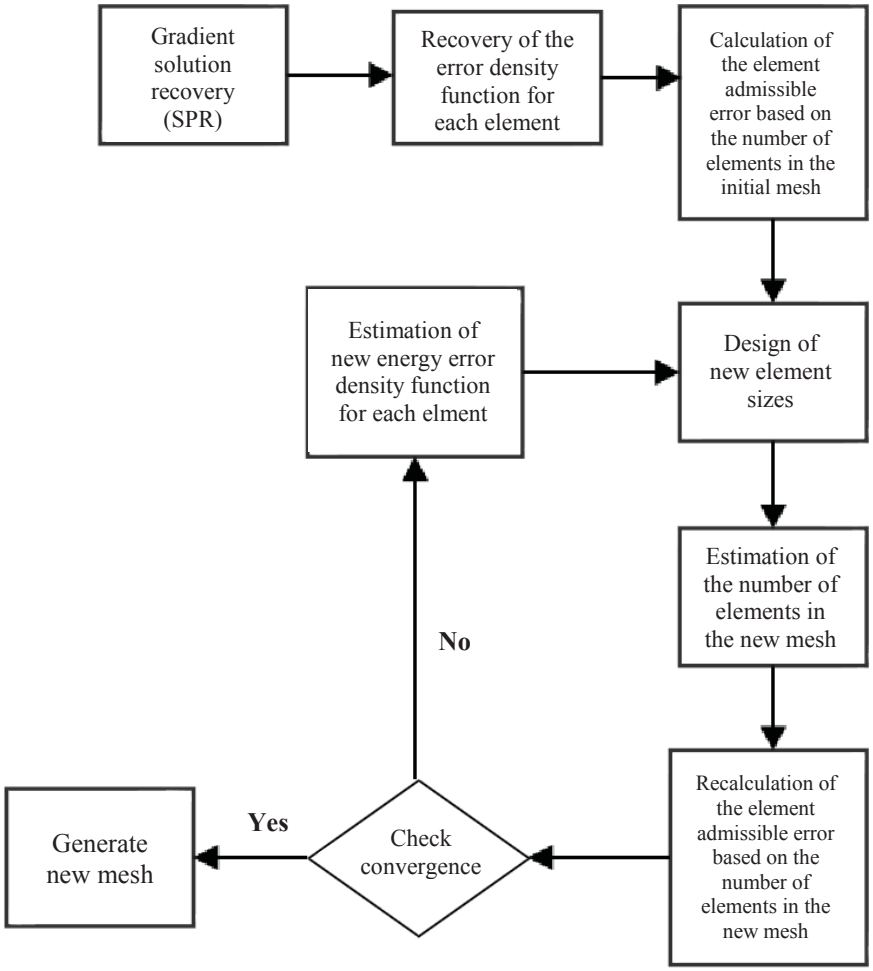

SOURCE: The author (2018).

5 RESULTS

In order to analyze the quality of the IEDR element design methodology, in this Chapter, results of four bidimensional problems found in the literature are solved: two of these problems are plane thermal conduction problems with squared shaped domains and the other two are plane elasticity problems, one with a squared shaped domain and the other with an L shaped domain which contains a stress singularity. These classic engineering problems are solved using h-adaptive FEM based on each of the remeshing methodologies aforementioned, the Ch^p, LB and IEDR methodologies. The error estimation process and initial meshes are the same across each methodology analyzed. Thus, the analysis exclusively focuses on each element design technique and avoids external influences.

Each h-adaptive process is carried out until a convergent mesh is attained, in which the mesh global energy error is lower than the estipulated admissible error, and, in some cases, additional iterations are analysed to describe the behavior of the process.

The problems discussed are evaluated in view of parameters of the h-adaptive process, discerning advantages and disadvantages of each methodology. The convergence curve of the process, the quality parameters of the mesh and the final mesh obtained are used to evaluate each process. This section does not include analysis of the error estimators since every methodology uses the same recovery method, thus, the same error estimation methodology.

5.1 NUMERICAL IMPLEMENTATION

The numerical implementation of the h-adaptive FEM is performed through the Matlab® software. In this algorithm, each adaptive strategy and analyzed problem is implemented separately using subfunctions. FIGURE 09 illustrates the implementation architecture for each of the adaptive strategies, where the element size design is done using the same estimated error differently.

FIGURE 9 – GENERIC h-ADAPTIVE PROCESS USING MATLAB® AND BAMG SOFTWARE.

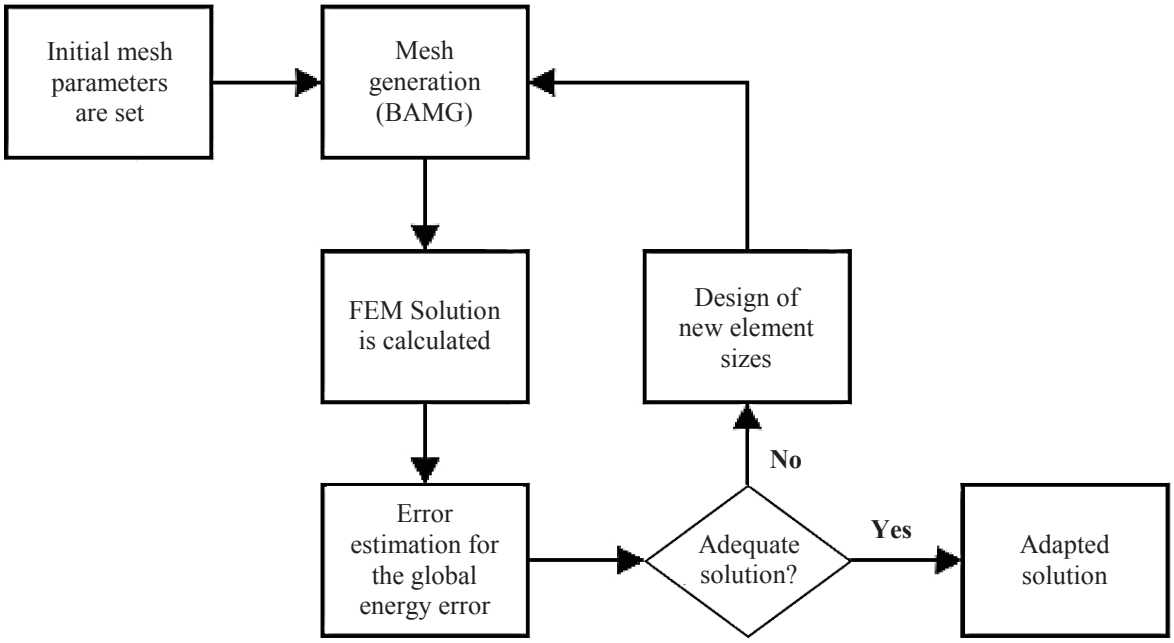

SOURCE: The author (2018).

In view of the numerical implementation, some remarks should be taken in consideration regarding the softwares and algorithm used:

- The error estimator used in every process is the SPR as proposed by Zienkiewicz and Zhu (1992b).
- The mesh generation is done via the Bidimensional Anisotropic Mesh Generator (BAMG) software (Hecht, 2006). This mesh generator is implemented to solely use nodal information related to the vertices of linear triangular elements. Thus, to generate quadratic triangular elements, two subfunctions were implemented in Matlab® by the author to add and remove the required edge nodes which characterize a quadratic triangular element, thus, making the use of this generator viable.
- The information regarding the element sizes are calculated with reference to the element barycenter location. Hence, an adjustment to this data had to be post-processed since the BAMG generator uses nodal parameters. FIGURE 9 illustrates the nodes in the barycenter of each element, where the nodal element size, h_{ie}, is calculated according to the element design strategies. For the vertex node as shown in the center of FIGURE 10, an inverse average of each element size in the patch of elements is used, $\overline{h}_{ie}$, given by

$$\overline{h}_{ie} = \frac{NP}{\sum_{ie=1}^{NP} \frac{1}{h_{ie}}} \tag{98}$$

FIGURE 10 – REPRESENTATION OF THE PATCH OF ELEMENTS ASSOCIATED TO THE CENTRAL NODES. BLACK DOTS REPRESENT ELEMENT SIZES SUPPLIED AS DATA.

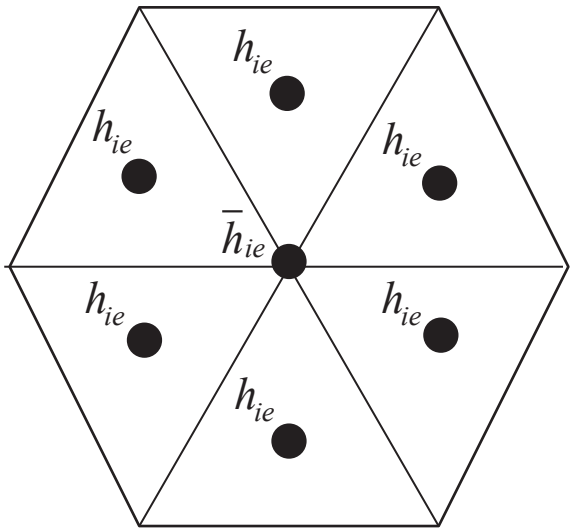

SOURCE: The author (2018).

where NP is the number of elements surrounding the vertex node.

- Also, the solution of each problem is validated using information given in the literature regarding each problem analyzed. It was ensured that each of the h-adaptive processes' solution converge to the analytical solution of the problem, the total strain energy meets the value presented in the literature and the sum of forces in the positive *x* and *y* directions were also validated.
- Limitations are imposed on the maximum element size and on the maximum refinement to guarantee the stability of the remeshing process and avoid distorted elements. The maximum size is defined as 20% of the characteristic domain size dimension and the maximum refinement is 10% of the original element size:

$$LC = 20\% \text{ and } ref_{max} = 10\% \tag{99}$$

- The numerical integration of the analytical loads is achieved using the Wandzurat quadrature with 25 points (WANDZURAT; XIAO, 2003).
- A constant value of $\overline{C} = 0,95$ is used to adjust the element size as described by Li and Bettess (1995).

5.2 PROBLEM 1 – ELLIPTIC TYPE THERMAL CONDUCTIVITY PROBLEM

A scalar bidimensional elliptic heat transfer problem (Poisson type problem) with homogeneous Dirichlet boundary conditions can be defined in a domain $\Omega = [0 \quad 1]^2 \subset R^2$, as

$$\begin{aligned} &Find\ T(x,y) \in H_0^1(\Omega) \\ &\int_\Omega (\nabla v)^T \boldsymbol{D}_g \nabla T \, d\Omega = \int_\Omega v f \, d\Omega, \quad \forall \quad v \in H_0^1(\Omega), \end{aligned} \tag{100}$$

where T is the analytical solution, $\boldsymbol{D}_g$ is a generic constutive tensor related to the problem, f is the scalar function of domain excitation, ∇ is the gradient differential operator, v is a function of a generic kinematically admissible variation and H_0^1 denotes first-order Hilbert space with compact support in Ω. The analytical solution of the problem is given by (modified from Mitchel, 2013)

$$T(x,y) = 2^{2(a+b)} x^a (1-x)^a y^b (1-y)^b, \tag{101}$$

where $a = 20$ and $b = 1$. FIGURE 11 shows graphical representations of the problem's analytical solution. The Ch^p, LB and IEDR based h-adaptive FEM methodologies are compared using LST elements.

FIGURE 11 – PROBLEM 1: ANALYTICAL SOLUTION.

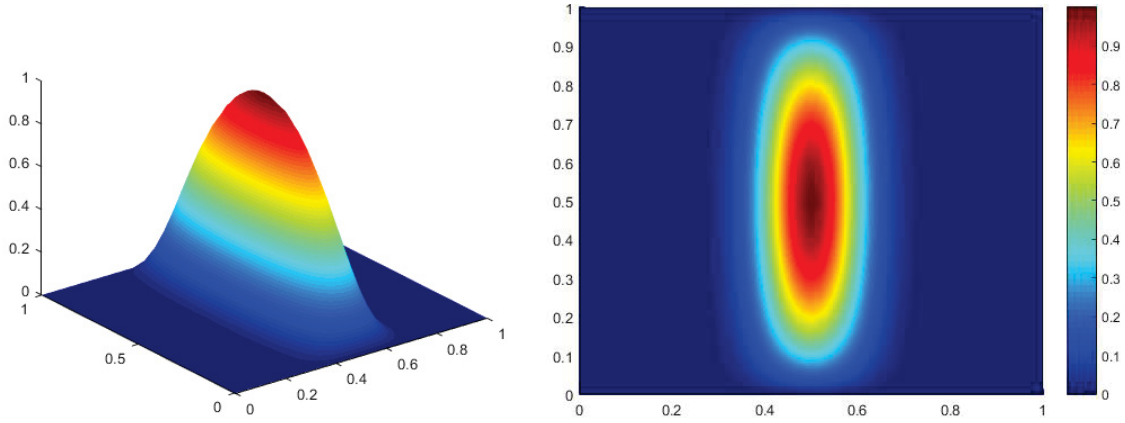

Isometric perspective. Top view (x-y).

SOURCE: The author (2018).

The initial mesh used by each of the methodologies is composed by 930 quasi-equilateral elements. FIGURE 12 illustrates the initial mesh and its energy error distribution. The stipulated global admissible error is $\bar{\eta} = 0.5\%$.

FIGURE 12 – PROBLEM 1: INITAL MESH AND ITS ERROR DISTRIBUTION, $\eta = 2.28\%$.

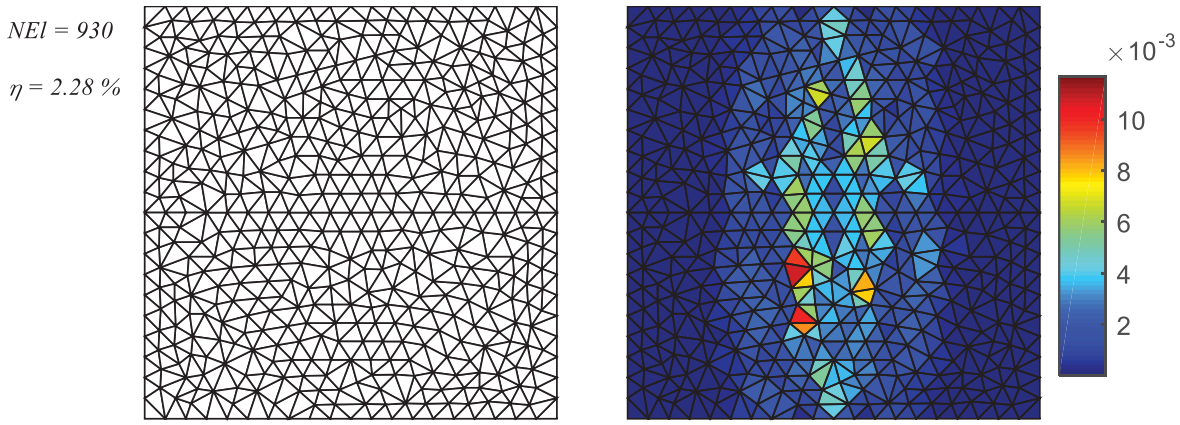

SOURCE: The author (2018).

In this problem, for each of the methodologies discussed, 3 adaptive iterations are completed such that the convergent mesh and stability of the techniques are analyzed. The resultant meshes are illustrated in FIGURE 13 to 15. FIGURE 13 shows that all 3 methodologies achieve the global admissible error, $\bar{\eta} = 0.5\%$, in the first iteration satisfying the convergence criterion. However, the meshes produced in the first iteration differ greatly between the Ch^p technique and LB and IEDR methodologies. The mesh produced by the Ch^p methodology presents a high number of elements and a global error percentage considerably lower than the admissible error indicating that the mesh is adapted with more elements than necessary. Furthermore, the error distribution in FIGURE 13 shows that the Ch^p technique produces high local errors in some regions while, in other regions, the error is much lower. On the other hand, the LB and IEDR techniques produced meshes, in the first iteration, with a lower number of elements, with 34.42% and 31.29% less degrees of freedom, respectively, when compared to the Ch^p technique. The subsequent meshes produced in iteration 2 and 3 also present better mesh parameters for the LB and IEDR techniques when compared to the renowned Ch^p technique, as shown in TABLE 2.

FIGURE 13 – PROBLEM 1: ITERATION 1, ADAPTED MESHES AND THEIR ERROR DISTRIBUTION FOR THE Ch^p, LB AND IEDR REMESHING STRATEGIES FOR LST ELEMENTS.

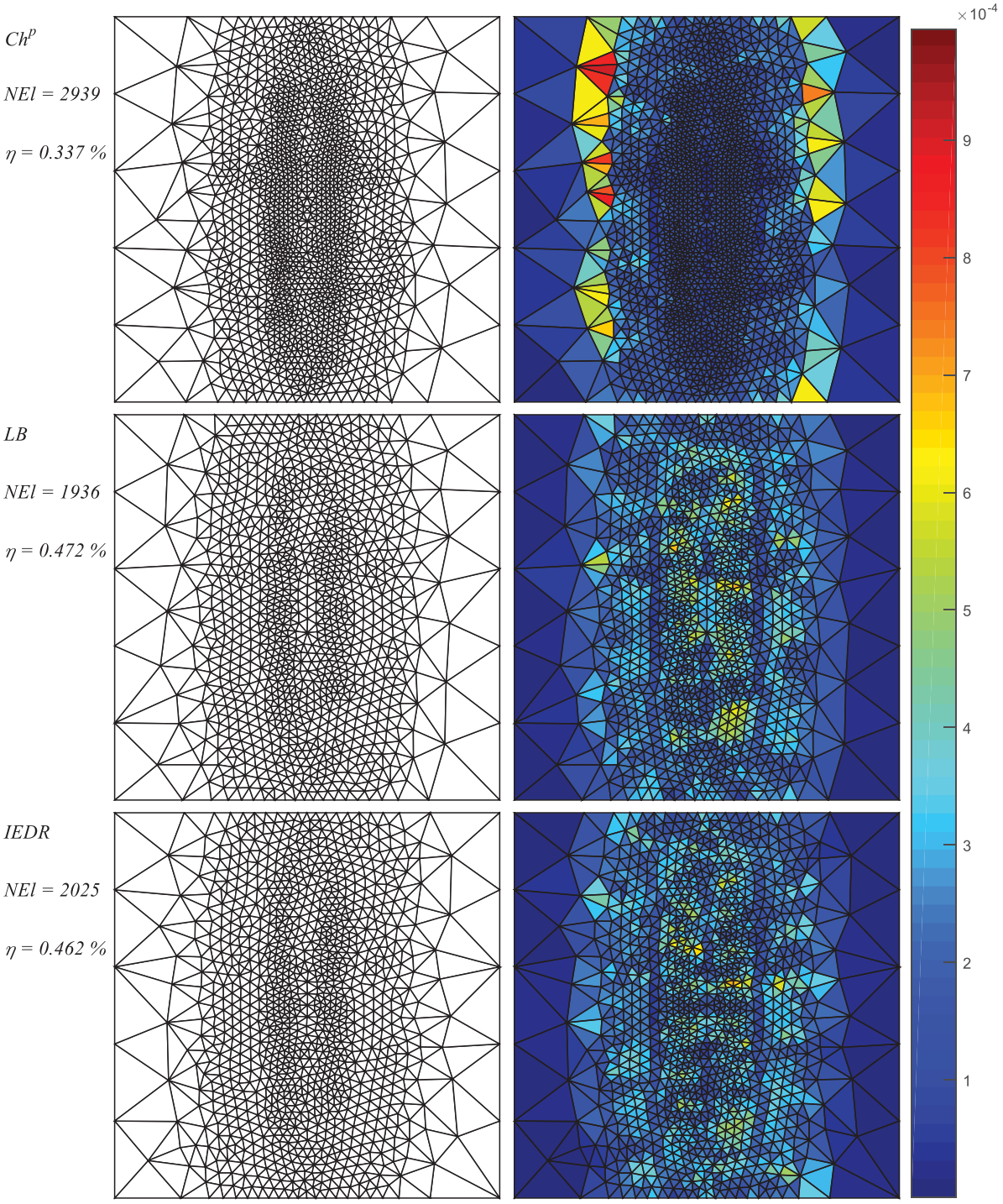

SOURCE: The author (2018).

TABLE 2 compares the characteristics of the adapted meshes for the first iteration of each process, *m=1*. This table shows a standard deviation of the error parameter, D_ζ, of 0.37 for the meshes produced by the IEDR and LB techniques whereas for the Ch^p technique the value of this parameter is 0.55. Thus, the first iteration of the adaptive process results in better

error equidistribution using the LB and IEDR element design methodologies when compared to the Ch^p technique.

TABLE 2 – PROBLEM 1: MESH PARAMETERS OF THE FIRST ITERATION.

h-adaptive Method	*Analytical error* (η)	*Effectivity index* (θ)	*Standard deviation of element error* (D_{ς})	*Number of degrees of freedom* (NDF)
Ch^p	0.34	1.11	0.55	5830
LB	0.47	1.10	0.37 (-32.7%)	3823 (-34.4%)
IEDR	0.46	1.10	0.37(-32.7%)	4000 (-31.3%)

SOURCE: The author (2018).

The meshes produced in the first iteration achieve inferior error in comparison to the stipulated admissible error, thus, these are said to be convergent meshes. Two subsequent iterations of the process are analyzed to further evaluate the behavior of each adaptive process. It is important to note that, even if the admissible error has been achieved, the h-adaptive process can continue producing divergent meshes. Here, the definition of the final mesh of the h-adaptive process is achieved for each methodology when no considerable changes in the mesh between iteration occurs. FIGURES 14 and 15 demonstrate the mesh produced in the second and third iteration, respectively. From these figures, little change it is noticeable between iterations in the number of elements and global error percentage for the meshes produced via the LB and IEDR – LB: 4.2% change in the number of elements between iterations 1 and 2, and 2.6% between iterations 2 and 3, IEDR: 7.1% change in the number of elements between iterations 1 and 2, and 5.3% between iterations 2 and 3– indicating that these processes have reached, approximately, their final mesh in only one iteration. Conversely, there is a substantial change in the number of elements for the meshes produced via the Ch^p technique – a 30,4% change in the number of elements between iteration 1 and 2, and a 8.5% change between iterations 2 and 3. Also, FIGURES 14 and 15 show that the meshes produced using this methodology have elements with higher local errors, indicated by the red elements in the error distribution figure, when compared to the IEDR and LB techniques.

FIGURE 14 – PROBLEM 1: ITERATION 2, ADAPTED MESHES AND THEIR ERROR DISTRIBUTION FOR THE Ch^P, LB AND IEDR REMESHING STRATEGIES FOR LST ELEMENTS.

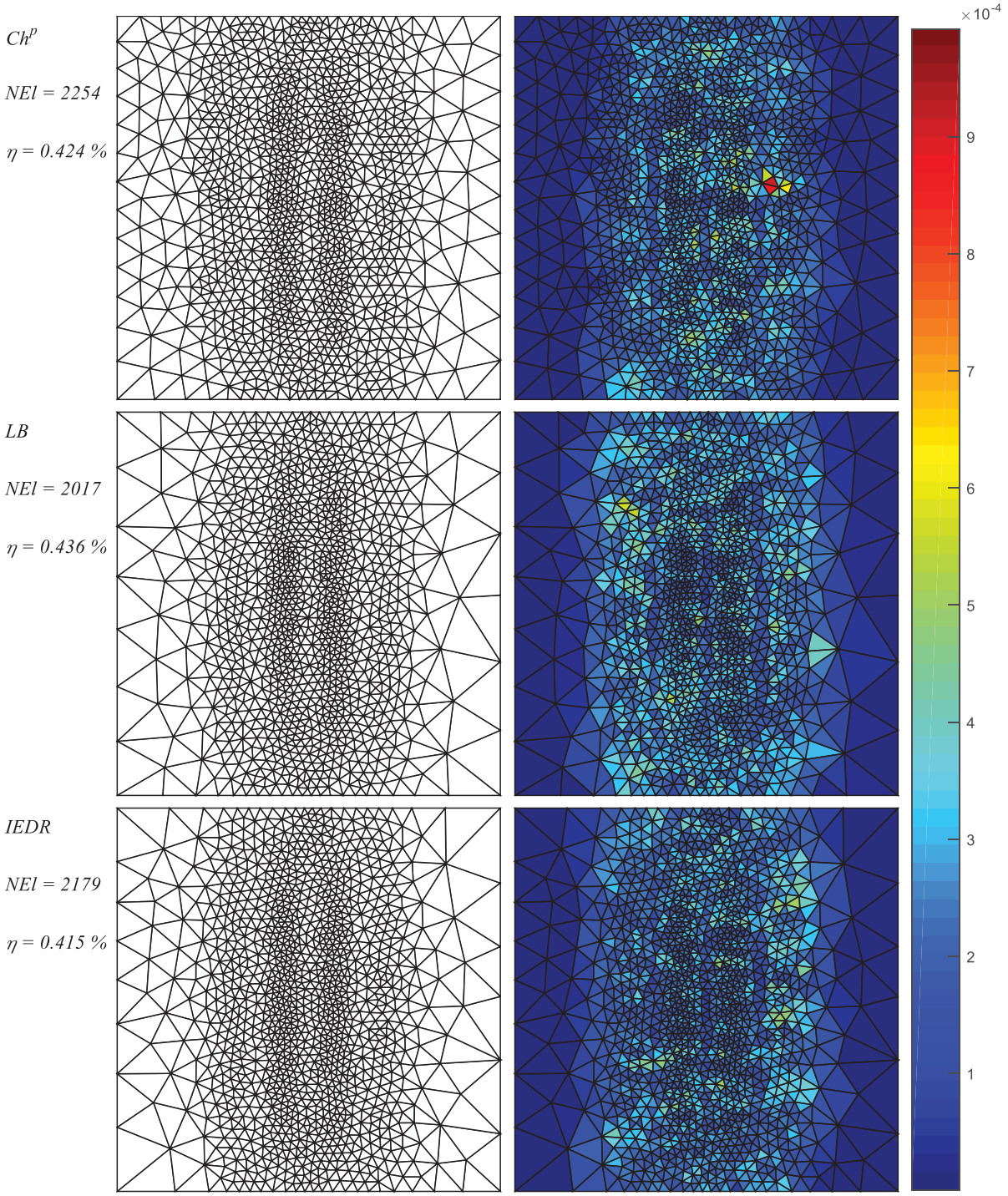

SOURCE: The author (2018).

FIGURE 15 – PROBLEM 1: ITERATION 3, ADAPTED MESHES AND THEIR ERROR DISTRIBUTION FOR THE Ch^p, LB AND IEDR REMESHING STRATEGIES FOR LST ELEMENTS.

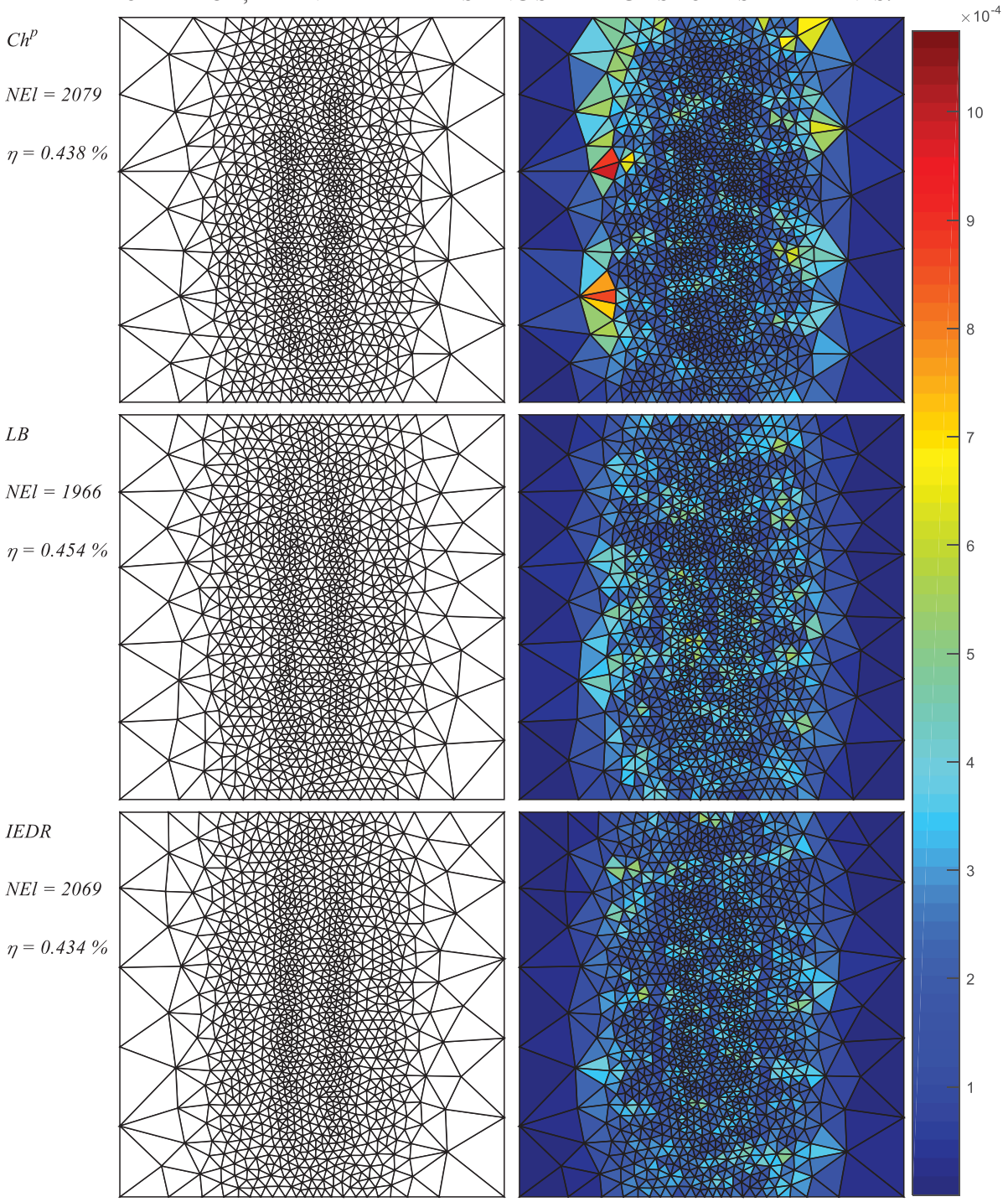

SOURCE: The author (2018).

TABLE 3 compares the characteristics of the initial and adapted meshes for the first, second and third iteration of each adaptive process for this problem. The meshes produced by the Ch^p methodology show poorer mesh quality parameters in relation to the meshes produced

by the LB and IEDR methodologies. As a reference, it is important to note that for an optimal mesh $\bar{\zeta}_{ave} = 1$, $\bar{\zeta}_{máx} = 1$ and $D_{\bar{\zeta}} = 0$.

TABLE 3 – PROBLEM 1: MESH PARAMETERS FOR THE h-ADAPTIVE PROCESSES BASED ON THE IEDR, LB AND Ch^p METHODOLOGIES.

h-adaptive Method		*Initial mesh*	*Mesh 1*	*Mesh 2*	*Mesh 3*
Ch^p	η	2.28	0.34	0.42	0.44
	NDF	1781	5830	4437	4110
	θ	1.11	1.31	1.09	1.19
	$\bar{\zeta}_{ave}$	2.64	0.58	0.76	0.81
	$\bar{\zeta}_{máx}$	24.66	3.73	3.26	3.39
	$D_{\bar{\zeta}}$	4.06	0.55	0.45	0.39
LB	η	2.28	0.47	0.44	0.45
	NDF	1781	3823	3980	3881
	θ	1.11	1.10	1.09	1.19
	$\bar{\zeta}_{ave}$	2.64	0.88	0.82	0.85
	$\bar{\zeta}_{máx}$	24.66	2.33	1.95	2.09
	$D_{\bar{\zeta}}$	4.06	0.37	0.34	0.34
IEDR	η	2.28	0.46	0.41	0.43
	NDF	1781	4000	4302	4086
	θ	1.11	1.10	1.09	1.10
	$\bar{\zeta}_{ave}$	2.64	0.86	0,78	0.82
	$\bar{\zeta}_{máx}$	24.66	2.35	1.82	1.90
	$D_{\bar{\zeta}}$	4.06	0.37	0.37	0.34

SOURCE: The author (2018).

FIGURE 16 shows the convergence curves of each h-adaptive process analyzed. In this graph, the logarithm of the number of degrees of freedom versus the logarithm of the error is plotted for each process. It is shown that all 3 methodologies achieve convergence related to the stipulated admissible global energy error in one iteration. Furthermore, the convergence curves for the processes based on the IEDR e LB methodologies show linearity, where the logarithm of the global energy error in the mesh decreases proportionally to the logarithm of the number of elements. On the contrary, the meshes obtained through the Ch^p

technique utilize a higher number of elements where the logarithm of the error does not change proportionally to the logarithm of the error, thus, a non-linear convergence curve is produced. In this technique, an overestimation of the required number of elements to achieve convergence is present. In the second and third iterations, this overestimation is adjusted incurring in additional computational costs in producing the final mesh for this formulation in comparison to the technique proposed in this dissertation, the IEDR technique. By comparing the IEDR and LB techniques, as shown in FIGURE 16, it is noticeable that both techniques show similar convergence curves. The LB methodology obtains meshes with a slightly lower number of elements, however no significant differences between the mesh parameters are present.

FIGURE 16 – PROBLEM 1: CONVERGENCE GRAPH FOR EACH ADAPTIVE PROCESS.

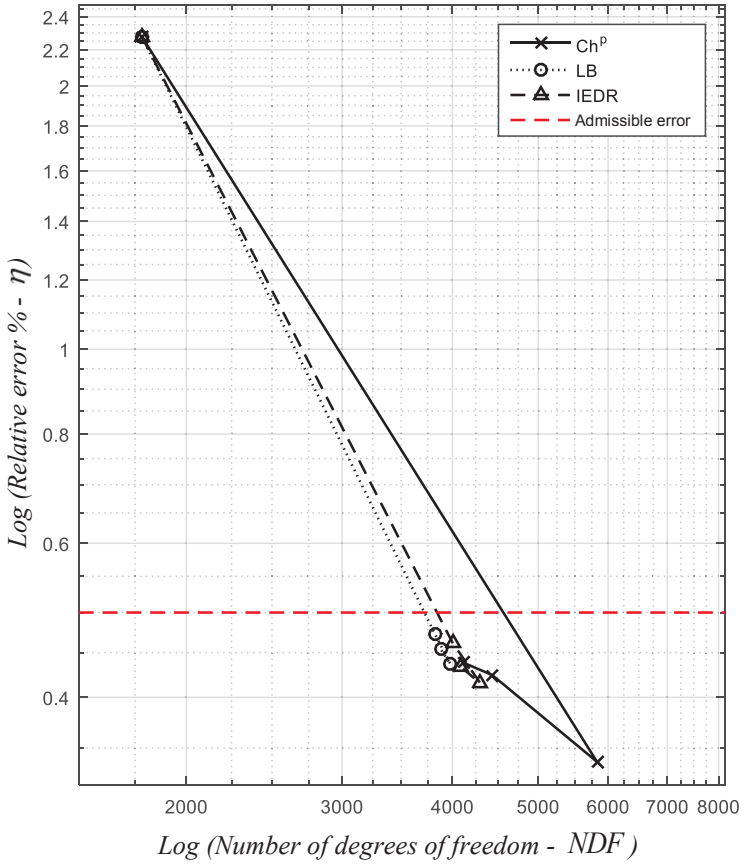

SOURCE: The author (2018).

5.3 PROBLEM 2 – ELLIPTIC TYPE THERMAL CONDUCTIVITY PROBLEM 2

In this elliptic problem (Poisson type) defined in a domain Ω and exclusively supported by a homogeneous Dirichlet boundary condition, the variational form of the problem for a given body load can be expressed as

$$\begin{aligned} &Find\ u(x,y) \in H_0^1(\Omega) \\ &\int_\Omega (\nabla v)^T \boldsymbol{D}_g \nabla u \, d\Omega = \int_\Omega vf \ d\Omega, \quad \forall \quad v \in H_0^1(\Omega), \end{aligned} \tag{102}$$

where u is the analytical solution of the problem. The domain load is applied such that the analitycal solution is given by (ZIENKIEWICZ; ZHU, 1992c)

$$u(x,y) = x(1-x)y(1-y)\arctan\left[\alpha'(\rho-\rho_0)\right], \tag{103}$$

where $\rho = (x+y)/\sqrt{2}$, $\rho_0 = 0.8$ and $\alpha' = 20$. FIGURE 17 illustrated the analytical solution of this problem.

FIGURE 17 – PROBLEM 2: ANALYTICAL SOLUTION.

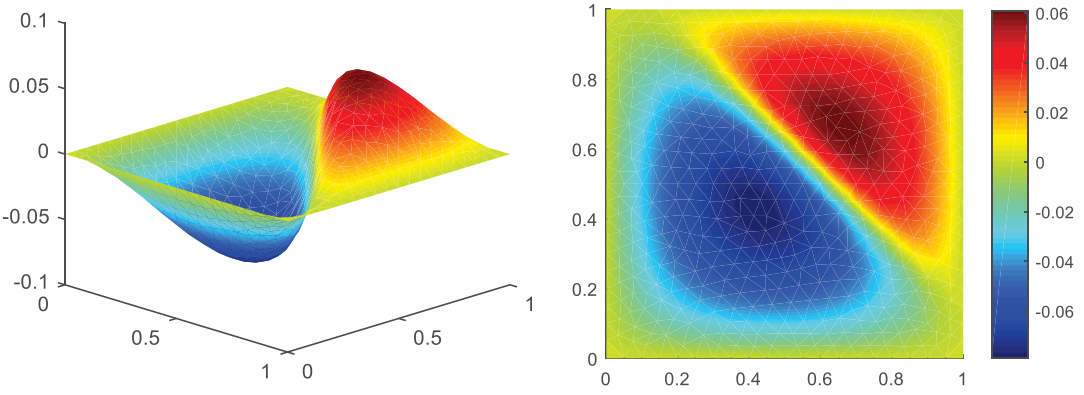

Isometric perspective. Top view (X-Y).

SOURCE: The author (2018).

The same admissible global error of the last problem is stipulated ($\bar{\eta} = 0.5\%$) and the initial mesh of 252 elements is shown in FIGURE 18. A coarser initial mesh is used in this problem to verify possible characteristics of the methodologies related to the low number of elements in the initial mesh. In such cases, the error estimation is poorer leading to difficulties

in accurate mesh design. The solution of this classic problem varies abruptly near the central diagonal region as shown by FIGURE 17.

FIGURE 18 – PROBLEM 2: INITIAL MESH.

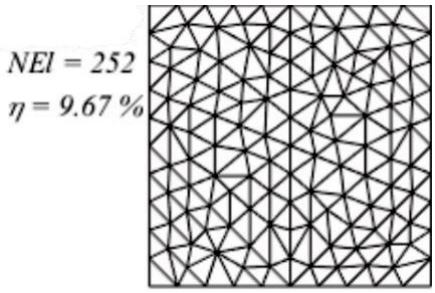

SOURCE: The author (2018).

The resultant adapted meshes and their error distribution for this problem using the Ch^p, LB and IEDR methodologies can be visualized in FIGURE 19. Again, it can be seen that the LB and IEDR h-adaptivity strategies applied to this problem produce meshes with uniformly distributed errors among the elements, whereas for the Ch^p technique, the error distribution show oscillatory behavior having regions where the error abruptly increases and decreases between iterations. This behavior of the Ch^p technique was indicated by Oñate and Bugeda (1993). In the first iteration, for example, the methodology produces small elements with low errors in the central diagonal region of the problem, however, in the second iteration, this same region of the mesh has bigger elements with higher errors. Consequentially, in the third iteration, the central diagonal region of the mesh contains smaller elements with low errors again. The same oscillatory behavior happens between the subsequent iterations. Conversely, the IEDR and LB methodologies, excluding the first iteration, present little changes in the mesh and error distribution between regions of the mesh. This indicates a more robust behavior for these two techniques. Also, the IEDR and LB methodologies are able to successfully adjust the element sizes in the presence of the abrupt change in the solution located at the central diagonal region of this problem.

FIGURE 19 – PROBLEM 2: ERROR DISTRIBUTION FOR 4 ITERATIONS OF THE IEDR, LB AND Ch^P ADAPTIVE PROCESSES.

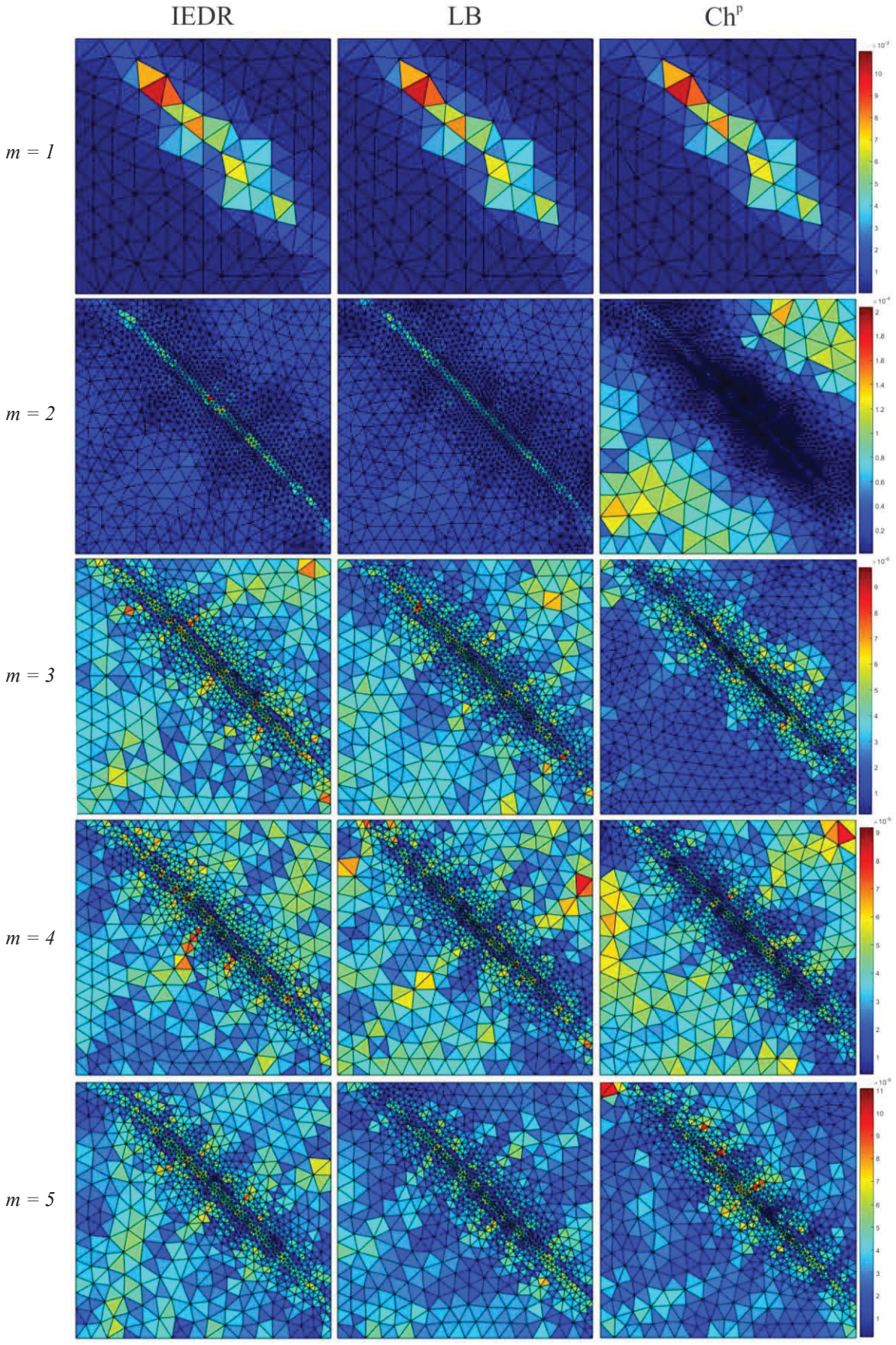

SOURCE: The author (2018).

In FIGURE 20, the convergence graphs of the h-adaptive processes are shown. It can be seen that the LB and IEDR techniques produce a final mesh in the second iteration, where no significant change is present between iterations. These meshes present a lower number of degrees of freedom when compared to the Ch^p technique. This phenomenon also occurred in the first problem.

FIGURE 20 – PROBLEM 2: CONVERGENCE GRAPH FOR EACH ADAPTIVE PROCESS.

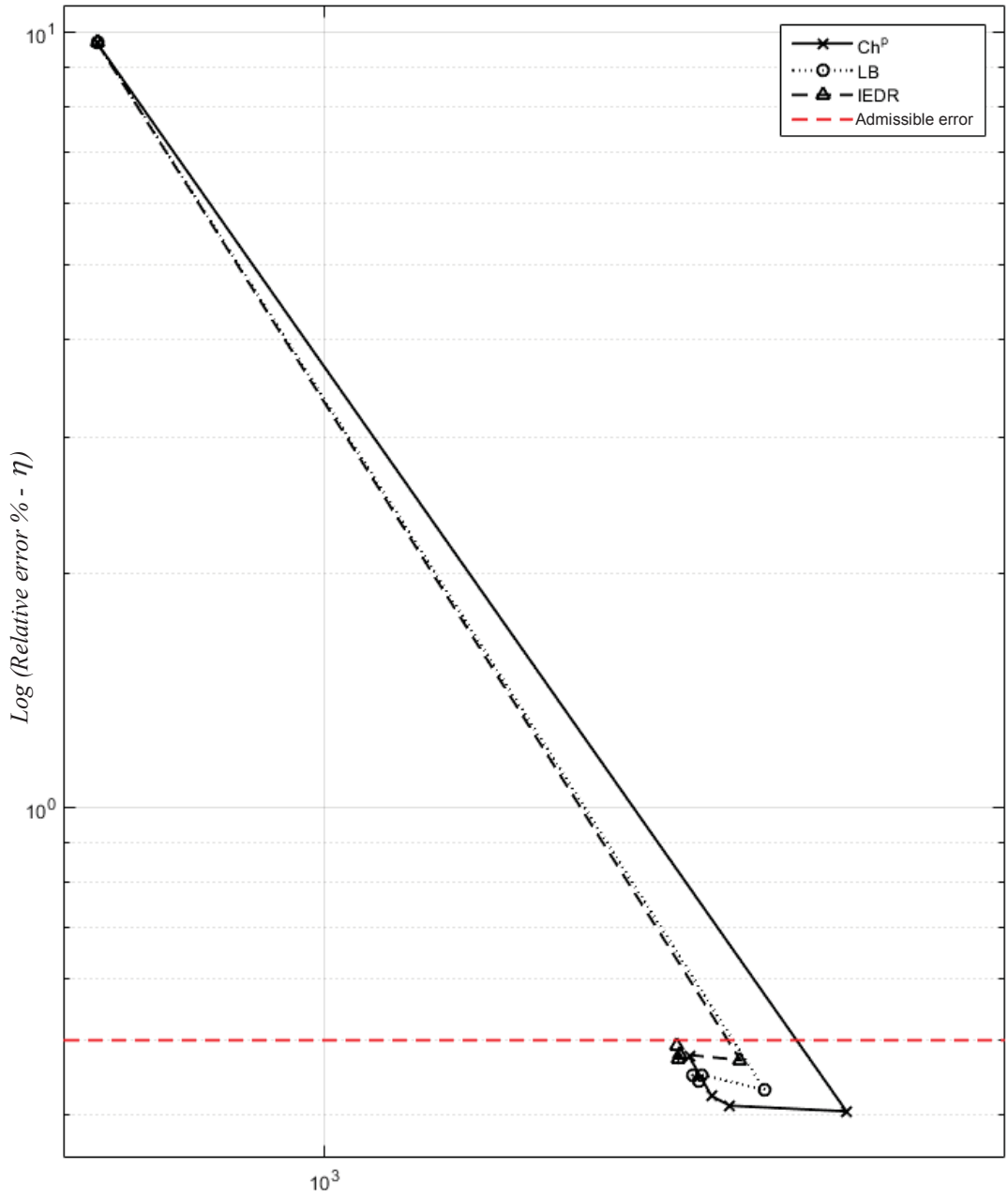

SOURCE: The author (2018).

Additionally, FIGURE 20 indicates that every h-adaptive process reaches the admissible global error value in a single iteration, even for a problem with higher gradient variation of the solution and a considerably coarser initial mesh. In this problem, it is shown that the meshes produced by the first iteration are not “final meshes”, where considerable change in the meshes are present between the first and second iterations for each process. The poor error estimation due to the coarse initial mesh causes difficulties for the h-adaptive processes to properly design the optimal element sizes. In this case, the IEDR technique presents better mesh parameters regarding the number of elements, closeness to the stipulated admissible error and standard deviation error parameter as shown in TABLE 4. This indicates that, even with poor error estimation, the methodology is still able to successfully predict with accuracy the required element sizes. The use of an error density function instead of pointwise element errors better describes the behavior of error for each element as it increases and decreases in size, in conjunction with the iterative adjustment process. Thus, the results show advantages in the use of the IEDR technique. Furthermore, as shown in FIGURE 20 and TABLE 4, the LB technique also produced similar meshes with mesh quality parameter superior to the Ch^p technique.

The standard deviation parameter, D_ζ, curve of each h-adaptive process is shown in FIGURE 21. The IEDR technique obtained meshes with a lower standard deviation of element errors than the Ch^p and similar to the LB based methodology, while using a lower number of elements. This indicates an effective error equidistribution in the mesh. Also, this parameter varies less between iterations indicating stability of the formulation.

FIGURE 21 – PROBLEM 2: STANDARD DEVIATION OF THE REFINEMENT PARAMETER FOR EACH h-ADAPTIVE PROCESS ITERATIONS.

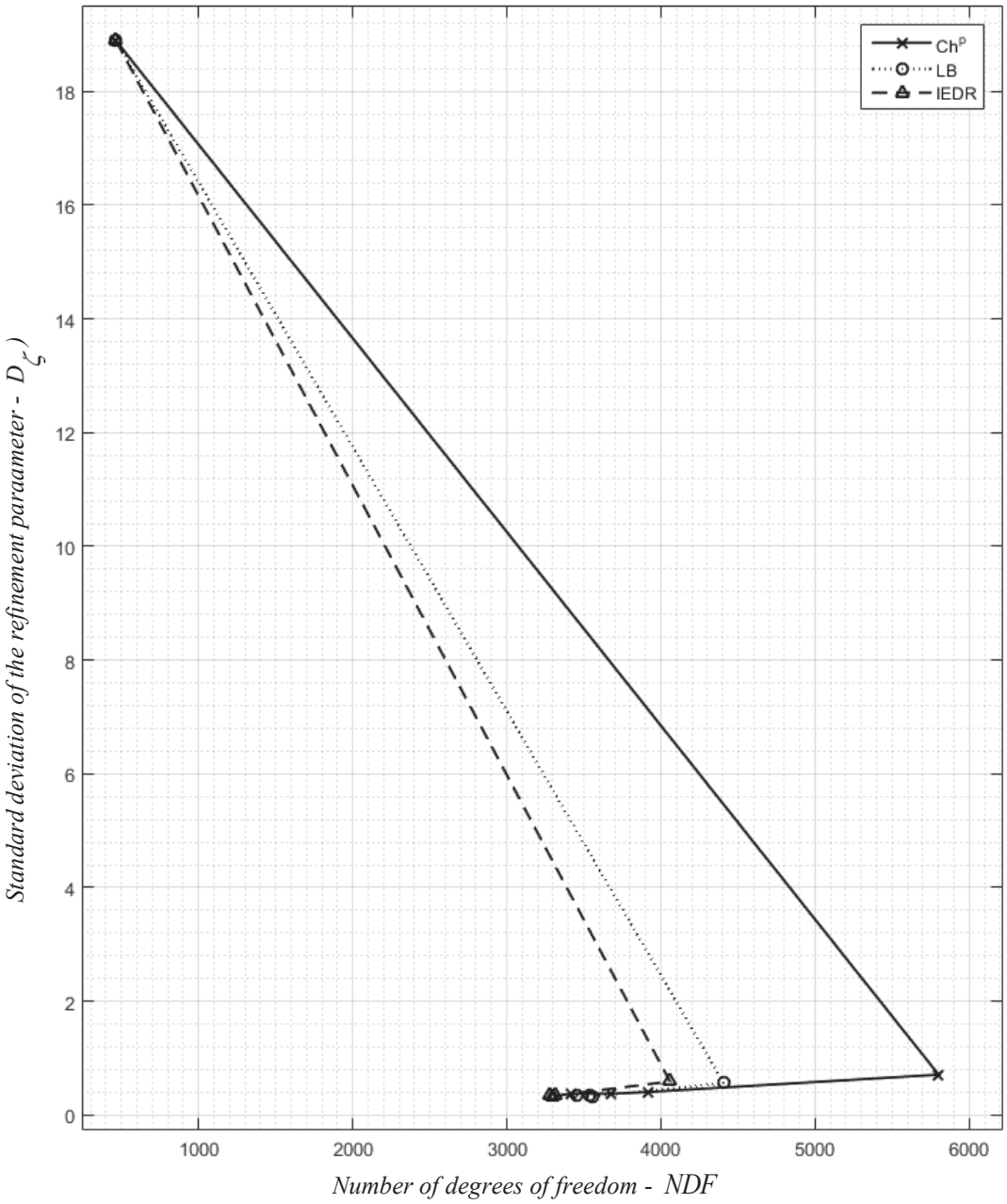

SOURCE: The author (2018).

TABLE 4 compares the characteristics of the initial and adapted meshes for the 4 iterations of each h-adaptive process based on the IEDR, LB and Ch^p methodologies for Problem 2. It is shown that the mesh quality parameters of the h-adaptive process based on the IEDR and LB methodologies are superior when compared to the classic Ch^p remeshing strategy for this problem, similarly to the characteristics discussed in Problem 1.

TABLE 4 – PROBLEM 2: MESH PARAMETERS FOR THE h-ADAPTIVE PROCESSES BASED ON THE IEDR, LB AND Ch^p METHODOLOGIES. IN RED, RELEVANT PARAMETERS OF COMPARISON ARE HIGHLIGHTED.

Method		*Initial mesh*	*Mesh 1*	*Mesh 2*	*Mesh 3*	*Mesh 4*
Ch^p	η	9.67	0.50	0.41	0.42	0.48
	NDF	465	5801	3916	3680	3417
	θ	1.28	1.05	1.11	1.09	1.11
	$\bar{\xi}_{ave}$	9.28	0.58	0.76	0.79	0.88
	$\bar{\xi}_{máx}$	103.8	5.00	2.06	2.25	2.75
	$D_{\bar{\xi}}$	18.89	0.71	0.40	0.37	0.38
LB	η	9.67	0.43	0.45	0.44	0.45
	NDF	465	4407	3557	3536	3454
	θ	1.28	1.09	1.09	1.09	1.10
	$\bar{\xi}_{ave}$	9.28	0.71	0.85	0.84	0.85
	$\bar{\xi}_{máx}$	103.8	3.30	2.30	2.29	2.09
	$D_{\bar{\xi}}$	18.89	0.56	0.33	0.34	0.34
IEDR	η	9.67	0.47	0.48	0.47	0.49
	NDF	465	4058	3311	3294	3273
	θ	1.28	1.09	1.09	1.10	1.09
	$\bar{\xi}_{ave}$	9.28	0.77	0.90	0.90	0.93
	$\bar{\xi}_{máx}$	103.8	5.51	2.38	2.24	2.20
	$D_{\bar{\xi}}$	18.89	0.59	0.34	0.32	0.34

SOURCE: The author (2018).

In this problem, the last mesh produced in the fourth iteration of the process is analyzed to evaluate the formulation of each methodology. The IEDR technique shows a convergent mesh with 5.53% less elements when compared to the LB technique and 4.40% less elements when compared to the mesh produced via the Ch^p methodology, while achieving a global analytical error percentage lower than the stipulated admissible global error. Further, the average value of the element error parameter is closer to 1 for the meshes produced through the IEDR technique when compared to the LB and Ch^p techniques and the standard deviation of the element error parameter is the same between the IEDR and LB techniques, and closer to 0 than the Ch^p technique.

5.4 PROBLEM 3 – PLANE ELASTICITY PROBLEM WITH SQUARED DOMAIN

An elliptical vectorial plane elasticity problem with homogeneous Dirichlet boundary conditions is defined in the variational form as

$$\begin{aligned} &Find\ \boldsymbol{u}(x,y) \in H_0^1(\Omega) \\ &\int_{\Omega} (\nabla \boldsymbol{v})^T\, \boldsymbol{D} \nabla \boldsymbol{u}\, d\Omega = \int_{\Omega} \boldsymbol{v}\boldsymbol{f}\ d\Omega, \quad \forall \quad \boldsymbol{v} \in H_0^1(\Omega), \end{aligned} \tag{104}$$

where a domain excitation is applied such that the solution is given by (ZIENKIEWICZ; TAYLOR, 2000)

$$\boldsymbol{u}(x,y) = \begin{Bmatrix} u_x \\ u_y \end{Bmatrix} = x(1-x)y(1-y)\arctan\left[\alpha(\rho-\rho_0)\right]\begin{Bmatrix} 1 \\ 1 \end{Bmatrix}, \tag{105}$$

where $\rho = (x+y)/\sqrt{2}$, $\rho_0 = 0.8$ and $\alpha = 20$. The same domain is used as the last problem, described by $\Omega = \left[0 \quad 1\right]^2 \subset R^2$. Plane stress state is assumed. TABLE 5 lists the properties of the plane stress state problem.

TABLE 5 – PROBLEM 3: PROBLEM PROPERTIES.

Modulus of Elasticity	Thickness	Poisson's ratio
$E = 1000$	$t = 1$	$\upsilon = 0,3$

SOURCE: The author (2018).

A lower admissible error is used in this problem ($\overline{\eta} = 0.2\%$) and the initial mesh is composed by 942 elements. FIGURE 17 shows the analytical solution of this problem given in each principal direction. It can be seen that the solution of this problem is a modification of Problem 2. FIGURE 22 illustrates the initial mesh used in the h-adaptive processes. This problem is used to analyze the techniques for plane elasticity problems, where every node has two degrees of freedom, and draw comparisons between the results found in Problem 2.

FIGURE 22 – PROBLEM 3: INITIAL MESH.

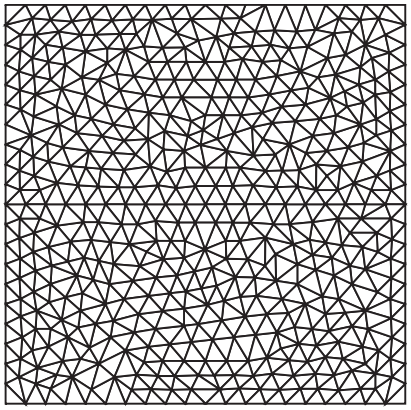

SOURCE: The author (2018).

FIGURE 23 shows the adapted meshes using each of analyzed adaptive methodologies based on the LB, IEDR and Ch^p element designs for 5 iterations of the process. The figure shows that the IEDR technique produce meshes with a lower number of elements for every adapted mesh in comparison with the LB and Ch^p techniques. Specifically, in the convergent mesh, given by the first iteration, the technique uses approximately 44% less elements than the Ch^p technique for that iteration and 2.3% less elements when compared to the LB technique. Also, after the first iteration, there is little change in the subsequent meshes design through the IEDR technique, varying between 3988 and 4052 elements, indicating that a final mesh based on the technique's formulation is achieved in the second iteration. The h-adaptive process based on the LB technique produce meshes similar to those based on the IEDR methodology, where small differences in the number of elements and analytical global errors are present.

Both, IEDR and LB techniques reach convergence by accurately defining suitable element sizes in the region of high variation in the solution located in the central diagonal part of the domain, whereas the Ch^p technique designs an unnecessary high number of elements in that critical region. Furthermore, by comparing iterations 2 and 3 of the adaptive process based on the Ch^p methodology, an oscillation of the element size definition is present in the critical region of high variation in the solution. This behavior is also present in Problem 1 and 2. Also, FIGURE 23 and TABLE 6 show similar results and behavior of each adaptive process as the problems discussed previously, even though a different problem is considered with a lower stipulated admissible error.

FIGURE 23 – PROBLEM 3: ADPTED MESHES PRODUCE FOR 5 ITERATIONS OF THE IEDR, LB E Ch^P ADAPTIVE PROCESSES.

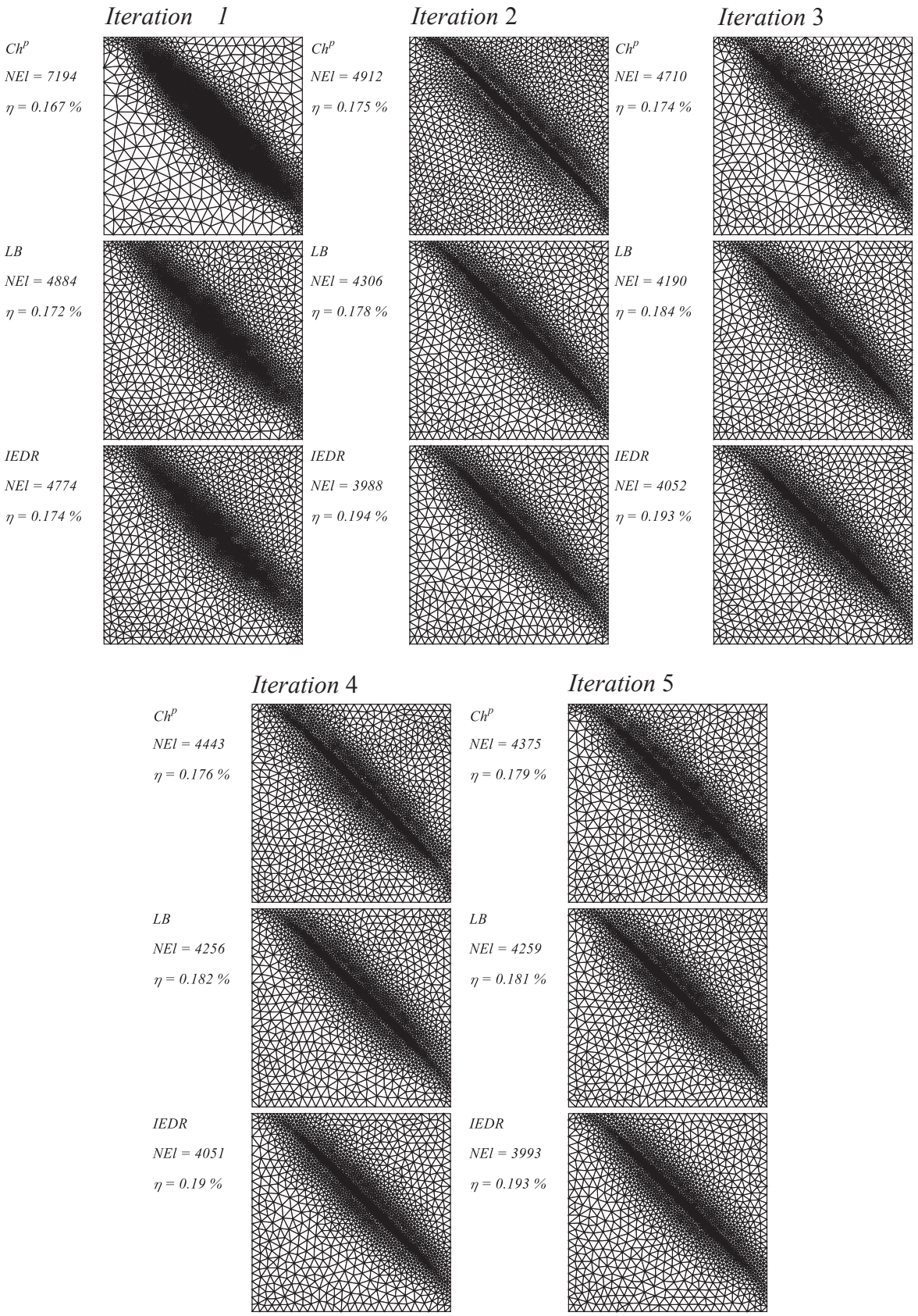

SOURCE: The author (2018).

TABLE 6 – PROBLEM 3: MESH PARAMETERS FOR THE h-ADAPTIVE PROCESSES BASED ON THE IEDR, LB AND Ch^p METHODOLOGIES. IN RED, RELEVANT PARAMETERS OF COMPARISON ARE HIGHLIGHTED.

Method		*Initial mesh*	*Mesh 1*	*Mesh 2*	*Mesh 3*	*Mesh 4*	*Mesh 5*
Ch^p	η	2.91	0.17	0.17	0.17	0.18	0.18
	NDF	3610	28570	19370	18630	17528	17280
	θ	1.23	1.04	1.10	1.07	1.09	1.07
	$\bar{\zeta}_{ave}$	5.92	0.59	0.78	0.81	0.83	0.85
	$\bar{\zeta}_{máx}$	168.49	6.37	3.24	2.48	2.26	2.33
	$D_{\bar{\zeta}}$	14.19	0.71	0.45	0.39	0.34	0.32
LB	η	2.91	0.17	0.18	0.18	0.18	0.18
	NDF	3610	19290	16998	16534	16798	16812
	θ	1.23	1.07	1.08	1.08	1.08	1.08
	$\bar{\zeta}_{ave}$	5.92	0.78	0.85	0.88	0.87	0.86
	$\bar{\zeta}_{máx}$	168.49	3.10	2.25	2.16	2.13	2.19
	$D_{\bar{\zeta}}$	14.19	0.41	0.30	0.30	0.30	0.30
IEDR	η	2.91	0.17	0.19	0.19	0.19	0.19
	NDF	3610	18846	15726	15982	15980	15748
	θ	1.23	1.07	1.08	1.08	1.08	1.08
	$\bar{\zeta}_{ave}$	5.92	0.80	0.93	0.92	0.91	0.92
	$\bar{\zeta}_{máx}$	168.49	3.34	2.49	2.51	2.51	2.58
	$D_{\bar{\zeta}}$	14.19	0.40	0.29	0.30	0.29	0.31

SOURCE: The author (2018).

TABLE 6 lists the mesh parameters of each of the 5 adaptive iterations of the IEDR, LB and Ch^p based h-adaptive processes for Problem 3. It is shown that the number of degrees of freedom required for this problem is considerably higher than the previous ones due to the low admissible error stipulated and the vectorial problem. Also, the table shows that the meshes produced by the IEDR and LB techniques present a lower number of elements, lower standard deviation of the error parameter, lower maximum refinement parameter and an avarage of the refinement parameter closer to 1 when compared to the h-adaptive process based on the Ch^p technique. This behavior follows the results shown previously in Problem 1 and 2 indicating that the Ch^p technique is not as effective in equidistibuting the element

errors. As emphasized in red in this table, the refinement parameter average, $\bar{\zeta}_{ave}$, is closer to the optimal value of 1 for the meshes produced by the IEDR methodology when compared to the LB e Ch^p element design techniques.

FIGURE 24 – PROBLEM 3: CONVERGENCE CURVES OF EACH ADAPTIVE PROCESS IEDR, LB AND Ch^p.

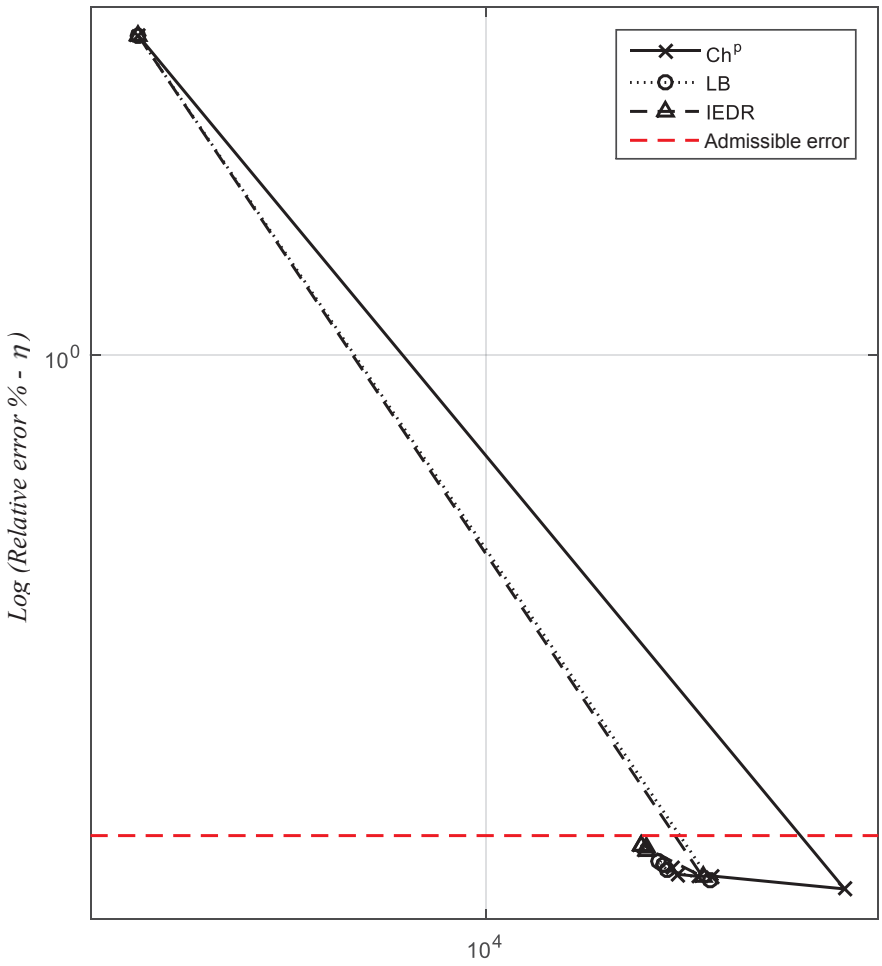

SOURCE: The author (2018).

The convergence graph of each process is shown in FIGURE 24 and 25. FIGURE 25 shows an enlarged view of the convergence graph in FIGURE 24 for iterations 1-5. The convergence curves for the IEDR and LB methodologies show that these adaptive processes reach convergence in the first iteration, where the global analytical error reaches the stipulated error, with a considerably lower number of degrees of freedom when compared to the Ch^p technique as visible in FIGURE 24. Also, the Ch^p technique overshoots the admissible error, producing a mesh with analytical error distant to that value. In an optimal mesh, the analytical error and admissible error should be equal. In terms of the behavior of the methodologies,

little differences in the meshes produced in iteration 2 to 5 are observed for the IEDR technique, whereas for the other techniques higher changes in the number of elements analytical error is present. All 3 methodologies analyzed show substantial mesh adjustments between the first and second iterations. This occurs due to the low admissible error of 0.2% which requires a significant increase in the number of elements in the first iteration when compared to the initial mesh, and, consequentially, loss of accuracy in the element design techniques is present. In the subsequent iterations, better error estimation is present due to the higher number of elements in the mesh.

FIGURE 25 – PROBLEM 3: ENLARGED VIEW OF THE CONVERGENCE CURVES OF EACH ADAPTIVE PROCESS IEDR, LB AND Ch^p.

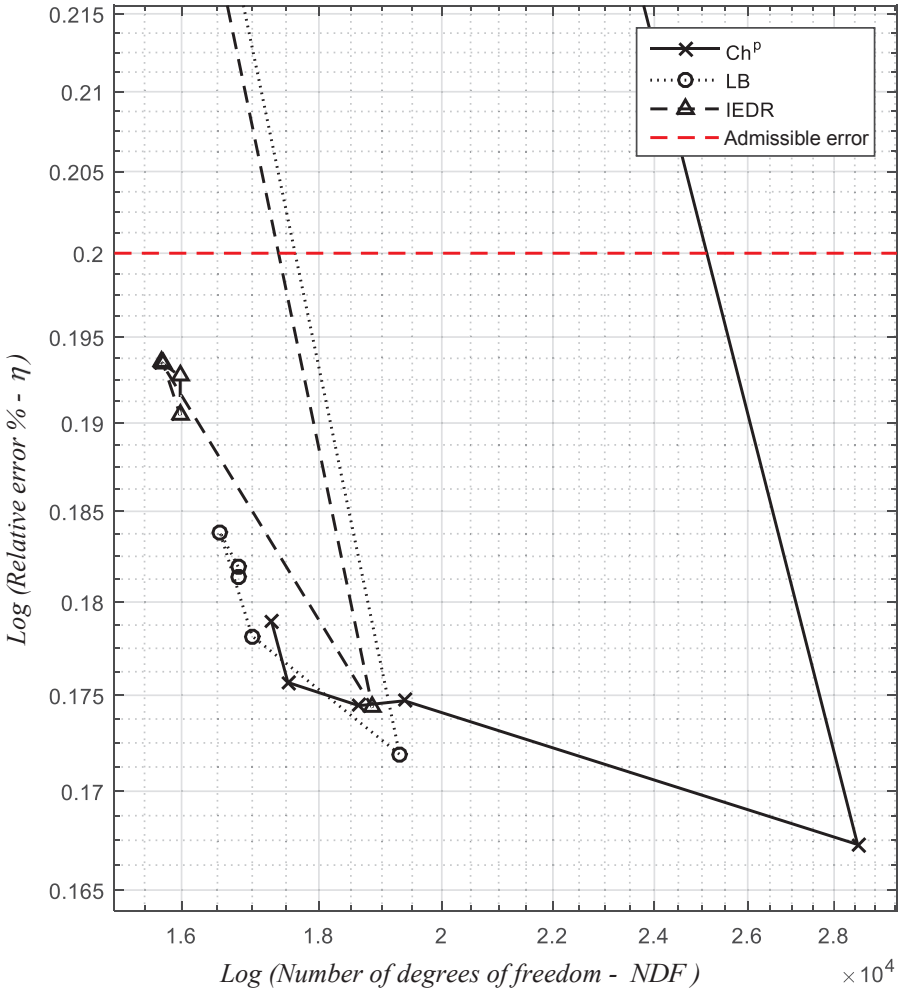

SOURCE: The author (2018).

5.5 PROBLEM 4 – PLANE ELASTICITY PROBLEM WITH SINGULARITY AND L SHAPED DOMAIN

The plane elasticity problem with an L domain is a classic problem of the Theory of Elasticity (SZABO; BABUSKA, 2011). The presence of a singularity in this problem provides difficulties in the design of suitable element sizes, making this problem important in the analysis of h-adaptivity strategies. Furthermore, this is a vector problem, which, differently from Problems 1 and 2, the solution has two dependent variables. The material properties and geometrical data are given in TABLE 7 for this plane strain problem:

FIGURE 26 – PROBLEM 4: MECHANICAL MODEL OF PROBLEM WITH L SHAPED DOMAIN.

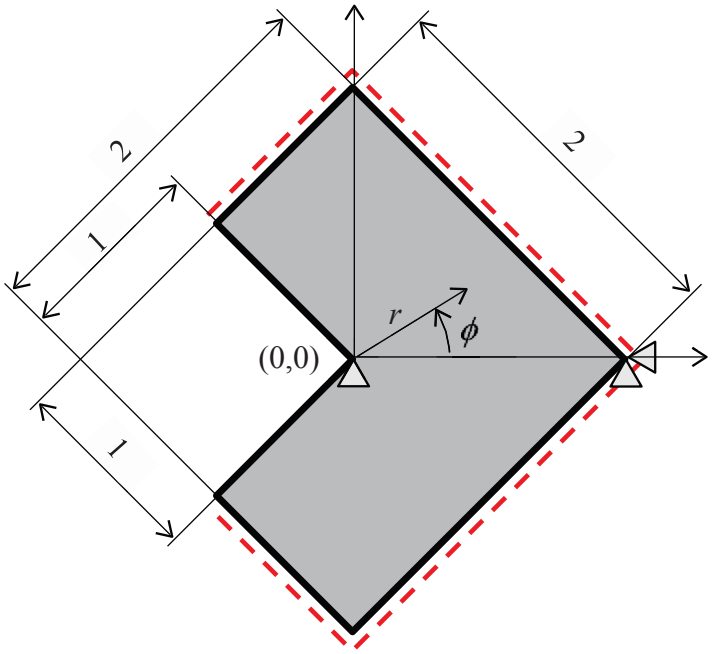

SOURCE: Modified from Díez; Ródenas and Zienkiewicz (2007).

TABLE 7 – PROBLEM 4: PROBLEM AND MATERIAL PROPERTIES.

Modulus of Elasticity	Thickness	Region of Singularity	Poisson's ratio
$E = 1000$	$t = 1$	$r = 0.005$	$\upsilon = 0,3$

SOURCE: The author (2018).

FIGURE 26 illustrates a mechanical model of the problem in analysis. Neumann boundary conditions are present on the outer edges of the domain. The stress components that describe the Neumann boundary condition are based on the first symmetric term (Mode I) of

the asymptotic expansion of the analytical solution around the central vertex (0,0) (SZABO; BABUSKA, 2011). Thus, the loads applied to the boundary of the domain (shown in red in FIGURE 26) are obtained through the solution of the stress fields given by (SZABO; BABUSKA, 2011)

$$\begin{aligned}
\sigma_{xx} &= \lambda r^{\lambda-1}\left[\left(2-Q_s\left(\lambda+1\right)\right)\cos\left(\left(\lambda-1\right)\phi\right)-\left(\lambda-1\right)\cos\left(\left(\lambda-3\right)\phi\right)\right] \\
\sigma_{yy} &= \lambda r^{\lambda-1}\left[\left(2-Q_s\left(\lambda+1\right)\right)\cos\left(\left(\lambda-1\right)\phi\right)+\left(\lambda-1\right)\cos\left(\left(\lambda-3\right)\phi\right)\right] \\
\sigma_{xy} &= \lambda r^{\lambda-1}\left[\left(Q_s\left(\lambda+1\right)\right)\text{sen}\left(\left(\lambda-1\right)\phi\right)+\left(\lambda-1\right)\text{sen}\left(\left(\lambda-3\right)\phi\right)\right]
\end{aligned} \tag{106}$$

where $Q_s = 0.543075579$, $\lambda = 0.544483737$, ϕ is the angle and *r* denotes de radius as shown in FIGURE 26. In this problem, the stress field is singular in the central vertex, at point (0,0) of FIGURE 26. The order of the singularity is given by λ. Rigid body movement is restricted, such that no body reactive forces are created as shown in FIGURE 26

Each element design methodology is based on the asymptotic convergence rate of the error as shown in Chapters 3 and 4. However, the presence of a singularity creates a critical region, as present in this problem near the re-entrant corner (0,0). The elements that share this region have a lower convergence rate as shown in Eq. (26) and Eq. (31) by the term $min\left(\lambda, p\right)$, i.e. the convergence rate is proportional to the minimum between the order of approximation or the regularity of the solution defined by the singularity. Hence, based on the formulation of each technique, the element design methodology, for these elements, is modified to account for the lower convergence rate of the singularity. TABLE 7 defines an arbritary radius of the singularity region as $r = 0.005$, where elements inside this radius (with origin at 0,0) are assumed to be affected by the singularity. Eq. (26), Eq. (31) and Eq. (97) are modified for elements in the singularity region.

For the Ch^p element design formulation, the order of singularity replaces the variable *p* in the element size formulation such that

$$\|\boldsymbol{e}\| \leq Ch^{min(\lambda,p)} \rightarrow \|\boldsymbol{e}\| \leq Ch^{0.544483737}, \tag{107}$$

The IEDR methodology, on the other hand, is only required to modify the convergence rate of its iterative process, given by α in Eq. (97). The resulting manipulation can be expressed as

$$C_i = D_i\left(\frac{h_{new}}{h_{old}}\right)^{2\alpha-i} \rightarrow C_i = D_i\left(\frac{h_{new}}{h_{old}}\right)^{2(1.544483737)-i}, \tag{108}$$

Similarly to the Ch^p element design formulation, the LB methodology is modified by replacing the value of the order of approximation, p, by the order of regularity of the solution. The convergence rate for the elements influenced by the singularity, for this methodology, can be expressed as

$$\|\boldsymbol{e}\|_{ie} \leq Ch^{min(\lambda,p)-n+2} \rightarrow \|\boldsymbol{e}\|_{ie} \leq Ch^{1.544483737}, \tag{109}$$

Eqs. (107) – (109) are valid exclusively in the region near the re-entrant corner. Therefore, a region composed by the elements between the radius r and point (0,0) was used as region of singularity, due to direct influence of the singularity into these elements. Further, the elements that are not located inside this radius maintain the original convergence rate, defined by the order of the element approximation, as indicated in Chapters 3 and 4.

The analytical solution of this problem is illustrated in FIGURE 27 for the displacement in the x and y directions. The initial mesh used for the h-FEM process has 166 triangular quadratic elements as shown in FIGURE 28. The admissible global error is set to 1% ($\bar{\eta} = 1\%$). Also, the solution of this problem shows abrupt changes in the gradient due to the presence of the singularity.

FIGURE 27 – PROBLEM 4: ANALYTICAL SOLUTION.

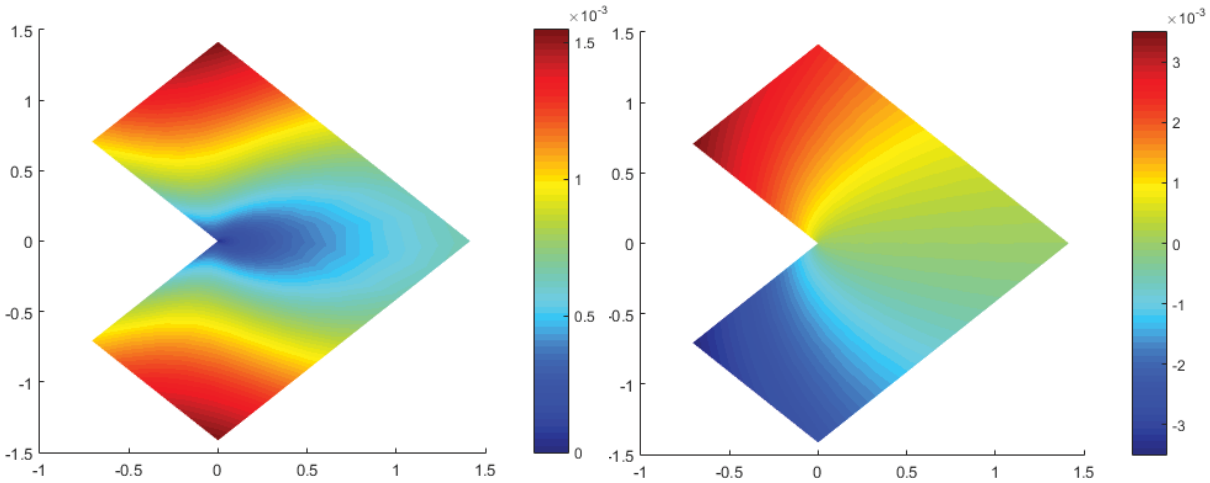

Top view (solution in the x direction) Top view (solution in the y direction)

SOURCE: The author (2018).

FIGURE 29 shows the convergence curves obtained through each of the h-adaptive finite element procedures based on the IEDR, LB and Ch^p element design methodologies. In this graph, the curves show that the IEDR and Ch^p methodologies reach convergence in 3 iterations while the LB technique requires 4 iterations.

FIGURE 28 – PROBLEM 4: INITIAL MESH AND ITS ERROR DISTRIBUTION.

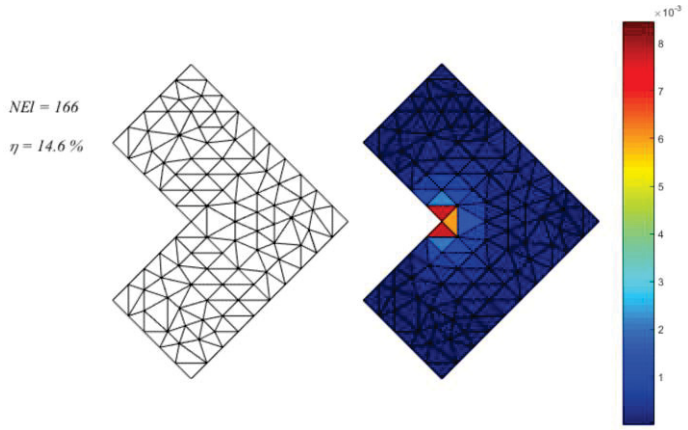

SOURCE: The author (2018).

FIGURE 29 – PROBLEM 4: CONVERGENCE CURVES OF EACH ADAPTIVE PROCESS IEDR, LB AND Ch^P.

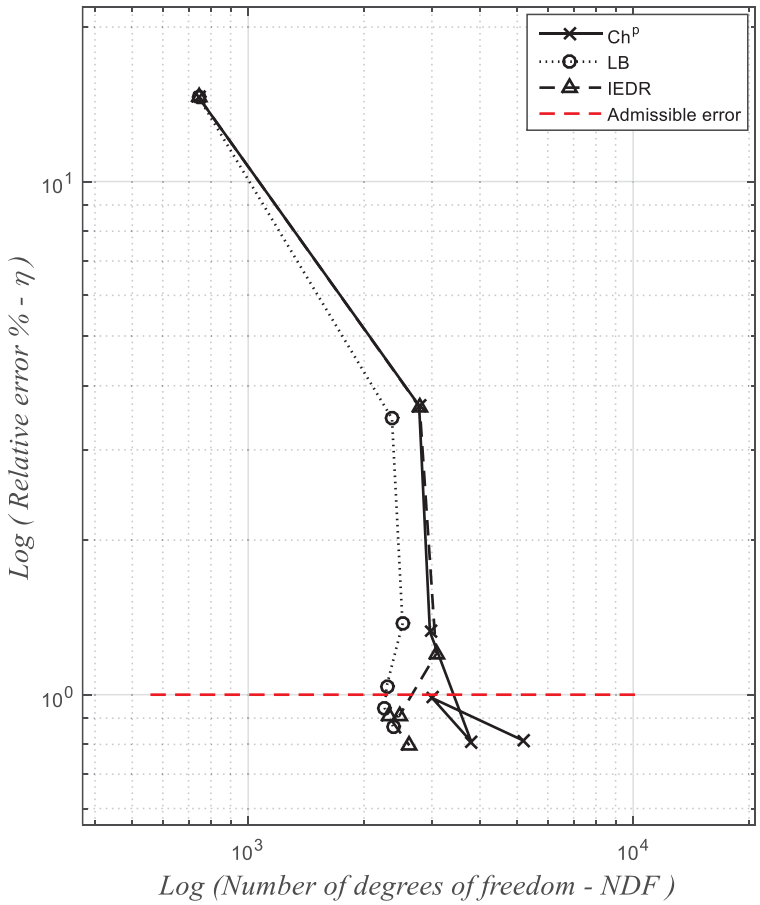

SOURCE: The author (2018).

Indeed, the h-adaptive FEM based on the IEDR methodology achieves convergence with 3 iterations producing a convergent mesh with considerably lower number of degrees in comparison with the Ch^p technique. In fact, the convergent mesh produced via the Ch^p has 913 elements, 156.6% more elements when compared to the 583 elements required by the IEDR technique. In the other hand, the LB methodology reaches convergence in 4 iterations with gradual adjustments in the mesh in order to equidistribute the error. Although the increased number of iterations required, this technique uses slightly less elements to achieve convergence. The convergence curves indicate that the IEDR technique present advantages related to the computational cost due to the use of less iterations while providing suitable mesh parameters for the convergent mesh. This indicates that, through the iterative process of estimating the new element's error density function, the IEDR technique is able to design element sizes in the critical singularity region effectively. Difficulties in predicting the element sizes in the critical region are due to the poor error estimation present.

FIGURE 30 illustrates the 3 meshes obtained through the h-adaptive IEDR remeshing methodology required to achieve convergence, where the global energy error of the mesh is lower than the admissible energy error. In this image, the first and second meshes produced present an elevated number of elements and, in the thid mesh, the excessive number of elements is adjusted. The mesh produced in the first iteration shows a prediction of high number of elements required to achieve an optimal mesh, thus, a generalized refinement of the mesh is carried out. The meshes produced in the second and third iterations through the IEDR methodology for this problem are relatively similar, with small changes present in the critical region of singularity.

FIGURE 30 – PROBLEM 4: ADAPTED MESHES NECESSARY TO ACHIEVE CONVERGENCE USING THE h-ADAPTIVE PROCESS BASED ON THE IEDR TECHNIQUE.

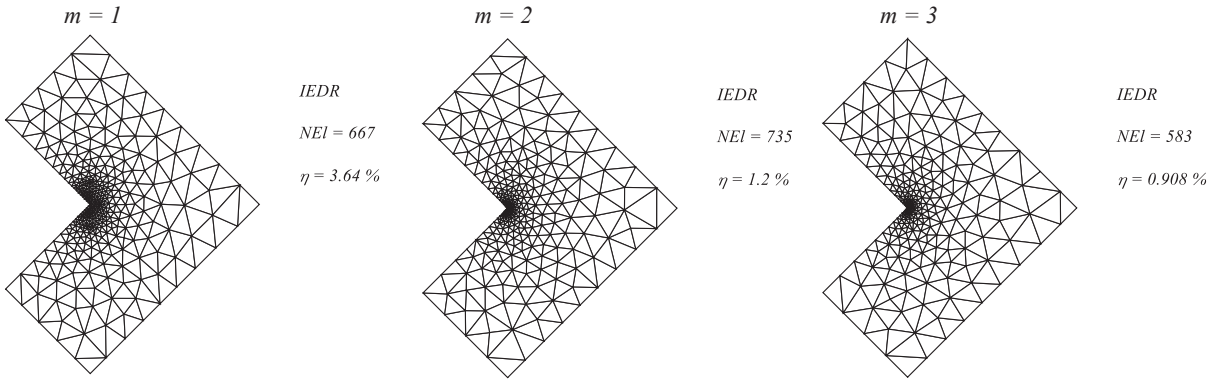

SOURCE: The author (2018).

FIGURES 31 and 32 show the meshes required to achieve the admissible global error using the Ch^p and LB methods, respectively. The meshes produced by the Ch^p method show the same oscillatory behavior as found in the previous examples, where the element sizes vary from being smaller in the critical region, in iterations 1 and 3 (m = 1 and m = 3), to being smaller in the whole domain as in iteration 2 (m = 2). The LB method, on the other hand, gradually refines the region of singularity, thus, requiring more iterations to achieve a convergent mesh in view of the admissible error.

FIGURE 31 – PROBLEM 4: ADAPTED MESHES NECESSARY TO ACHIEVE CONVERGENCE USING THE h-ADAPTIVE PROCESS BASED ON THE Ch^p TECHNIQUE.

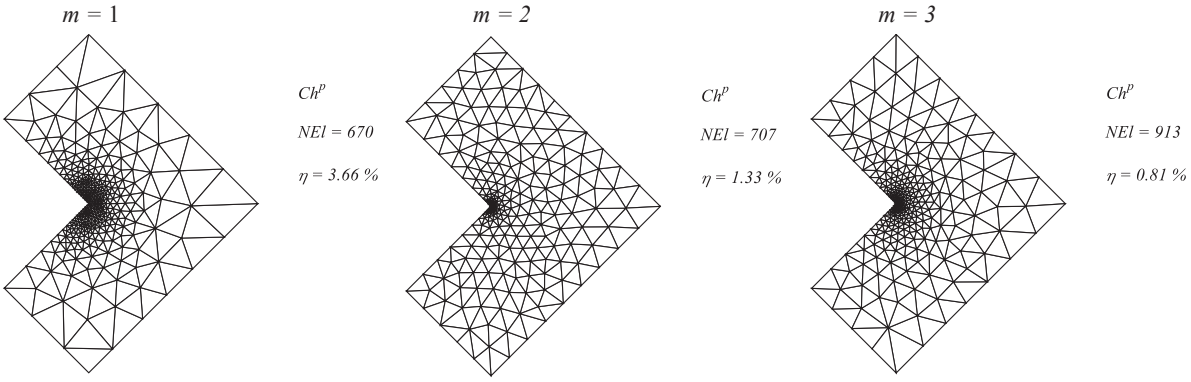

SOURCE: The author (2018).

FIGURE 32 – PROBLEM 4: ADAPTED MESHES NECESSARY TO ACHIEVE CONVERGENCE USING THE h-ADAPTIVE PROCESS BASED ON THE LB TECHNIQUE.

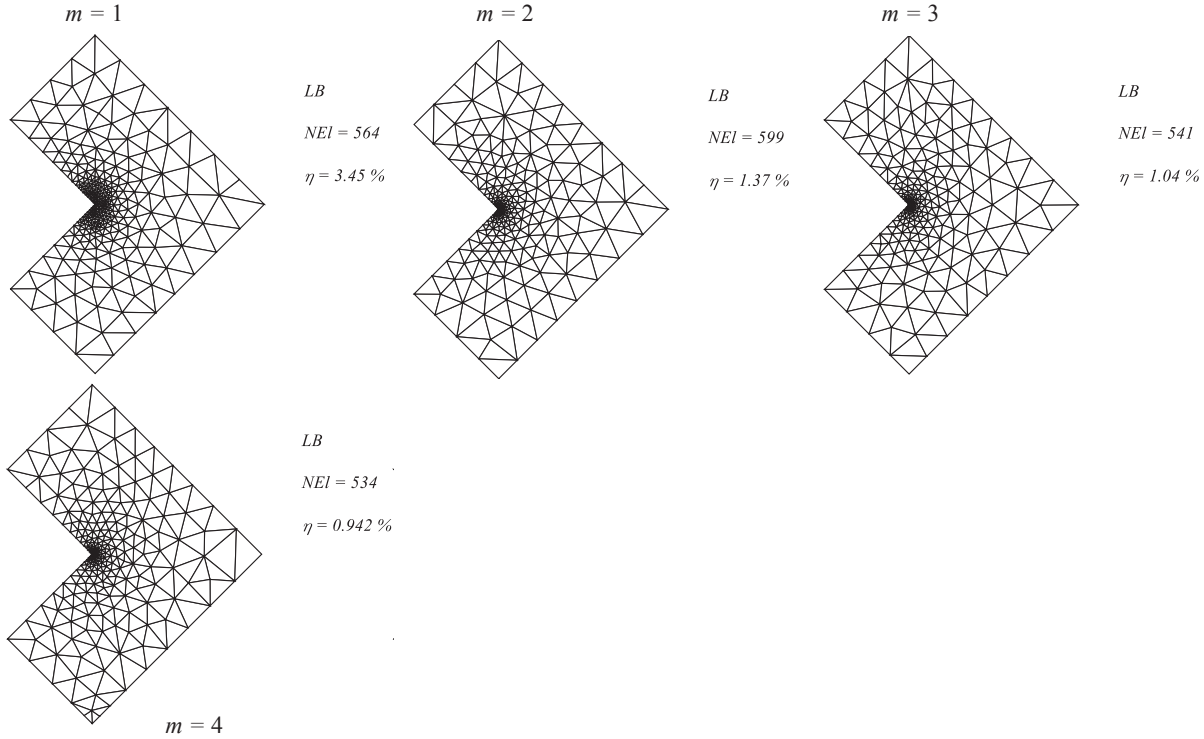

SOURCE: The author (2018).

In TABLE 8, the mesh parameters for 5 iterations of the adaptive processes are shown. Even though a convergent mesh is achieved after 3 or 4 iterations, additional iterations are analysed to assess the stability of each result. The mesh quality parameters obtained through the IEDR and LB methodologies show better characteristics, in broad terms, than the mesh parameters obtained through the Ch^p methodology. Specifically, the standard deviation of the element error is closer to 0, the maximum error parameter is lower, and the average of error parameter is closer to 1 for the IEDR and LB methodologies.

TABLE 8 – PROBLEM 4: MESH PARAMETERS FOR THE h-ADAPTIVE PROCESSES BASED ON THE IEDR, LB AND Ch^p METHODOLOGIES.

Method		*Initial Mesh*	*Mesh 1*	*Mesh 2*	*Mesh 3*	*Mesh 4*	*Mesh 5*
Ch^p	η	14.61	3.66	1.33	0.81	0.98	0.81
	NDF	743	2779	2965	3797	3007	5195
	θ	0.72	0.84	0.95	1.07	1.11	1.08
	$\bar{\zeta}_{ave}$	4.89	1.05	0.77	0.61	0.75	0.53
	$\bar{\zeta}_{máx}$	108.3	50.95	14.31	4.39	8.57	3.60
	$D_{\bar{\zeta}}$	14.30	3.50	1.10	0.66	0.69	0.78
LB	η	14.61	3.45	1.37	1.04	0.94	0.87
	NDF	743	2363	2517	2289	2263	2379
	θ	0.72	0.86	0.91	1.64	1.06	1.07
	$\bar{\zeta}_{ave}$	4.89	1.10	0.85	0.88	0.88	0.83
	$\bar{\zeta}_{máx}$	108.3	44.93	14.91	7.20	4.51	2.56
	$D_{\bar{\zeta}}$	14.30	3.27	1.09	0.57	0.36	0.31
IEDR	η	14.61	3.64	1.20	0.91	0.91	0.80
	NDF	743	2789	3077	2465	2319	2621
	θ	0.72	0.82	0.91	1.02	1.07	1.12
	$\bar{\zeta}_{ave}$	4.89	1.01	0.70	0.79	0.85	0.75
	$\bar{\zeta}_{máx}$	108.3	51.7	14.65	5.82	3.79	4.19
	$D_{\bar{\zeta}}$	14.30	3.50	1.02	0.49	0.34	0.38

SOURCE: The author (2018).

FIGURE 33 shows an enlarged view of the error distribution near the singularity for the first 3 iterations of each h-adaptive process. The figure shows a similar element sizes and error distributions near the re-entrant vertex for the LB and IEDR techniques, while the Ch^p

methodology produces a higher number of elements. Also, the IEDR methodology designed gradually decreasing element sizes towards the singularity vertex, whereas the Ch^p methodology produced equally small element sizes distributed in the region nearby the vertex. The LB methodology designed slightly bigger elements while using a lower number of elements, thus requiring another iteration to achieve convergence of 1% error.

FIGURE 33 – PROBLEM 4: ENLARGED VIEW OF ERROR DISTRIBUTION NEAR THE RE-ENTRANT VERTEX FOR 3 ITERATIONS OF EACH METHODOLOGY.

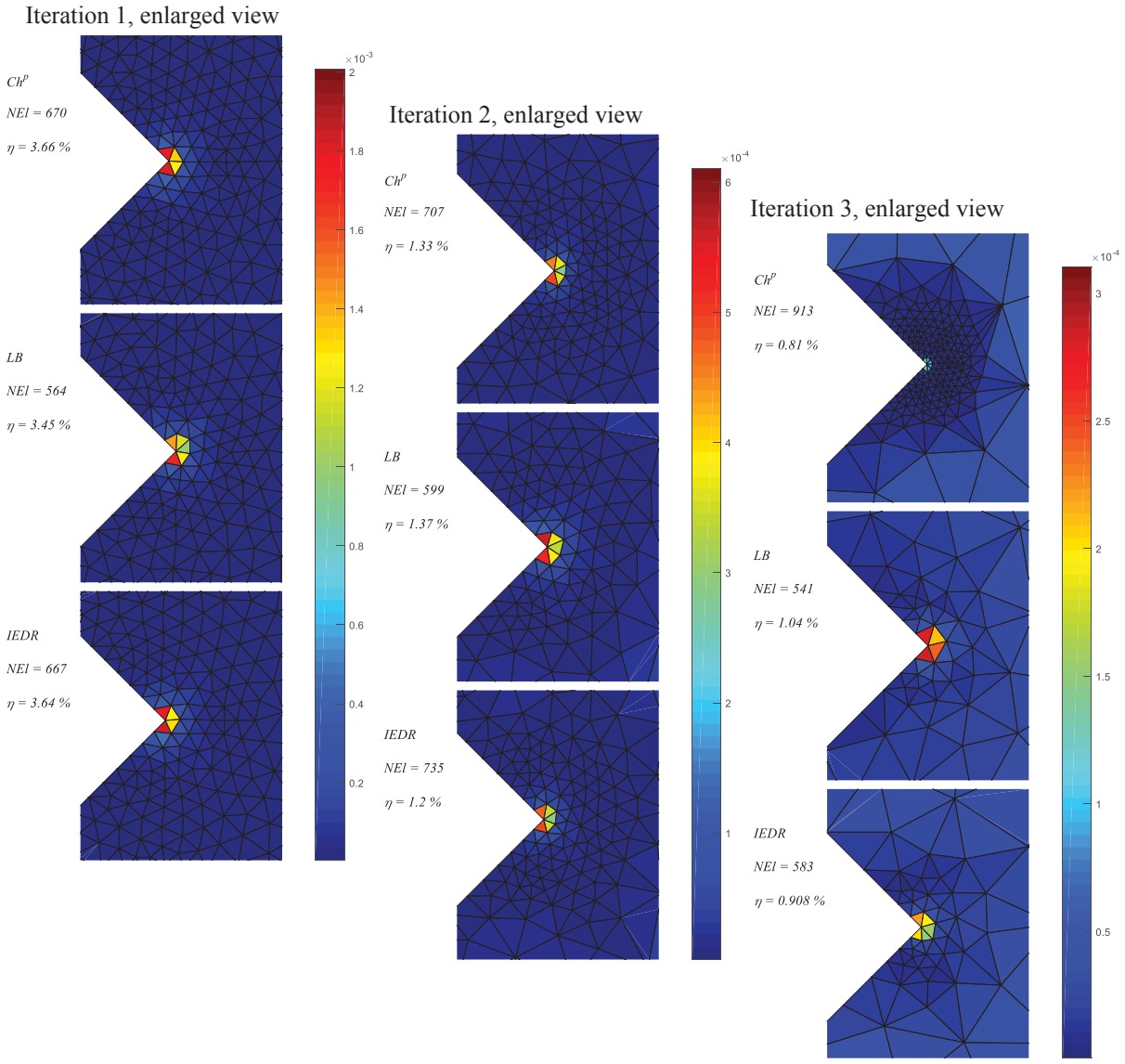

SOURCE: The author (2018).

6 FINAL CONSIDERATIONS

6.1 CONCLUSION

In this dissertation, the analysis and the numerical implementation of a new element design methodology for the h-adaptive mesh refinement process considering approximately isotropic elements of quadratic order is studied. The formulation is developed based on the IEDR technique previously developed for linear triangular elements in the literature. This methodology innovates by recovering an error density function for each element instead of using a scalar value. As shown, for Poisson type heat transfer elliptic problems, the methodology based on the IEDR remeshing strategy produced meshes, in each iteration, with quality parameters comparable to the LB methodology and superior in comparison to the commonly used Ch^p element design methodology. The technique obtained improved results by allocating refined elements in regions of the solution with higher change in gradients while allocating coarser elements in regions of the solution with lower change in gradients. Furthermore, as shown in Problem 3 and 4, the methodology successfully refined linear elastic problems. In problem 4, where a stress singularity is present, the mesh required one less iteration than the methodology based on the LB remeshing strategy to achieve convergence and presented better mesh parameters than the methodology based on the Ch^p element design technique. The results show, in every problem analyzed, that the IEDR technique as proposed produces meshes, overall, with superior mesh quality parameters when compared to the Ch^p technique.

Thus, it can be concluded that the IEDR technique, as seen from the results and formulation, addresses the approximate errors, through the recovery of an error density function, in such a manner that more information is used to design the new element sizes. Also, the developed formulation makes use of an iterative process that estimates the optimal number of elements required in the new mesh. Therefore, the methodology tends to achieve convergence in less iterations and better mesh quality parameters than the Ch^p technique. On the other hand, for the first 3 problems analyzed, the proposed element design methodology obtains meshes similar to those obtained through the LB element design methodology, which also predicts the optimal number of elements. Still, for the problems with higher complexity such as Problem 4, the IEDR technique achieves convergence with less iterations than the LB element design methodology. This indicates that the LB technique tends to smooth the mesh

excessively when compared to the IEDR technique, requiring more iterations to accurately design fine elements for regions with concentrated high errors, such as regions with singularities.

The IEDR technique obtained meshes with adequate quality parameters for every problem analyzed when compared to the other techniques and reached convergence with 3 iterations for the problem with singularity. These results demonstrate that the IEDR technique is as versatile as the LB methodology while obtaining better meshes when compared to the Ch^p technique. Thus, the proposed IEDR methodology for quadratic triangular elements is an effective alternative to the commonly used techniques discussed, providing a lower computational cost, due to the use of less elements, in obtaining an optimal solution. Also, through the recovery of an error density function, the methodology can be used in the anisotropic h-adaptive FEM, where elongated elements are designed to accommodate the required solution. The use of anisotropic elements has resulted in higher convergence rates with a considerably lower number of elements, as shown by Silva (2017). The LB and Ch^p techniques are not able to produce anisotropic meshes.

The element design methodology developed in this study for the h-adaptive FEM using quadratic elements, called IEDR, was based on fundamental concepts of meh adaptivity, thus, the technique can be utilized in tridimensional problems as well as elements with different geometries. These extensions were not part of the scope of this study.

6.2 RECOMMENDATIONS

The current work proposed an extension and evaluation of the IEDR element design methodology for quadratic elements. To achieve these goals, a new iterative process of *a posteriori* estimation of the error density function is introduced and results are shown in Chapter 5. In this context, some aspects of this methodology can be improved in future efforts. Thus, suggestions for future works are:

I. Extension of the proposed methodology to higher element orders of approximation;
II. Extension of the technique regarding the application of anisotropic elements;
III. Extension of the methodology to other types of adaptivity processes such as: hp-FEM, hr-FEM, multigrid adaptivity and others;

IV. Application of the technique in practical engineering problems with high complexity, such as, for example, bone remodeling problems, crack growth analysis with enriched elements, porous media fluid flow, thermomechanical coupled problems and vibration problems.

V. Undertake a study to assess, specifically, the computational costs related to the number of iterations of the adaptive process, the number of elements and order of element approximation such that a computational cost function can be developed, and an optimization of such function is possible.

7 REFERENCES

AINSWORTH, M.; ODEN, J. T. **A Posteriori Error Estimation in Finite Element Analysis**. 1ª. ed. John Wiley and Sons, 2000.

AINSWORTH, M.; ODEN, J. T. A unified approach to a posteriori error estimation using element residual methods. **Numerische Mathematik**, v. 65, p. 23–50, 1993a.

AINSWORTH, M.; ODEN, J. T. A posteriori error estimators for second order elliptic systems: Part 1. Theoretical foundations and a posteriori error analysis. **Computers and Mathematics with Applications**, v. 25, p. 101–113, 1993b.

AINSWORTH, M.; ODEN, J. T. A posteriori error estimators for second order elliptic systems: Part 2. An Optimal Order Process for Calculating Self-Equilibrating Fluxes. **Computers and Mathematics with Applications**, v. 26, p. 75–87, 1993c.

BABUSKA, I.; RHEINBOLDT, W. C. A posteriori error analysis of finite element solutions for one-dimensional problems. **SIAM Journal on Numerical Analysis**, v. 18, p. 565–589, 1981.

BABUSKA, I.; RHEINBOLDT, W. C. Error estimates for adaptive finite element computations. **SIAM Journal on Numerical Analysis**, v. 15, p. 736–754, 1978.

BANK, R. E., WIESER, A. Some a posteriori error estimators for elliptic partial differential equations. **Mathematics of Computation**, v. 44, p. 283–301, 1985.

BANK, R., XU, J. Asymptotically exact a posteriori error estimators, part I: grids with superconvergence. **Journal of Numerical Analysis**, v. 41, p. 2294–2312, 2003.

BARLOW, J. Optimal stress locations in finite element models. **International Journal for Numerical Methods in Engineering**, v. 10, p. 243–251, 1976.

BERTSEKAS, D. P. **Constrained Optimization and Lagrange Multiplier Methods.** Athena Scientific, Belmont, MA, EUA, 1996.

BOROOMAND, B.; ZIENKIEWICZ, O. C. Recovery by equilibrium patches. **International Journal for Numerical Methods in Engineering**, v. 40, p. 137–154, 1997

CAO, W. On the superconvergence patch recovery techniques for the linear finite element approximation on anisotropic meshes. **Journal of Computational and Applied Mathematics**, v. 265, p. 33-51, 2014.

COOK, R. D., *et al.*. **Concepts and Applications of Finite Element Analysis.** 4. ed., John Wiley & Sons, INC. 2002.

DEMKOWICZ, L, ODEN, J. T. On a mesh optimization method based on a minimization of interpolation errors. **Computer Methods in Applied Mechanics and Engineering**, v. 25, p. 5568, 1986.

DÍEZ, P., RÓDENAS, J. J., ZIENKIEWICZ, O. C. Equilibrated patch recovery error estimates: simple and accurate upper bounds of the error. **International Journal for Numerical Methods in Engineering**, v. 69, p. 2075–2098, 2007.

FRAYSSE F.; VALERO E.; RUBIO G. Quasi-*a priori* truncation error estimation and higher order extrapolation for non-linear partial differential equations. **Journal of Computational Physics**, v. 253, p. 389-404, 2013.

GONZÁLEZ-ESTRADA O. A., *et al*.. Mesh adaptivity driven by goal-oriented locally equilibrated superconvergent patch recovery. **Computer Mechanics**, v. 53, p, 957-976, 2014.

GRÄTSCH, T.; BATHE, J. K. A posteriori error estimation techniques in practical finite element analysis. **Computers and Structures**, v. 83, p. 235–265, 2005.

HECHT, F. New development in FreeFem++. **Journal of Numerical Mathematics**, v. 20, p. 251–266, 2012.

HUANG, Y., XU, J. Superconvergence of quadratic finite elements on mildly structured grids. **Mathematics of Computation**, v. 77, p. 1253–1268, 2008.

HUANG, Y.; YI, N. The superconvergent cluster recovery method. **Journal of Scientific Computing**, v. 44, p. 301–322, 2010.

JOHNSON, C.; HANSBO, P. Adaptive finite element methods in computational mechanics. **Computer Methods in Applied Mechanics and Engineering**, v. 101, p. 143–181, 1992.

KATRAGADDA, P.; GROSSE, I. R. A posteriori error estimation and adaptative mesh refinement for combined thermal-stress finite element analysis. **Computers & Structures**, v. 59, p. 1149–1163, 1996.

LI, L. *et al*. Theoretical formulations for adaptive finite element computations. **Communications in Numerical Methods in Engineering**, v. 11, p. 857–868, 1995.

LI, L., BETTESS, P. Notes on mesh optimal criteria in adaptive finite element computations. **Communications in Numerical Methods in Engineering**, v. 11, p. 911–915, 1995.

MITCHELL, W. F. A collection of 2D elliptic problems for testing adaptive grid refinement algorithms. **Applied Mathematics and Computation**, v.220, p. 350–364, 2013.

NADAL E. *et al.*. A recovery-explicit error estimator in energy norm for linear elasticity. **Computer Methods in Applied Mechanics and Engineering**, v. 287, p. 172-190, 2015.

NICOLAS G., et al. Improved adaptive mesh refinement for conformal hexahedral meshes. **Advances in Engineering Software**, v. 102, p. 14–28, 2016.

NOVOTNY, A. A.; FANCELLO, E. A. Um refinamento h, p e hp adaptativo na análise de flexão de placas semi-espessas. **Revista Internacional de Métodos Numéricos para Cálculo y Diseño en Ingeniería**, v. 14, p. 25–48, 1998.

ONÃTE, E.; BUGEDA, G. A study of mesh optimality criteria in adaptive finite element analysis. **Engineering Computations**, v. 10, p. 307–321, 1993.

PEREIRA, J. T.; SILVA, J.; GONÇALVES, J. C. L. Método dos elementos finitos h-adaptativo: uma nova técnica para projeção isotrópica do tamanho elementar. **XXXVII Iberian Latin American Congress on Computational Methods in Engineering**, Brasília, Brasil. 2016.

PRUDHOMME, S. *et al.*. Practical methods for a posteriori error estimation in engineering applications. **International Journal for Numerical Methods in Engineering**, v. 56, p. 1193–1224, 2003.

RAJENDRAN, S.; LIEW, K. M. Optimal stress sampling points of plane triangular elements for patch recovery of nodal stresses. **International Journal for Numerical Methods in Engineering**, v. 58, p. 579-607, 2003.

REDDY, J. N. **An Introduction to the Finite Element Method**. 3. ed. Mc Graw Hill, 2006.

SILVA, J. **Análise de Estimadores de Erro a posteriori Aplicados ao Método dos Elementos Finitos Utilizando Refino h-adaptativo**. 2015. Dissertação (Mestrado em Engenharia Mecânica) – Programa de Pós-Graduação em Engenharia Mecânica, Universidade Federal do Paraná, Curitiba, Brasil. 2015

SILVA, J. **Otimização Estrutural Topológica Utilizando o Método dos Elementos Finitos h-adaptativo Fundamentado na Recuperação da Densidade do Erro Isotrópica e Anisotrópica**. Tese (Doutorado em Engenharia Mecânica) – Programa de Pós-Graduação em Engenharia Mecânica, Universidade Federal do Paraná, Curitiba, Brasil. 2017

SILVA, J.; SILVA, F. E. C.; PEREIRA, J. T.; GONÇALVES, J. C. L. Análise de diferentes estimadores de erro a posteriori aplicados a problemas bidimensionais utilizando refino h-adaptativo. **Congresso Nacional de Matemática Aplicada à Indústria (CNMAI)**, Caldas Novas, Brasil. 2015.

STEWART, J. R.; HUGHES, T. J. R. An a posteriori error estimator and hp-adaptive strategy for finite element discretizations of the Helmholtz equation in exterior domains. **Finite Elements in Analysis and Design**, v. 25, p. 1–26, 1997.

SZABÓ, B., BABUSKA, I. **Introduction to Finite Element Analysis: Formulation, Verification and Validation.** 1. ed. Wiley, 2011.

UBERTINI, F. Patch recovery based on complementary energy. **International Journal for Numerical Methods in Engineering**, v. 59, p. 1501–1538, 2004.

WANDZURAT, S., XIAO, H. Symmetric quadrature rules on a triangle. **Computers & Mathematics with Applications**, v. 45, p. 1829–1840, 2003.

WIBERG, N. – E.; ABDULWAHAB, F. An efficient postprocessing technique for stress problems based on superconvergent derivatives and equilibrium. **Numerical Methods in Engineering**, p. 25–32, 1992.

WIBERG, N. – E.; ABDULWAHAB, F. Patch recovery based on superconvergent derivatives and equilibrium. **International Journal for Numerical Methods in Engineering**, v. 36, p. 2703–2724, 1993.

WIBERG, N. – E.; ABDULWAHAB, F.. Error Estimation with postprocessed finite element solutions. **Computers & Structure**s, v. 64, p. 113–137, 1997.

WIBERG, N. – E.; ABDULWAHAB, F.; ZIUKAS, S. Enhanced superconvergent patch recovery incorporating equilibrium and boundary conditions. International Journal for **Numerical Methods in Engineering**, v. 37, p. 3417–3440, 1994.

WIBERG, N. – E.; LI, X. D. A postprocessed error estimate and an adaptive procedure for the semidiscrete finite element method in dynamic analysis**. International Journal for Numerical Methods in Engineering**, v. 37, p. 3585– 3603, 1994.

ZHANG, Z. M. Ultraconvergence of the patch recovery technique. **Mathematics of Computation**, v. 65, p. 1431–1437, 1996.

ZHANG, Z. M. Ultraconvergence of the patch recovery technique II. **Mathematics of Computation**, v. 69, p. 141–158, 2000.

ZHANG, Z.; NAGA, A. Validation of the a posteriori error estimator based on polynomial preserving recovery for linear elements. **International Journal for Numerical Methods in Engineering**, v. 61, p. 1860–1893, 2004.

ZHANG, Z; NAGA, A. A new finite element gradient recovery method: superconvergence property. **SIAM Journal on Numerical Analysis**, v. 26, p. 1192– 1213, 2005.

ZHU, M., MENG, L. The derivative ultraconvergence for quadratic triangular finite elements. **Journal of Computational Mathematics**, v. 22, p. 857–864, 2004.

ZIENKIEWICZ, O. C; BOOROMAND, B.; ZHU, J.Z. Recovery procedures in error estimation and adaptivity Part I: Adaptivity in linear problems. **Computer Methods in Applied Mechanics and Engineering**, v. 76, p. 111–125, 1999.

ZIENKIEWICZ, O. C.; TAYLOR, R. L. **The Finite Element Method – Volume 1: The Basis**. 5. ed. Butterworth Heinemann, 2000.

ZIENKIEWICZ, O. C.; ZHU, J. Z. A simple error estimator and adaptive procedure for practical engineering analysis. **International Journal for Numerical Methods in Engineering**, v. 24, p. 337–357, 1987.

ZIENKIEWICZ, O. C.; ZHU, J. Z. The superconvergent patch recovery and a posteriori error estimates. Part 1: the recovery technique. **International Journal for Numerical Methods in Engineering**, v. 32, p. 1331–1364, 1992a.

ZIENKIEWICZ, O. C.; ZHU, J. Z. The superconvergent patch recovery and a posteriori error estimates. Part 2: Error estimates and adaptivity. **International Journal for Numerical Methods in Engineering**, v. 33, p. 1365–1382, 1992b.

ZIENKIEWICZ, O.C; ZHU, J.Z. The superconvergent patch recovery (SPR) and adaptive finite element refinement. **Computer Methods in Applied Mechanics and Engineering**, v. 101, p. 207-224, 1992.

ZIENKIEWICZ, O. C.; ZHU, J. Z.; WU, J. Superconvergent patch recovery technique — some further tests. **Communications in Numerical Methods in Engineering**, v. 9, p. 251–258, 1993.

ZIENKIEWICZ, O.C; ZHU, J.Z. Superconvergence and the superconvergent patch recovery. **Finite Element in Analysis and Design**, v. 19, p. 11–23, 1995.